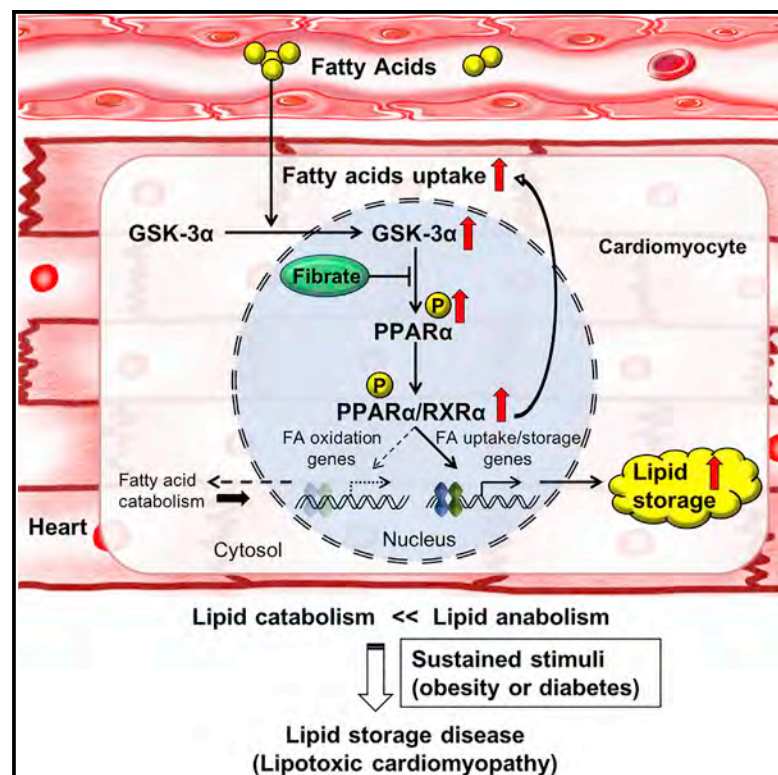


Cell Metabolism

Glycogen Synthase Kinase-3 α Promotes Fatty Acid Uptake and Lipotoxic Cardiomyopathy

Graphical Abstract



Authors

Michinari Nakamura, Tong Liu, Seema Husain, ..., Bin Tian, Hong Li, Junichi Sadoshima

Correspondence

sadoshju@njms.rutgers.edu

In Brief

Nakamura et al. investigate the mechanisms underlying the development of lipotoxic cardiomyopathy. Fatty-acid-induced upregulation of GSK-3 α acts as a central regulator of cardiac fatty acid metabolism by stimulating a biased PPAR α transcriptional response via Ser280 phosphorylation, favoring fatty acid uptake. A reversal of Ser280 phosphorylation attenuates lipotoxicity.

Highlights

- Fatty acids upregulate GSK-3 α , which in turn phosphorylates PPAR α at Ser280
- Ser280 phosphorylation stimulates biased gene expression, favoring fatty acid uptake
- PPAR α -Ser280 phosphorylation promotes the development of lipotoxic cardiomyopathy
- Fibrates inhibit Ser280 phosphorylation, thereby reversing cardiac lipotoxicity

Glycogen Synthase Kinase-3 α Promotes Fatty Acid Uptake and Lipotoxic Cardiomyopathy

Michinari Nakamura,¹ Tong Liu,² Seema Husain,³ Peiyong Zhai,¹ Junco S. Warren,⁴ Chiao-Po Hsu,⁵ Takahisa Matsuda,¹ Christopher J. Phiel,⁶ James E. Cox,⁷ Bin Tian,³ Hong Li,² and Junichi Sadoshima^{1,8,*}

¹Department of Cell Biology and Molecular Medicine, Cardiovascular Research Institute, Rutgers New Jersey Medical School, Newark, NJ, USA

²Center for Advanced Proteomics Research, Department of Biochemistry & Molecular Biology, Rutgers New Jersey Medical School, Newark, NJ, USA

³Department of Microbiology, Biochemistry, and Molecular Genetics, Rutgers New Jersey Medical School, Newark, NJ, USA

⁴Nora Eccles Harrison Cardiovascular Research and Training Institute and Department of Internal Medicine, University of Utah School of Medicine, Salt Lake City, UT, USA

⁵Division of Cardiovascular Surgery, Department of Surgery, Taipei Veterans General Hospital, National Yang-Ming University School of Medicine, Taipei City, Taiwan

⁶Department of Integrative Biology, University of Colorado Denver, Denver, CO, USA

⁷Metabolomics Core Research Facility and Department of Biochemistry, University of Utah, Salt Lake City, UT, USA

⁸Lead Contact

*Correspondence: sadoshju@njms.rutgers.edu

<https://doi.org/10.1016/j.cmet.2019.01.005>

SUMMARY

Obesity induces lipotoxic cardiomyopathy, a condition in which lipid accumulation in cardiomyocytes causes cardiac dysfunction. Here, we show that glycogen synthase kinase-3 α (GSK-3 α) mediates lipid accumulation in the heart. Fatty acids (FAs) up-regulate GSK-3 α , which phosphorylates PPAR α at Ser280 in the ligand-binding domain (LBD). This modification ligand independently enhances transcription of a subset of PPAR α targets, selectively stimulating FA uptake and storage, but not oxidation, thereby promoting lipid accumulation. Constitutively active GSK-3 α , but not GSK-3 β , was sufficient to drive PPAR α signaling, while cardiac-specific knock-down of GSK-3 α , but not GSK-3 β , or replacement of PPAR α Ser280 with Ala conferred resistance to lipotoxicity in the heart. Fibrates, PPAR α ligands, inhibited phosphorylation of PPAR α at Ser280 by inhibiting the interaction of GSK-3 α with the LBD of PPAR α , thereby reversing lipotoxic cardiomyopathy. These results suggest that GSK-3 α promotes lipid anabolism through PPAR α -Ser280 phosphorylation, which underlies the development of lipotoxic cardiomyopathy in the context of obesity.

INTRODUCTION

Fatty acids (FAs) are major substrates for ATP generation in oxidative tissues, including the adult heart (Lopaschuk et al., 2010). Derangement in FA metabolism has significant consequences for cellular functions, leading to organ failure. Decreases in the level of FA oxidation (FAO) are a common feature of heart failure (Neubauer, 2007), a condition in which cardiac

output is decreased because of the dysfunction or death of individual cardiomyocytes (CMs). In lipotoxicity, an imbalance between the uptake or synthesis of FA and its consumption results in intracellular accumulation of lipid intermediates, which induces cellular dysfunction and death in non-adipose tissues, including the kidney, liver, skeletal muscle, and heart (Goldberg et al., 2012). Lipotoxic cardiomyopathy is the major mechanism through which patients with insulin resistance, diabetes, and obesity develop cardiac hypertrophy and dysfunction (Schilling and Mann, 2012) and is an important cause of heart failure with preserved ejection fraction (HFpEF). However, how the balance of FA metabolism is disrupted in obesity remains poorly understood.

Peroxisome proliferator-activated receptor α (PPAR α) is a nuclear receptor transcription factor that plays a key role in regulating FA metabolism in the heart (Vega and Kelly, 2017). Genetic overexpression of PPAR α in the heart mimics the phenotype of lipotoxic cardiomyopathy (Finck et al., 2002), whereas knock-down of PPAR α attenuates lipotoxic cardiomyopathy (Finck et al., 2003), suggesting that PPAR α plays an important role in the pathogenesis of lipotoxic cardiomyopathy. However, how endogenous PPAR α is functionally modulated in the presence of obesity and diabetes and how its modification contributes to lipotoxicity remain poorly understood. In particular, given that PPAR α broadly controls expression of genes involved in FA metabolism, including uptake, storage, and oxidation, it remains unclear how changes in the level or the activity of PPAR α alone can cause the imbalance between the various FA metabolic mechanisms, which in turn leads to accumulation of lipid intermediates in CMs.

Through our extensive search for the molecular mechanism mediating lipotoxic cardiomyopathy in mouse models of obesity and diabetes induced by high-fat diet (HFD) consumption and genetic alteration, we found that activation of glycogen synthase kinase-3 α (GSK-3 α), an isoform of GSK-3, is essential for the induction of lipotoxic cardiomyopathy. Thus, the goal in this study was to elucidate the molecular mechanism by which GSK-3 α

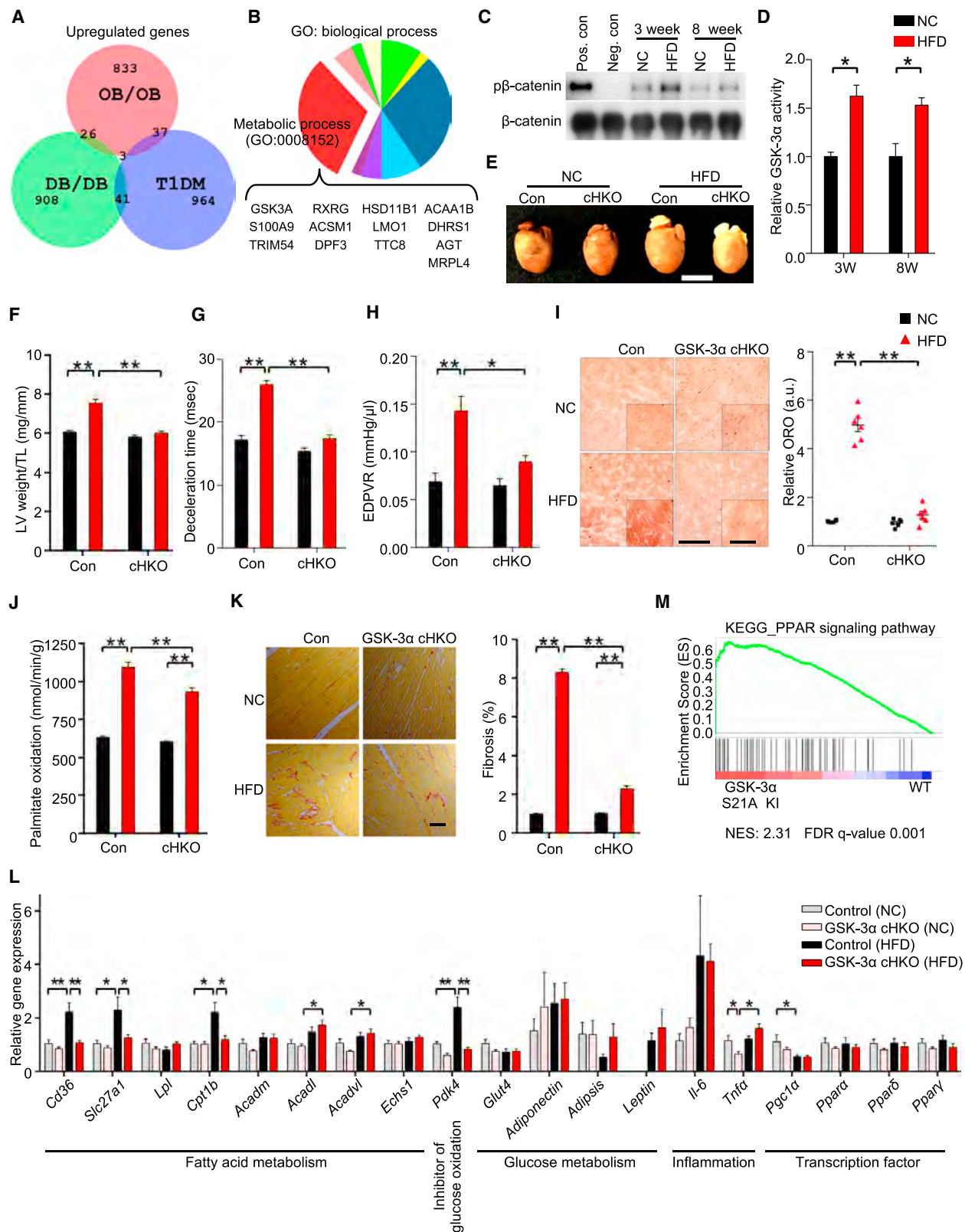


Figure 1. Cardiac-Specific GSK-3 α Haploinsufficiency Ameliorates High-Fat-Diet (HFD)-Induced Lipotoxic Cardiomyopathy

(A) Area-proportional Venn diagram representing the 26 genes significantly ($p < 0.05$) upregulated both in ob/ob (GEO: GSE16790) and db/db (GEO: GSE36875) mouse hearts but not in streptozotocin-induced diabetic hearts (type 1 DM) (GEO: GSE5606).

(legend continued on next page)

controls lipid accumulation in CMs in the presence of metabolic syndrome. Our results show that FAs upregulate nuclear GSK-3 α , which phosphorylates PPAR α at Ser280 in the ligand-binding domain (LBD). This modification induces transcription of genes involved in FA uptake and storage, but not oxidation. Our data suggest that GSK-3 α acts as an FA sensor in CMs, stimulating lipid uptake and promoting its accumulation in CMs through biased activation of PPAR α , and that this process underlies the development of lipotoxic cardiomyopathy in obesity and diabetes.

RESULTS

Cardiac-Specific Haploinsufficiency of GSK-3 α Ameliorates HFD-Induced Cardiomyopathy

In order to elucidate changes in the signaling mechanism during the development of lipotoxic cardiomyopathy, we analyzed publicly available gene expression datasets from the hearts of obese (GEO: GSE16790) and diabetic mice (GEO: GSE36875). In order to distinguish the mechanism of cardiomyopathy caused by obesity or type 2 diabetes, on which we are focusing, from that caused by type 1 diabetes, we excluded gene sets upregulated in streptozotocin-induced diabetic hearts (GSE5606). Twenty-six genes were upregulated in the hearts of both obese and diabetic mice (Figure 1A). Consistent with the nature of obesity-related cardiomyopathy, analysis of Gene Ontology terms showed that the metabolic process (GO: 0008152) containing 13 genes represented the largest biological process among the 26 overlapping genes wherein GSK-3 α was the only kinase (Figure 1B). We validated the upregulation of GSK-3 α in a diet-induced obese model. Obesity induced by HFD (60% kcal from fat) consumption elicited lipotoxic cardiomyopathy with accumulation of intramyocardial lipid in the heart. In line with the paper by Bigger and Abel (2009), we also identified insulin resistance in the heart, as evidenced by decreased Akt phosphorylation in response to insulin (Figure S1A). Since Akt, which negatively regulates GSK-3 α , is downregulated and GSK-3 α is translocated to the nucleus in response to stress (Azoulay-Alfaguter et al., 2011) (Figure S4A), we evaluated the activity of GSK-3 α in the nucleus in response to HFD, using immune complex *in vitro* kinase assays with recombinant β -catenin as a substrate. GSK-3 α was activated by HFD consumption (Figures 1C and 1D). GSK-3 α was similarly activated in genetically

obese mouse (*ob/ob*) hearts (Figure S1B). These results suggest that the activity of GSK-3 α is significantly increased in the hearts of HFD-fed mice and genetically obese mice.

In order to examine the functional significance of GSK-3 α activation in the heart in response to HFD consumption, we fed cardiac-specific GSK-3 α heterozygous (*het*) knockout (GSK-3 α cHKO) and *het* floxed (control) mice with an HFD for up to 14 weeks (Figure S1C). Although there was no difference in body weight gain, food intake, or systemic insulin resistance between control and GSK-3 α cHKO mice (Figures S1D–S1F), there was a clear attenuation in HFD-induced cardiac and individual CM hypertrophy in GSK-3 α cHKO mice (Figures 1E, 1F, and S1G). Left ventricular (LV) systolic function was preserved in both groups (Figure S1H) after HFD consumption. However, the HFD induced diastolic dysfunction in control mice, as evidenced by a longer deceleration time of the transmitral flow observed via Doppler echocardiography, a left upward shift of the slope of the end-diastolic pressure-volume (PV) relation loop (EDPVR), and an increase in Tau in PV loop analyses (Pacher et al., 2008) (Figures 1G, 1H, and S1I–S1K). The HFD-induced diastolic dysfunction was significantly alleviated in GSK-3 α cHKO mice. HFD consumption did not affect maximum LV pressure or stroke work in either control or GSK-3 α cHKO mice (Figures S1L and S1M). These results indicate that HFD-mediated cardiac hypertrophy (lipotoxic cardiomyopathy) may not be induced by altered blood pressure within 3 months and that suppression of hypertrophy does not lead to markedly elevated wall stress; thus, the overall function of the heart in GSK-3 α cHKO mice is improved. Together, these results suggest that aberrant activation of GSK-3 α plays a critical role in the development of cardiomyopathy in response to HFD consumption.

Intramyocardial lipid accumulation, as assessed by oil red O staining, and palmitic acid oxidation, assessed using ^3H -palmitic acid, were increased in control mouse hearts in response to an HFD but were markedly attenuated in GSK-3 α cHKO mice (Figures 1I and 1J). A Seahorse analysis indicated that the mitochondrial FAO rate was also increased in CMs isolated from the hearts of control mice fed an HFD but was significantly suppressed in CMs isolated from the hearts of GSK-3 α cHKO mice fed an HFD (Figures S2A–S2D). In addition, picric acid sirius red staining showed reduced cardiac fibrosis in GSK-3 α cHKO mice compared with control mice (Figure 1K). Glycogen storage in

(B) Pie chart illustrating the percent composition of Gene Ontology biological processes of the 26 common genes found in (A). Metabolic process (GO: 0008152) contains the largest gene set (13 genes), among which only GSK-3 α is a kinase.

(C) Immunoblots to evaluate nuclear GSK-3 α activity in the hearts of wild-type (WT) mice fed an HFD or normal chow (NC) for the indicated periods. GSK-3 α was immunoprecipitated from the nuclear fraction of heart lysates, followed by *in vitro* kinase assays with recombinant β -catenin. Recombinant GSK-3 α protein was used as a positive control, and IP with immunoglobulin G (IgG) was used as a negative control.

(D) Quantification of the nuclear GSK-3 α activity in (C) ($n = 3$).

(E–L) GSK-3 α cardiac-specific heterozygous knockout (GSK-3 α cHKO) mice and heterozygous floxed (control) mice were fed an HFD or NC for 14 weeks. (E) Photograph of the hearts of control and GSK-3 α cHKO mice fed an HFD or NC. (F) Left ventricular (LV) weight normalized by tibia length, a marker of cardiac hypertrophy ($n = 8$ [NC] and 22–24 [HFD]). (G and H) Diastolic function, as indicated by deceleration time ($n = 8$ –15) (G), and the slope of the end-diastolic pressure-volume (PV) relation (EDPVR) ($n = 5$ [NC] and 9 [HFD]) (H). (I) Lipid accumulation in the hearts (oil red O staining, left). Scale bar, 100 μm . Inset scale bar, 20 μm . Quantification of myocardial lipid accumulation (right) ($n = 6$). (J) Palmitate oxidation in the hearts ($n = 8$ –9 [NC] and 17 [HFD]). (K) Picric acid sirius red (PASR) staining, indicating cardiac fibrosis (left). Scale bar, 100 μm . Percentage of PASR-positive areas (right) ($n = 4$). (L) mRNA expression related to cardiac metabolism, inflammation, and transcription factors in the hearts ($n = 6$).

(M) Gene set enrichment analysis plot of Kyoto Encyclopedia of Genes and Genomes (KEGG). PPAR signaling signatures in GSK-3 α S21A knockin (KI) and WT mice fed NC. NES denotes normalized enrichment score. FDR denotes false discovery rate. Error bars indicate SEM. * $p < 0.05$, ** $p < 0.001$.

See also Figures S1 and S2 and Table S1.

Table 1. Top 10 Upregulated KEGG Gene Sets in GSK-3 α KI (versus WT) Mouse Heart

	GS Follow Link to MSigDB	Size	ES	NES	NOM p Value	FDR q Value
1	KEGG_COMPLEMENT_AND_COAGULATION_CASCADES	45	0.76	2.52	0	0
2	KEGG_PPAR_SIGNALING_PATHWAY	60	0.66	2.31	0	0.001
3	KEGG_GLYCINE_SERINE_AND_THREONINE_METABOLISM	28	0.74	2.22	0.001	0.001
4	KEGG_CYSTEINE_AND_METHIONINE_METABOLISM	29	0.72	2.15	0	0.002
5	KEGG_SPLICEOSOME	90	0.48	1.77	0	0.131
6	KEGG_PHENYLALANINE_METABOLISM	16	0.65	1.75	0.019	0.135
7	KEGG_TRYPTOPHAN_METABOLISM	33	0.56	1.74	0.006	0.131
8	KEGG_BASAL_TRANSCRIPTION_FACTORS	30	0.57	1.72	0.012	0.131
9	KEGG_PROTEASOME	42	0.53	1.72	0.011	0.123
10	KEGG_AMINO_SUGAR_AND_NUCLEOTIDE_SUGAR_METABOLISM	42	0.54	1.71	0.001	0.115

The PPAR signaling pathway is most significantly enriched among energy metabolism-related gene sets in the hearts of GSK-3 α knockin (KI) mice compared to wild-type (WT) mice at 3 months of age, a time point before the development of cardiomyopathy in GSK-3 α KI mice.

the heart was not significantly altered by GSK-3 α suppression (Figures S2E and S2F). Notably, GSK-3 β cHKO mice developed cardiac systolic dysfunction and more prominent myocardial lipid accumulation than control mice in response to an HFD (Figures S2G and S2K), suggesting that the role of GSK-3 is isoform dependent. The HFD upregulated mRNA expression of genes involved in FA metabolism in control mice, whereas these changes were attenuated in GSK-3 α cHKO mice (Figure 1L). In contrast, gene expression of inflammatory cytokines and other transcription factors related to cardiac metabolism did not differ significantly between control and GSK-3 α cHKO mice fed an HFD. These results indicate that alleviation of diet-induced cardiomyopathy and metabolic remodeling in GSK-3 α cHKO mice may be mediated, at least in part, at the level of transcription of genes involved in FA metabolism.

Since an HFD activates GSK-3 α , we hypothesized that activation of GSK-3 α is sufficient to deregulate expression of FA-metabolism-related genes. We analyzed microarray data obtained from the hearts of GSK-3 α S21A homozygous knockin (KI) mice harboring constitutively active GSK-3 α and wild-type (WT) mice fed normal chow (NC) (Matsuda et al., 2008). Although there was no overt cardiac phenotype at the age of 3 months, the gene set enrichment analysis (GSEA) showed that, in the hearts of GSK-3 α S21A KI mice, PPAR signaling is the most significantly enriched among the upregulated gene sets related to energy metabolism (Figure 1M; Tables 1 and S1). In contrast, GSK-3 β S9A homozygous KI mice, harboring constitutively active GSK-3 β , displayed downregulation of genes involved in cardiac FA metabolism (Figure S2L). One PPAR target gene, *CD36*, was significantly increased in GSK-3 α S21A KI mice (Figure S2M). Consistent with the increased *CD36* mRNA expression, both palmitate uptake into the heart and intramyocardial lipid accumulation were increased in GSK-3 α S21A KI mice (Figures S2N and S2O). These results are also consistent with the absence of an increase in expression of *CD36* in response to HFD consumption in GSK-3 α cHKO mice (Figure 1L), which could partially explain the lower FAO, potentially resulting from less

FA import, in GSK-3 α cHKO mice. Taken together, these results indicate that upregulation of GSK-3 α , but not GSK-3 β , positively regulates lipid metabolism through PPAR modification in the heart.

GSK-3 α Phosphorylates PPAR α at Ser280 Located in the Ligand-Binding Domain

Since the PPAR α transcription factor plays a major role in the regulation of FA metabolism in the heart, we examined the physical interaction between GSK-3 α and PPAR α . Yellow fluorescent protein (YFP)-tagged PPAR α pulled down endogenous GSK-3 α , but not GSK-3 β , in CMs (Figures 2A and S3A). Anti-FLAG immunoprecipitation (IP) assays showed that GSK-3 α and PPAR α interact with one another in mouse hearts overexpressing FLAG-tagged PPAR α (Figure 2B). CoIP assays also revealed that endogenous GSK-3 α and endogenous PPAR α interact with one another in CMs *in vitro* (Figure 2C). In addition, *in vitro* binding assays using recombinant GST-PPAR α and recombinant GSK-3 α or GSK-3 β showed that GSK-3 α , but not GSK-3 β , directly interacts with PPAR α (Figures 2D and S3B). We further evaluated which amino acids of PPAR α are involved in the interaction with endogenous GSK-3 α , using truncated recombinant GST-PPAR α and CM lysates (Figures 2E and 2F). Although full-length (FL) and N-terminally truncated (T5) GST-PPAR α were able to pull down endogenous GSK-3 α , C-terminally truncated GST-PPAR α (T1–T4) and GST alone failed to pull down GSK-3 α , suggesting that the LBD of PPAR α interacts with GSK-3 α (Figure 2G).

We then hypothesized that GSK-3 α phosphorylates PPAR α . *In vitro* kinase assays showed that both GST-PPAR α -FL and a PPAR α fragment (amino acids 170–430) containing the LBD are phosphorylated by GSK-3 α (Figure S3C). Furthermore, mass spectrometry analysis showed that Ser280 of PPAR α , located in the LBD and highly conserved in PPAR α across species, is phosphorylated by GSK-3 α (Figures 2H and S3D). We therefore generated an antibody against PPAR α phosphorylated at Ser280. This antibody effectively detected GST-tagged WT

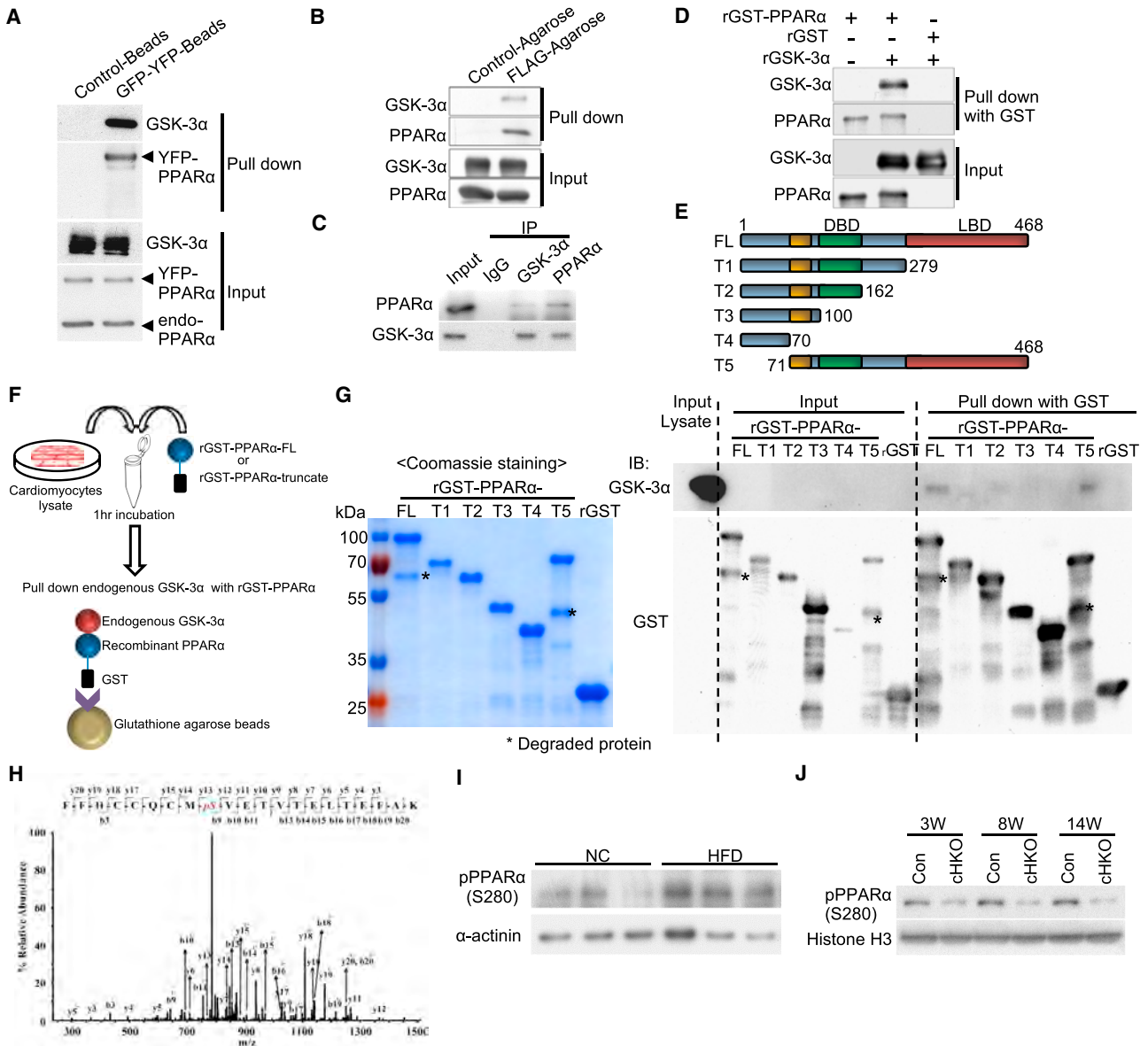


Figure 2. GSK-3 α Physically Interacts with and Phosphorylates PPAR α at Ser280 in Cardiomyocytes (CMs) and in the Heart

(A and B) IP assays to test the interaction between endogenous GSK-3 α and exogenously expressed PPAR α . YFP-tagged PPAR α or FLAG-tagged PPAR α was overexpressed in CMs using adenovirus (A) or in transgenic mouse hearts under the control of the α MHC promoter (B), respectively.

(C) CoIP assays testing the interaction between endogenous GSK-3 α and endogenous PPAR α in CMs.

(D) *In vitro* binding assays testing the direct interaction between recombinant (r) GSK-3 α and rPPAR α .

(E–G) IP assays to identify the amino acids in PPAR α responsible for the interaction with endogenous GSK-3 α . (E) Schematic representation of rGST-fused PPAR α fragments. (F) Schema of the IP assays. rGST-fused-PPAR α -full-length (FL) or truncated PPAR α (T1–T5) was incubated with lysates extracted from cultured CMs, followed by pull-down with glutathione-sepharose and immunoblotting with anti-GSK-3 α antibody. (G) Coomassie Brilliant Blue staining of rGST-PPAR α -FL or truncated rGST-PPAR α (T1–T5) (left). Immunoblots testing the binding of endogenous GSK-3 α to rGST-PPAR α -FL or T1 to T5 (right).

(H) Mass spectrometry analysis of the rGST-PPAR α protein phosphorylated by GSK-3 α in a kinase reaction. The tandem mass spectrometry (MS/MS) spectrum of the PPAR α residue corresponding to Ser280 was increased at 80 Da, indicating phosphorylation.

(I) Immunoblots showing Ser280 phosphorylation of endogenous PPAR α in the hearts of WT mice fed a high-fat diet (HFD) or normal chow (NC) for 3 weeks. α -sarcomeric actinin was used as a loading control.

(J) Immunoblots showing pPPAR α (S280) in the hearts of control or GSK-3 α chKO mice fed an HFD for the indicated period.

See also Figure S3.

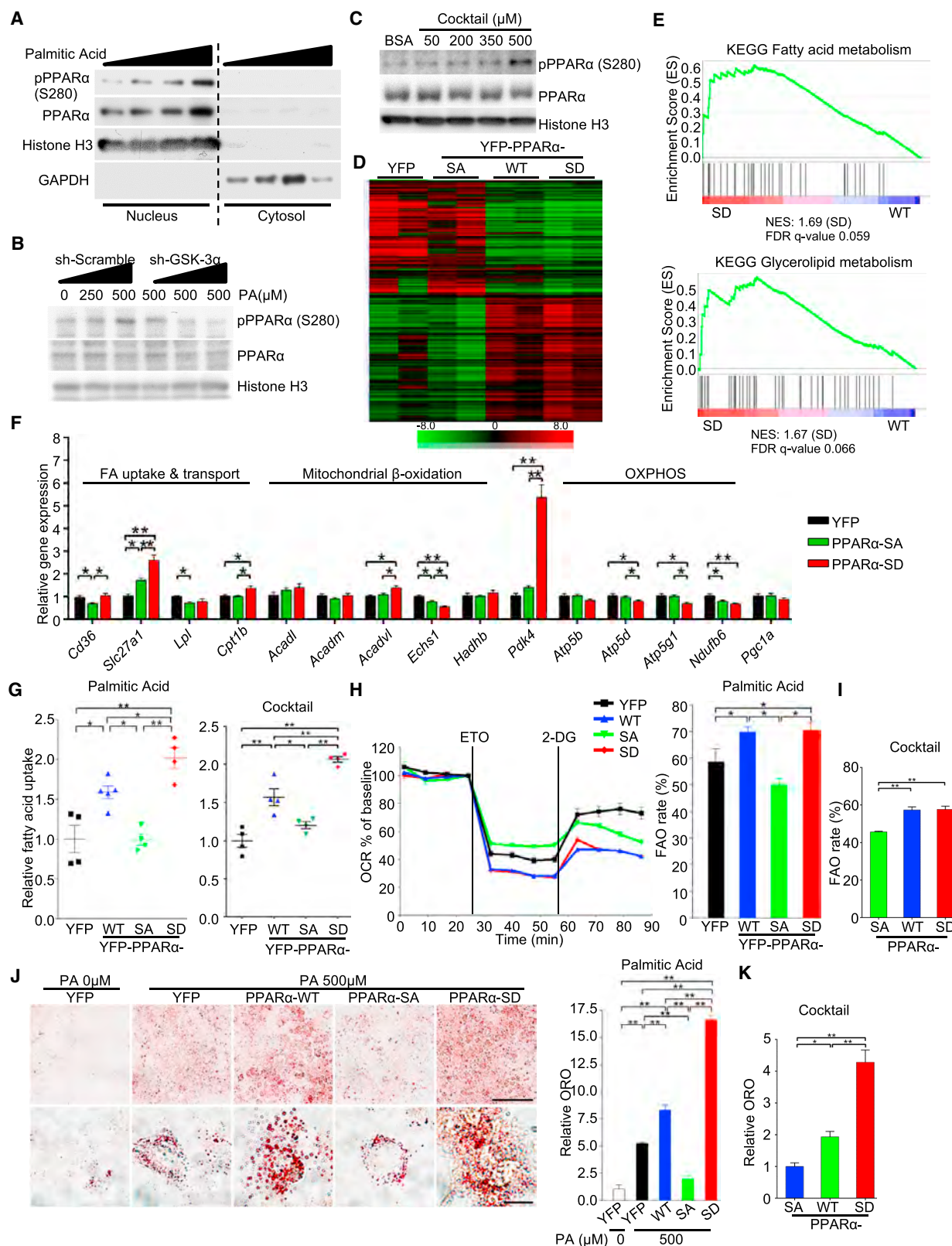


Figure 3. Ser280 Phosphorylation Stimulates a Subset of PPAR α Targets and Promotes Fatty Acid Uptake in Cardiomyocytes

(A) Immunoblots showing subcellular localization and expression of p-PPAR α (Ser280) in cultured cardiomyocytes (CMs) treated with BSA-palmitic acid (PA) (0–500 μ M) for 9 h.

(legend continued on next page)

PPAR α , but not GST-tagged PPAR α -S280A, a non-phosphorylatable mutant, after *in vitro* kinase assays with GSK-3 α (Figures S3E and S3F). Using this antibody, we confirmed that YFP-tagged PPAR α -WT, but not PPAR α -S280A, was phosphorylated in the presence of GSK-3 α overexpression but not GSK-3 α knockdown in CMs (Figure S3G). YFP-tagged PPAR α -S280D, a phospho-mimetic mutant, was detected by the phospho-specific antibody even in cells in which GSK-3 α was knocked down. Immunoblot analyses using this antibody showed that Ser280 phosphorylation of endogenous PPAR α was increased in control mouse hearts in response to HFD consumption (Figures 2I and S3H), whereas there was significantly less Ser280 phosphorylation in GSK-3 α cHKO mouse hearts (Figures 2J and S3I). Taken together, these data indicate that GSK-3 α directly interacts with PPAR α at the LBD and phosphorylates PPAR α at Ser280 in the heart and that Ser280 phosphorylation of PPAR α is increased by HFD consumption through GSK-3 α activation.

GSK-3 α -Mediated Phosphorylation Enhances PPAR α Transcriptional Activity

We examined the functional role of PPAR α -Ser280 phosphorylation. First, we investigated whether the phosphorylation status of endogenous PPAR α is altered by FAs through GSK-3 α in CMs *in vitro*. Bovine serum albumin (BSA)-conjugated palmitic acid, a major saturated FA in mammals, increased the nuclear localization of GSK-3 α in CMs within 1 h, whereas GSK-3 β was located diffusely in CMs, as shown by immunofluorescence staining (Figure S4A). The activity of GSK-3 α in the nucleus was increased in response to palmitic acid, as determined by immune complex *in vitro* kinase assays of the nuclear fraction of CMs (Figure S4B). In association with the enhanced GSK-3 α activity, PPAR α -Ser280 phosphorylation in the nuclear fraction was increased by palmitic acid in a dose-dependent manner (Figure 3A), an effect that was suppressed in the presence of adenovirus (ad)-mediated knockdown of GSK-3 α (ad-short-hairpin [sh] RNA-GSK-3 α) (Figures 3B and S4C). Since saturated FAs (such as palmitic acid), monounsaturated FAs (such as oleic acid), and polyunsaturated FAs (such as linoleic acid), have distinct effects on metabolic diseases (Roberts et al., 2014), we examined the

impact of unsaturated FAs and an FA cocktail containing palmitic acid, oleic acid, and linoleic acid on the GSK-3 α -PPAR α axis. Both oleic acid and the cocktail induced nuclear localization of GSK-3 α and PPAR α -Ser280 phosphorylation, an effect similar to that of palmitic acid. On the other hand, GSK-3 α localization was unaffected and PPAR α -Ser280 phosphorylation decreased in the presence of linoleic acid (Figures 3C and S4D–S4F). These results suggest that palmitic acid, oleic acid, and the FA cocktail, but not linoleic acid, increase PPAR α -Ser280 phosphorylation through GSK-3 α in the CM nucleus *in vitro*.

Next, we examined the effect of Ser280 phosphorylation on PPAR α transcriptional activity in response to palmitic acid in CMs. Knockdown of GSK-3 α by ad-shRNA-GSK-3 α abolished the palmitic acid-induced increase in PPAR α activity (Figure S4G). The effect of PPAR α -Ser280 phosphorylation on its activity was further elucidated using PPAR α -WT, PPAR α -S280A, and PPAR α -S280D. Whereas PPAR α reporter activity dose dependently increased in response to palmitic acid in PPAR α -WT-transduced H9C2 cells, it was significantly attenuated in PPAR α -S280A-transduced H9C2 cells (Figure S4H). Conversely, PPAR α -S280D increased transcriptional activity independently of palmitic acid. These results suggest that GSK-3 α positively regulates PPAR α activity through Ser280 phosphorylation. Since PPAR γ , another PPAR isoform, is phosphorylated at Ser273 by ERK and CDK5 in adipose tissue in obesity (Banks et al., 2015; Choi et al., 2010), we evaluated the phosphorylation status of PPAR γ at Ser273. Neither palmitic acid nor changes in GSK-3 α expression altered the PPAR γ -Ser273 phosphorylation level in CMs (Figures S4I and S4J).

To demonstrate the functional role of PPAR α phosphorylation, we performed an RNA sequencing (RNA-seq) analysis of H9C2 cells transduced with PPAR α -WT, PPAR α -S280A, PPAR α -S280D, or YFP as a control. The results indicated that PPAR α phosphorylation induces global changes in gene expression (Figure 3D). Ingenuity pathway analysis showed that phosphorylation of PPAR α significantly alters energy metabolism (Figure S4K). Furthermore, GSEAs showed that FA- and glycerolipid-metabolism-related gene sets are significantly enriched in PPAR α -S280D-transduced cells relative to PPAR α -WT

- (B) Immunoblots examining the involvement of GSK-3 α in the BSA-PA-induced increase in PPAR α phosphorylation at Ser280 in CMs. CMs transduced with adenovirus harboring shRNA-GSK-3 α or scramble were treated with the indicated concentrations of PA, followed by nuclear extraction and immunoblotting.
- (C) Immunoblots showing the expression of p-PPAR α (Ser280) in the nucleus of CMs treated with BSA-fatty acid cocktail for 9 h.
- (D) Clustergram heatmap of RNA sequencing (RNA-seq) data. H9C2 cells were transduced with PPAR α -wild type (WT), -S280A (SA) or -S280D (SD) mutant, or YFP alone as a control. Gene sets having (1) a fold difference of 1.5 or more between SA and SD and (2) a WT expression level located between SD and SA are shown in the heatmap.
- (E) Gene set enrichment analysis plots of PPAR α -SD (versus WT) showing upregulated signatures related to energy metabolism. Gene expression was determined by RNA-seq data.
- (F) qRT-PCR validation of expression of genes related to lipid metabolism and oxidative phosphorylation in CMs transduced with adenovirus harboring a YFP-PPAR α -S280A or -S280D mutant or YFP alone as a control (n = 8–10).
- (G) Fatty acid uptake into CMs transduced with the indicated adenovirus. ³H-palmitate (left) and combined ³H-palmitate and ³H-oleate (right) incorporation into CMs was measured by scintillation counting (n = 4–5).
- (H) Relative oxygen consumption rate (OCR) of CMs transduced with the indicated adenovirus was measured in a 24-well Seahorse experiment in the presence of 500 μ M BSA-PA. Mitochondrial fatty acid oxidation (FAO) was evaluated by etomoxir-inhibitable OCR. Histograms show FAO rate (the ratio of FAO versus total OCR) (n = 5).
- (I) FAO rate in CMs transduced with the indicated adenovirus, measured in a 96-well Seahorse experiment in the presence of 500 μ M BSA-fatty acid cocktail (n = 8).
- (J and K) Oil red O staining of CMs transduced with the indicated adenovirus in the presence or absence of BSA-PA (500 μ M) (n = 5) (J) or in the presence of BSA-fatty acid cocktail (500 μ M) (n = 6) (K). BSA alone was used as a control (PA 0 μ M). Scale bars, 100 μ m (upper panel) and 20 μ m (lower panel). Error bars indicate SEM. *p < 0.05, **p < 0.001.

See also Figure S4 and Table S2.

(Figure 3E; Table S2). Gene expression changes were further examined in CMs by quantitative RT-PCR (Figure 3F). PPAR α -S280D increased expression of genes related to FA uptake and pyruvate dehydrogenase (PDH) kinase 4 (*PDK4*), which inactivates the PDH complex and inhibits glucose oxidation, but genes related to β -oxidation and mitochondrial oxidative phosphorylation were mostly either unchanged or decreased (Figure 3F). These results suggest that PPAR α -Ser280 phosphorylation upregulates expression of genes involved in FA uptake and storage but not utilization.

We next investigated the functional significance of PPAR α phosphorylation in CMs. Consistent with the gene expression patterns, transduction with PPAR α -S280D markedly enhanced uptake of BSA-palmitic acid and BSA-FA cocktail into CMs compared to transduction with either PPAR α -WT or PPAR α -S280A (Figure 3G). The oxygen consumption rate (OCR) inhibitable with etomoxir, a Cpt1 inhibitor, was evaluated as a measure of mitochondrial FAO in CMs using a Seahorse analyzer (Kim et al., 2013). Despite a significant increase in FA uptake in CMs expressing the PPAR α -S280D mutant compared with those expressing PPAR α -WT, FAO was not further increased in PPAR α -S280D-transduced CMs compared with PPAR α -WT-transduced CMs (Figures 3H, 3I, and S4L), suggesting that CMs expressing PPAR α -S280D accumulate more lipids than those expressing PPAR α -WT (Figures 3J, 3K, and S4M). Taken together, these results suggest that Ser280 phosphorylation of PPAR α may shift FA metabolism to FA uptake and storage, thereby promoting lipid accumulation.

Phosphorylation of PPAR α at Ser280 Increases Both Interaction between PPAR α and RXR α and Specific DNA Binding

We investigated the mechanism by which Ser280 phosphorylation enhances PPAR α activity. YFP-tagged PPAR α -S280A and -S280D mutants were both found primarily in the nucleus (Figure S5A), indicating that Ser280 phosphorylation does not affect the nuclear localization of PPAR α . PPAR α heterodimerizes with retinoid X receptor (RXR) and binds to the PPAR response element (PPRE) to activate transcription (Evans and Mangelsdorf, 2014). IP assays showed that heterodimerization with RXR α occurs more efficiently in PPAR α -S280D than in PPAR α -WT or PPAR α -S280A (Figure 4A). Although PPAR α activity can be altered by recruitment of Sirt1 to PPAR α (Oka et al., 2011), interaction with Sirt1 was phosphorylation independent (Figure S5B). According to the three-dimensional structure of PPAR α previously analyzed by X-ray crystallography (Xu et al., 2002), Ser280 is located on helix 3 near His440 and Lys448/449, basic residues on helix 11 across the ligand-binding pocket (Figure S5C). Thus, we predict that Ser280 phosphorylation shortens the distance between Ser280 and His440 or Lys448/449 through increased electrostatic interaction, which could allow the activating function-2 (AF-2) on helix 12 to adopt a more stable and active conformation in an agonist-independent manner (Figure S5D). In fact, *in vitro* PPAR α reporter assays showed that combined mutations replacing His440 and Lys448/449 with uncharged amino acids suppressed the activity of PPAR α -S280D to a level similar to that of PPAR α -WT (Figures 4B and S5E), consistent with the aforementioned hypothesis.

Next, we asked whether increased association of PPAR α -S280D with RXR α enhances DNA binding. We compared the chromatin association of the PPAR α -WT, PPAR α -S280A, and PPAR α -S280D alleles using chromatin IP (ChIP) assays. PPAR α -S280D exhibited enhanced chromatin association with the promoters of genes involved in FA uptake and transport in CMs compared to PPAR α -WT, whereas PPAR α -S280A exhibited less chromatin association than PPAR α -WT (Figures 4C and S5F). However, DNA binding of PPAR α -S280D was unchanged or decreased compared to PPAR α -WT and PPAR α -S280A when we used primers for the promoters of genes encoding mitochondrial FAO proteins (Figures 4D and S5F).

We further investigated the underlying mechanisms by which Ser280-phosphorylated PPAR α preferentially stimulates FA uptake-related genes rather than oxidation-related genes. First, we evaluated whether the binding affinity of PPAR α to the PPRE is altered by the phosphorylation, using a double-stranded oligo pull-down assay. The oligos containing the PPRE/DR1 sequences in the uptake-related gene promoters were able to pull down phosphorylated recombinant GST-PPAR α to a greater extent than those containing the PPRE/DR1 sequences in the oxidation-related gene promoters (Figure 4E). On the other hand, the binding ability of PPAR α to the PPRE sequences of the oxidation-related genes was higher when PPAR α was not phosphorylated at Ser280 (recombinant GST-PPAR α -S280A). These results suggest that phosphorylation at Ser280 is sufficient to change the DNA-binding preference of PPAR α , even in the absence of other proteins.

In order to test whether differences in the PPRE/DR1 sequence confer a preference for recruiting either Ser280-phosphorylated or unphosphorylated PPAR α and, consequently, selective control of FA uptake versus oxidation, we first inspected PPRE/DR1 sequences in the promoters of genes upregulated by PPAR α -S280D versus S280A to generate PPRE/DR1 motifs (Figure S5G). The genes identified by the PPAR α -S280D-related PPRE/DR1 motif were more frequently observed in the gene set identified by the FA uptake-related PPRE/DR1 motif than in that associated with the oxidation-related PPRE/DR1 motif (Figure 4F). These results indicate that the selective control of FA uptake versus oxidation by PPAR α -Ser280 phosphorylation is modulated at least in part by the PPRE/DR1 sequence. Together, these findings suggest that GSK-3 α -mediated phosphorylation of PPAR α at Ser280 increases the interaction between PPAR α and RXR α and the binding of PPAR α to specific PPREs, thereby stimulating a subset of PPAR α target genes favoring FA uptake and storage (Figure S5H).

PPAR α Phosphorylation Is Critical for HFD-Induced Lipid Derangement in the Heart

In order to demonstrate the functional significance of PPAR α -Ser280 phosphorylation in the heart *in vivo* in response to an HFD, we generated KI mice in which the Ser280 residue in PPAR α was replaced with Ala (PPAR α -S280A KI mice) on the C57BL/6J background, using homologous recombination in embryonic stem cells (ESCs) (Figures S6A–S6D). Since homozygous KI mice were embryonic lethal, we used het KI mice for further characterization. The cardiac phenotype of the het KI mice was normal at 18 weeks of age. We first evaluated how the lack of PPAR α -Ser280 phosphorylation affects metabolites

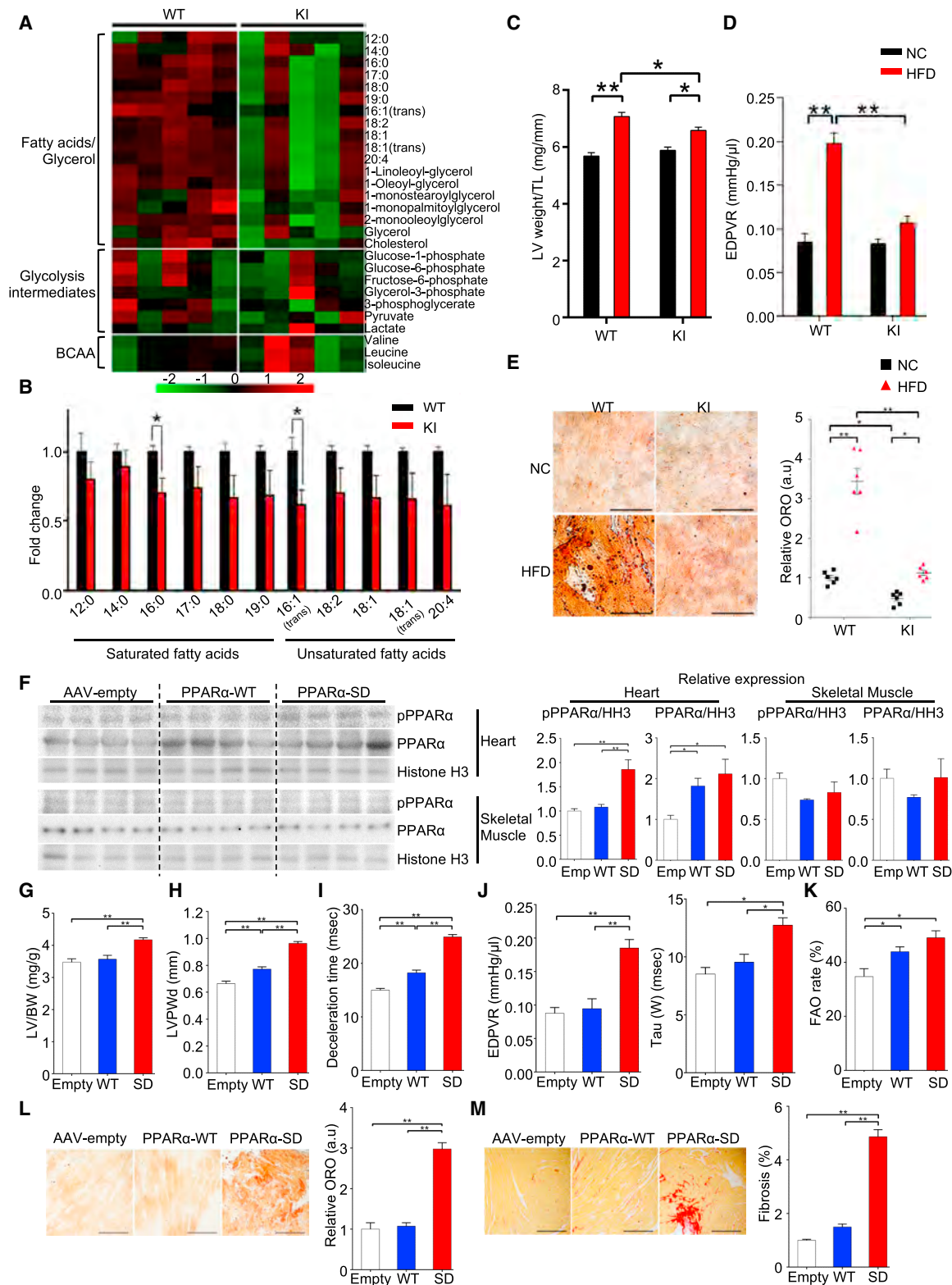


Figure 5. Phosphorylation of PPAR α at Ser280 Is Critical for the Development of Lipotoxic Cardiomyopathy

(A) Heatmap of metabolites associated with fatty acids-glycerol, glycolysis, and BCAA metabolism in the hearts of wild-type (WT) and heterozygous PPAR α -S280A knockin (KI) mice at baseline, measured by metabolomics.

(B) Histograms showing myocardial free fatty acids in the hearts of WT and heterozygous PPAR α -S280A KI mice (n = 5).

(legend continued on next page)

preserved ejection fraction (Figures 5G–5J and S6L–S6N). Lung weight normalized by body weight was increased in PPAR α -S280D-expressing mice, suggesting that PPAR α phosphorylation leads to the development of HFpEF (Figure S6K). Despite an increase in FAO rate (Figures 5K and S6O), PPAR α -S280D induced cardiac lipid accumulation to a markedly greater degree than PPAR α -WT or AAV-empty injection, accompanied by increased cardiac fibrosis (Figures 5L and 5M). These results suggest that PPAR α phosphorylation at Ser280 is sufficient to induce lipid accumulation and cardiomyopathy.

PPAR α Ligands Inhibit GSK-3 α -Mediated Phosphorylation of PPAR α

Fenofibrate is a U.S. Food and Drug Administration-approved PPAR α agonist. Given that GSK-3 α interacts with and phosphorylates PPAR α in the LBD, we asked whether fenofibrate alters the status of Ser280 phosphorylation. Interestingly, fenofibrate inhibited PPAR α -Ser280 phosphorylation in a dose-dependent manner in CMs in the presence of palmitic acid or the FA cocktail (Figures 6A, S7A, and S7B). Another PPAR α agonist, WY-14643, also inhibited GSK-3 α -mediated PPAR α -Ser280 phosphorylation *in vitro*, as well as palmitic acid-induced Ser280 phosphorylation in cultured CMs (Figures S7C and S7D).

We also tested whether fenofibrate inhibits PPAR α -Ser280 phosphorylation in the heart *in vivo* and whether it ameliorates HFD-induced lipid dysregulation and cardiac dysfunction. Mice were fed *ad libitum* with an HFD in the presence or absence of 0.2% (wt/wt) fenofibrate (Haemmerle et al., 2011) for the indicated periods (Figure S7E). Consistent with the *in vitro* results, fenofibrate treatment suppressed HFD-induced PPAR α -Ser280 phosphorylation in the heart (Figures 6B and S7F). Systolic function was preserved in both the control and fenofibrate groups (Figure S7G), but fenofibrate significantly attenuated cardiac hypertrophy and diastolic dysfunction (Figures 6C, 6D, and S7H–S7K). Although fenofibrate decreased palmitate oxidation in the hearts of mice fed an HFD (Figure S7L), it significantly suppressed HFD-induced lipid accumulation in the heart (Figure 6E).

In order to test whether fenofibrate directly affects lipid metabolism in CMs, *in vitro* experiments were conducted. Fenofibrate enhanced the transcriptional activity of PPAR α in both the absence and presence of low concentrations of palmitic acid in CMs (Figure S7M), confirming the role of fenofibrate as a PPAR α agonist. However, fenofibrate decreased FA-induced PPAR α activation in the presence of high concentrations of palmitic acid (Figure S7M). Although fenofibrate suppressed PPAR α reporter gene activity in response to a high concentration of palmitic acid in H9C2 cells transduced with PPAR α -WT, it failed to

suppress the PPAR α activity in those transduced with PPAR α -S280D (Figure 6F), suggesting that fenofibrate-induced suppression of PPAR α activity in the presence of a high concentration of palmitic acid is mediated through suppression of PPAR α -Ser280 phosphorylation. To further demonstrate the functional alterations in lipid metabolism in response to fenofibrate, CMs transduced with either PPAR α -WT or PPAR α -S280D were treated with either a low (50 μ M) or high (500 μ M) concentration of palmitic acid or the FA cocktail. Seahorse analyses showed that fenofibrate suppressed the FAO rate at high, but not low, concentrations of FAs in CMs expressing PPAR α -WT. However, fenofibrate did not affect the mitochondrial FAO rate at either low or high concentrations of FAs in CMs expressing PPAR α -S280D (Figure 6G; data using the cocktail not shown). Similarly, although intracellular lipid accumulation, evaluated with oil red O staining, induced by a high concentration of palmitic acid was suppressed by fenofibrate in CMs expressing PPAR α -WT, it was not affected by fenofibrate in CMs expressing PPAR α -Ser280D (Figure 6H). These results indicate that fenofibrate acts as a PPAR α agonist at low concentrations of FAs but suppresses FA metabolism in the presence of high concentrations of FAs, by inhibiting PPAR α -Ser280 phosphorylation (Figure S7N).

Next, we examined the mechanisms by which fenofibrate decreases Ser280 phosphorylation. GSK-3 α and YFP-tagged PPAR α physically interact with one another in a palmitic acid concentration-dependent manner, as evaluated with pull-down assays (Figures 6I and 6J) and *in situ* proximity ligation assays (Figure 6K). Fenofibrate inhibited the interaction between endogenous GSK-3 α and YFP-tagged PPAR α in CMs. Taken together, these results suggest that fenofibrate negatively regulates PPAR α phosphorylation in CMs by inhibiting the interaction between GSK-3 α and PPAR α , thereby suppressing PPAR α activity and normalizing lipid derangement in the heart in the presence of high concentrations of FA.

Finally, we examined GSK-3 α activity in human failing hearts. Diabetic patients showed a reduction in the ratio of Ser21-phosphorylated versus total GSK-3 α (Figures 6L and S7O; Table S4), indicating enhanced GSK-3 α activity in the presence of diabetes in human hearts.

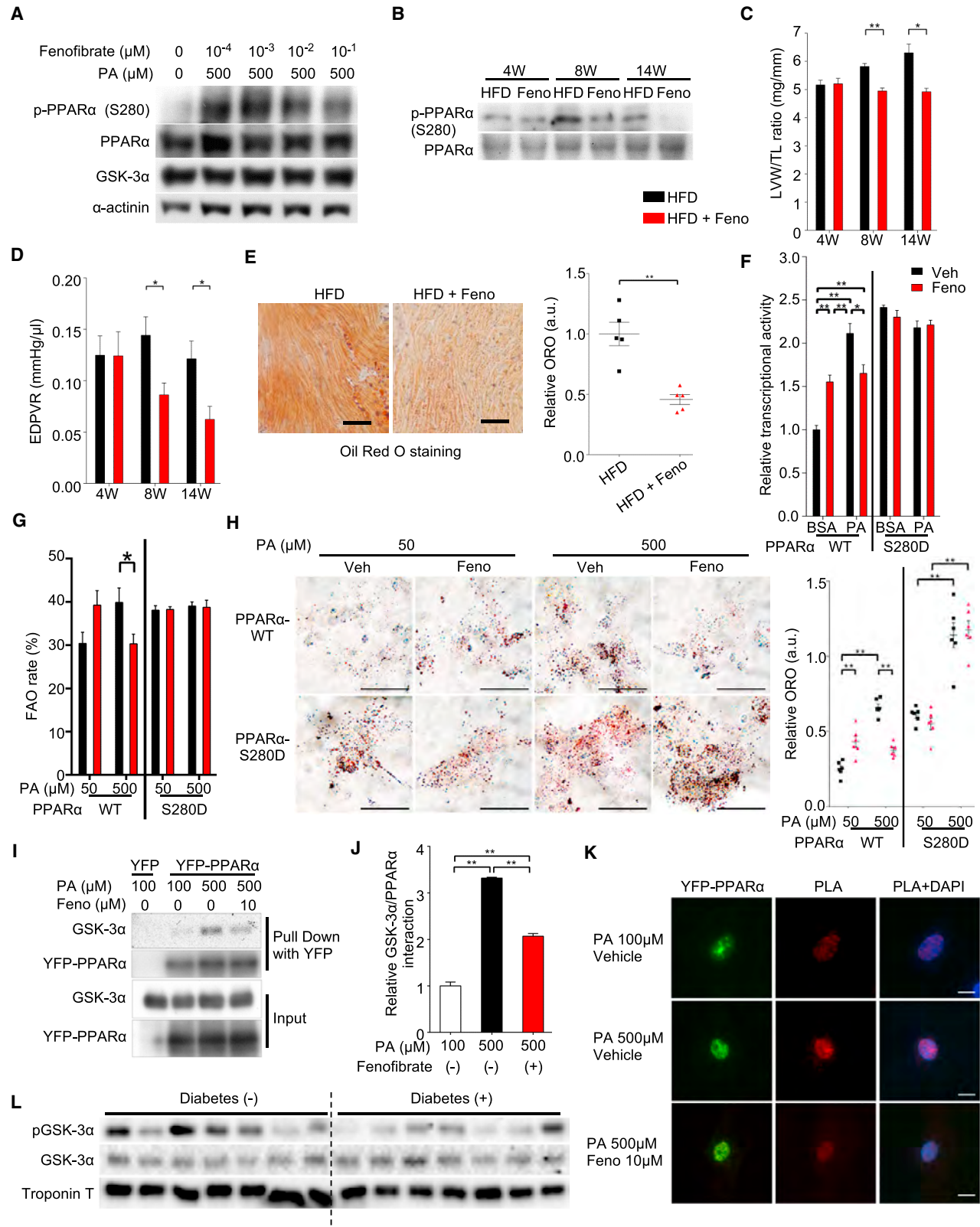
DISCUSSION

In this study, we show that GSK-3 α acts as a key kinase controlling lipid uptake and storage through PPAR α phosphorylation. FAs upregulate nuclear GSK-3 α , which phosphorylates PPAR α at Ser280, selectively stimulating transcription of genes involved

(C–E) WT and heterozygous PPAR α -S280A KI mice were fed a high-fat diet (HFD) or normal chow (NC) for 8 weeks. (C) Left ventricular (LV) weight normalized by tibia length (n = 5). (D) The slope of the end-diastolic pressure-volume (PV) relation (EDPVR), a marker of diastolic function (n = 5–8). (E) Oil red O staining of the heart sections (left). Scale bar, 50 μ m. Quantification of myocardial lipid accumulation (right) (n = 6).

(F–M) Either PPAR α -WT or PPAR α -S280D (SD) mutant was expressed in the hearts of WT mice (C57BL/6J background) fed NC for 8 weeks via adeno-associated virus (AAV)-mediated gene delivery. AAV-empty injection (Emp or Empty) was performed as a control. (F) Representative immunoblots showing the expressions of p-PPAR α (Ser280), PPAR α -S280D, and total PPAR α in the heart and skeletal muscle. Histogram indicates the expression levels relative to histone H3 (n = 8). (G) LV weight normalized by tibia length (n = 5–7). (H) LV posterior wall thickness on diastole (LVPWd), a marker of hypertrophy (n = 5–6). (I) Deceleration time, a marker of diastolic function (n = 5–6). (J) The slopes of EDPVR (left) and Tau (right), both markers of diastolic function (n = 4–6). (K) Fatty acid oxidation (FAO) rate in CMs isolated from the hearts of mice transduced with the indicated AAV (n = 5). (L) Oil red O staining of the heart sections (left). Scale bars, 50 μ m. Quantification of myocardial lipid accumulation (right) (n = 4–6). (M) Picric acid sirius red (PASR) staining indicating cardiac fibrosis in the heart sections (left) and the percentage of PASR-positive areas (right). Scale bars, 200 μ m (n = 4–7). Error bars indicate SEM. *p < 0.05, **p < 0.001.

See also Figure S6 and Table S3.



(legend on next page)

in FA uptake and storage without affecting those involved in FAO. The resultant imbalance between lipid uptake and consumption leads to intracellular lipid accumulation in metabolic syndrome. We propose that the GSK-3 α -PPAR α pathway is an essential mediator of FA uptake and storage.

Ligand-Independent PPAR α Activation through Ser280 Phosphorylation

Our results suggest that Ser280 phosphorylation stimulates PPAR α function independently of ligands. The Ser280 residue of PPAR α is located in helix 3 (H3) within the LBD (Zoete et al., 2007). Based on the crystal structure of the PPAR α LBD (Xu et al., 2002) and PPRE luciferase reporter assays, we predict that phosphorylation of PPAR α -Ser280 enhances its electrostatic interaction with His440 and Lys448/449, basic residues on helix 11 (H11), thereby shortening the distance between H3 and H11 and allowing the adjacent helix 12 (H12), containing AF-2, to fold up against the LBD core, creating a lid over the ligand-binding pocket even in the absence of endogenous ligands. PPAR α -Ser280 phosphorylation also enhances the binding of PPAR α to the PPRE in the promoters of genes involved in FA uptake but not mitochondrial FAO. Thus, it is likely that Ser280 phosphorylation affects the function of PPAR α through multiple mechanisms by allosterically affecting the structure of PPAR α . This, in turn, allows Ser280-phosphorylated PPAR α to selectively activate transcription of genes involved in FA uptake and storage but not utilization; this selectivity is modulated at least in part by the PPRE sequence.

Previous investigations have shown that PPAR γ is phosphorylated by ERK/CDK5 at Ser273 in adipose tissues in a model of obesity (Banks et al., 2015; Choi et al., 2010). Although both Ser280 in PPAR α and Ser273 in PPAR γ are located in the LBD, there is no amino acid sequence homology between the regions adjacent to PPAR α Ser280 and PPAR γ Ser273. Consistently, neither FAs nor changes in GSK-3 α activity alter the level of PPAR γ -Ser273 phosphorylation in CMs. Furthermore, although fenofibrate inhibits phosphorylation of PPAR α at Ser280 by competing with GSK-3 α , it does not inhibit phosphorylation of PPAR γ at Ser273 (Figure S7P). More importantly, phosphoryla-

tion of PPAR α at Ser280 and that of PPAR γ at Ser273 affect distinct sets of downstream genes and exhibit distinct functional consequences, namely promoting FA uptake and lipotoxicity in the heart and lipid-independent insulin resistance in adipose tissue, respectively.

GSK-3 in Metabolism

GSK-3 α and GSK-3 β share 98% sequence similarity in their catalytic domains and phosphorylate some common targets *in vitro*. However, genetic deletion of GSK-3 β in mice causes embryonic lethality, whereas deletion of GSK-3 α does not, suggesting that GSK-3 α and GSK-3 β have distinct biological targets (Hoefflich et al., 2000). The differences in the amino acid sequences at the N and C termini confer distinct substrate specificities, and the difference in subcellular localization between GSK-3 α and GSK-3 β allows them to phosphorylate distinct substrates as well. Here, only GSK-3 α , but not GSK-3 β , translocates to the nucleus and interacts with PPAR α in CMs in response to FAs. Interestingly, although downregulation of GSK-3 α in CMs inhibited the development of cardiomyopathy in response to HFD consumption, downregulation of GSK-3 β exacerbated HFD-induced cardiomyopathy. Constitutively active GSK-3 α and GSK-3 β regulate expression of genes involved in FA uptake and transport in diametrically opposite directions. Elucidating the molecular mechanisms allowing GSK-3 α and GSK-3 β to exert opposite functions is important because none of the currently available small molecule inhibitors for GSK-3 are isoform specific, and, thus, the beneficial effect of GSK-3 α inhibition upon lipotoxic cardiomyopathy could be diminished or overwhelmed by the detrimental effect of GSK-3 β inhibition. In theory, only the unique actions of GSK-3 α ought to be targeted for the treatment of lipotoxic cardiomyopathy.

GSK-3 has recently been shown to act as a glucose sensor in B cells in the germinal center (Jellusova et al., 2017): GSK-3 is inactivated in the presence of abundant glucose, promoting cell growth and proliferation, whereas GSK-3 is activated under conditions of glucose deprivation, increasing glycolysis, and energy production. Glucose and FA metabolism are often reciprocally regulated. According to the Randle hypothesis, FA suppresses

Figure 6. Fenofibrate, a PPAR α Ligand, Inhibits GSK-3 α -Mediated PPAR α -Ser280 Phosphorylation, Thereby Ameliorating Lipotoxic Cardiomyopathy

(A) Immunoblots examining the effect of fenofibrate, a PPAR α agonist, on PPAR α -Ser280 phosphorylation in cardiomyocytes (CMs) in the presence or absence of 500 μ M BSA-palmitic acid (PA).

(B–E) Wild-type (WT) mice were fed a high-fat diet (HFD) in the presence or absence of fenofibrate (Feno) for the indicated periods, as shown in Figure S7C.

(B) Immunoblots examining the effect of fenofibrate on PPAR α -Ser280 phosphorylation in the hearts. (C) Left ventricular (LV) weight normalized by tibia length (n = 8–12). (D) The slope of the end-diastolic pressure-volume (PV) relation (EDPVR), a marker of diastolic function (n = 5–11). (E) Oil red O staining of heart sections after 14 weeks of HFD in the presence or absence of fenofibrate (left). Scale bar, 100 μ m. Quantification of myocardial lipid accumulation (right) (n = 5).

(F) The differential effect of fenofibrate on PPRE-luciferase reporter activity in H9C2 cells transduced with PPAR α -WT or PPAR α -S280D mutant in the presence of a high concentration of fatty acid (500 μ M PA) or BSA control. YFP alone was used for background extraction (n = 6).

(G) Fatty acid oxidation (FAO) rate in CMs in the presence of 50 μ M or 500 μ M PA. Total oxygen consumption rate (OCR) in CMs transduced with the indicated adenoviruses was measured by 96-well Seahorse experiment, and mitochondrial FAO was evaluated by etomoxir-inhibitable OCR (n = 18–23 [WT] and 6–7 [S280D]). (H) Oil red O staining of rat neonatal CMs transduced with the indicated adenovirus in the presence or absence of fenofibrate with 50 μ M or 500 μ M BSA-PA (left). Scale bar, 50 μ m. Quantification of myocardial lipid accumulation (right) (n = 6).

(I and J) IP assays showing the interaction between endogenous GSK-3 α and YFP-PPAR α or YFP alone as a control in CMs treated with 100 μ M or 500 μ M BSA-PA in the presence or absence of 10 μ M fenofibrate (I) and quantification of the data (n = 4) (J).

(K) Proximity ligation assay (PLA) showing the *in situ* interaction between endogenous GSK-3 α and YFP-PPAR α in CMs treated with 100 μ M or 500 μ M PA in the presence or absence of 10 μ M fenofibrate. PLA was performed using anti-GSK-3 α and anti-GFP-YFP antibodies. Red color indicates localization in close proximity. Scale bar, 10 μ m.

(L) Immunoblots examining GSK-3 α activity in failing human hearts in the presence (n = 7) or absence (n = 14) of diabetes.

See also Figure S7 and Table S4.

glucose oxidation and induces insulin resistance in muscles through an increase in intracellular citrate concentration (Randle et al., 1963). Alternatively, FA negatively regulates glucose oxidation through DAG-mediated activation of PKC θ and IRS-1 and the subsequent inhibition of PI3K and GLUT4 translocation (Samuel and Shulman, 2012; Shulman, 2014). Our results represent another important mechanism in the heart by which FAs negatively regulate glucose oxidation: increases in FAs activate GSK-3 α , which in turn upregulates *PDK4* through PPAR α phosphorylation. We propose that glucose and FA metabolism may be coordinately regulated via GSK-3 α in the heart and that the GSK-3 α -PPAR α axis is a major mechanism in the induction of lipotoxic cardiomyopathy in obesity. Since expression of GSK-3 α is increased in the presence of FAs, GSK-3 α and PPAR α may constitute a feedforward mechanism that not only contributes to myocardial energy production in the intact heart, such as during fasting, but also facilitates the progression of lipotoxic cardiomyopathy in metabolic syndrome. It is tempting to speculate that mammals, including humans, have developed this mechanism to allow the heart to promote FA uptake and storage without stimulating FAO or consequent production of reactive oxygen species when fat is abundant in preparation for future use as a backup when fat is less available.

Bidirectional Role of Fibrates in Cardiac Lipid Metabolism

Fenofibrate is a synthetic PPAR α agonist that has been shown to stimulate FA metabolism in the liver and skeletal muscle. However, the pharmacological action of fenofibrate in the heart remains elusive because fenofibrate fails to alter myocardial FA metabolism in healthy human volunteers and, conversely, decreases FA metabolism in the hearts of mice fed an HFD (Sarma et al., 2012). Here, we demonstrate that fenofibrate inhibits PPAR α activity by blocking GSK-3 α -mediated PPAR α phosphorylation in the presence of high concentrations of FAs in CMs. GSK-3 α is translocated into the nucleus in the presence of high concentrations of FAs, where it phosphorylates PPAR α . Since GSK-3 α and fenofibrate both bind to the PPAR α LBD, fenofibrate can competitively inhibit the access of GSK-3 α to the LBD of PPAR α and inhibit Ser280 phosphorylation.

It should be noted that the effectiveness of fenofibrate for the treatment of patients with diabetes remains controversial. Although a recent meta-analysis showed that fibrates have an additive cardioprotective effect upon statin therapy in humans (Silverman et al., 2016), the ACCORD (Action to Control Cardiovascular Risk in Diabetes) trial had previously showed little or no effect of combination therapy with fenofibrate and simvastatin compared to simvastatin alone in patients with diabetes (ACCORD Study Group et al., 2010). Given the aforementioned difficulty in developing an isoform-specific inhibitor for GSK-3 α and the absence of an approved drug for lipotoxic cardiomyopathy in the clinical setting, interventions directly and selectively suppressing PPAR α phosphorylation at Ser280 may be more effective as a treatment for lipotoxic cardiomyopathy than either GSK-3 inhibitors or fenofibrate. PPAR α has cell-type-specific roles. For example, enhanced PPAR α activity in muscle or liver is protective against diet-induced obesity or diabetes (Finck et al., 2005; Kersten et al., 1999). Furthermore, transcription may be regulated in a cell-type-specific manner (Gosselin

et al., 2014; Heinz et al., 2015). Thus, whether PPAR α -Ser280 phosphorylation also contributes to FA metabolism in other cell types remains to be elucidated.

Increasing evidence suggests that the FA composition of fats, including monounsaturated or polyunsaturated FAs and even-chain or odd-chain saturated FAs, the total and individual concentrations of FAs, and the ratio of saturated to unsaturated FAs all have distinct effects on cellular metabolism, thereby either promoting or preventing metabolic syndrome and cardiovascular diseases. Thus, it is challenging to conduct an *in vitro* study that faithfully mimics the FA composition observed in HFD models *in vivo*. The palmitic acid concentration in human plasma ranges from 25 to 2,500 μ M, and the level of PPAR α phosphorylation at Ser280 in CMs *in vitro* in response to the FA concentrations we used is comparable to those in the hearts of mice fed either an HFD or a control diet *in vivo*. Therefore, the experiments conducted using a range of 0–500 μ M BSA-conjugated FAs in CMs *in vitro* closely resemble human lipotoxic cardiomyopathy in terms of lipid accumulation and altered cellular metabolism. It would be interesting to investigate the impact of additional single FAs or multiple FAs in combination with different ratios on the Ser280 phosphorylation level in the future.

Limitations of Study

The HFD we used for the *in vivo* study contained lard-based fats. It would be important to identify the key components of the fat or the ratio of each FA in the blood that is critical for the induction of PPAR α phosphorylation and the development of lipotoxic cardiomyopathy *in vivo*. In addition, the specific combination of FAs that would faithfully replicate *in vivo* conditions of HFD consumption for *in vitro* studies remains to be established. Although our results suggest that the PPRE/DR1 sequence plays a critical role in mediating the effect of Ser280 PPAR α phosphorylation on the biased control of FA metabolism, the possibility remains that the effect of Ser280 PPAR α phosphorylation is mediated through either a DNA-binding-motif-independent mechanism or indirect regulation of FA metabolism.

In summary, we demonstrate that GSK-3 α acts as a central regulator of cardiac FA metabolism by stimulating a biased PPAR α transcriptional response through Ser280 phosphorylation and consequent changes in the structure of PPAR α . Activation of GSK-3 α under conditions similar to metabolic syndrome contributes to the development of lipotoxic cardiomyopathy by inducing an imbalance between FA uptake/storage and catabolism in CMs. We show that a reversal of Ser280 phosphorylation of PPAR α normalizes lipotoxicity and cardiac dysfunction, representing a promising therapeutic intervention to combat lipotoxic cardiomyopathy in patients with metabolic syndrome.

STAR★METHODS

Detailed methods are provided in the online version of this paper and include the following:

- KEY RESOURCES TABLE
- CONTACT FOR REAGENT AND RESOURCE SHARING
- EXPERIMENTAL MODEL AND SUBJECT DETAILS
 - Mice
 - Gene Targeting Mouse

- Human Samples from Explanted Hearts
- Cell Line
- Primary Rat Neonatal Cardiomyocytes
- **METHOD DETAILS**
 - Antibodies and Reagents
 - Adenovirus Constructs
 - Adeno-Associated Virus
 - Recombinant Proteins
 - *In Vitro* Kinase Assay
 - Mass Spectrometry
 - RNA-Seq Library Preparation, Sequencing, and Data Analysis
 - Quantitative RT-PCR
 - Metabolomics Analysis
 - Immunoblotting
 - Subcellular Fractionation
 - Immunoprecipitation
 - Immune Complex *In Vitro* Kinase Assay
 - *In Vitro* Binding Assays
 - Reporter Gene Assay
 - Chromatin Immunoprecipitation (ChIP) Assay
 - *In Vitro* Oligo Pull-Down Assay
 - Generation of the PPRE/DR1 Sequence Logos
 - Echocardiography
 - Pressure-Volume (PV) Loop Analysis
 - Metabolic Assay
 - Adult CMs Isolation and Metabolic Assay
 - Fatty Acid Oxidation
 - Fatty Acid Uptake *In Vitro*
 - Palmitate Uptake into the Heart *In Vivo*
 - Oil Red O Staining
 - Immunohistochemistry
 - Immunofluorescence Staining
 - Proximity Ligation Assay
- **QUANTIFICATION AND STATISTICAL ANALYSIS**
- **DATA AND SOFTWARE AVAILABILITY**

SUPPLEMENTAL INFORMATION

Supplemental Information includes seven figures and five tables and can be found with this article online at <https://doi.org/10.1016/j.cmet.2019.01.005>.

ACKNOWLEDGMENTS

We thank Dr. Peter S. Klein for providing us with GSK-3 α heterozygous floxed mice, Daniela Zablocki for critical reading of the manuscript and Mayumi Nakamura for the graphics, Dr. Richard Kitsis for his help in generating PPAR α -S280A KI mice, and Dr. Shinichi Oka for technical suggestions. This work was supported in part by U.S. Public Health Service grants HL67724, HL91469, HL102738, HL112330, and AG23039 (to J.S.). This work was also supported by the Leducq Foundation Transatlantic Network of Excellence (to J.S.), American Heart Association Founders Affiliate Postdoctoral Fellowship (14POST18870094) and Scientist Development Grant (17SDG33660358) (to M.N.), and DRC at Washington University Grant (No. 5 P30 DK020579) (to J.S.W.). The mass spectrometry data were obtained from an Orbitrap instrument funded in part by an NIH grant (NS046593) for the support of the Rutgers University Neuroproteomics Core Facility.

AUTHOR CONTRIBUTIONS

M.N. and J.S. designed the experiments and wrote the paper; M.N. conducted the *in vitro* and *in vivo* experiments; M.N., P.Z., and T.M. conducted the animal

experiments and analyses; T.L. and H.L. conducted the mass spectrometry analyses; M.N., S.H., and B.T. conducted the gene expression analyses; J.S.W. and J.E.C. conducted the metabolomic analyses; C.-P.H. provided the human heart samples; C.J.P. generated the GSK-3 β floxed mice; J.S. supervised the study and generated project resources. All authors reviewed and commented on the manuscript.

DECLARATION OF INTERESTS

The authors declare no competing interests.

Received: May 4, 2018

Revised: November 27, 2018

Accepted: January 10, 2019

Published: February 7, 2019

REFERENCES

- ACCORD Study Group, Ginsberg, H.N., Elam, M.B., Lovato, L.C., Crouse, J.R., 3rd, Leiter, L.A., Linz, P., Friedewald, W.T., Buse, J.B., Gerstein, H.C., et al. (2010). Effects of combination lipid therapy in type 2 diabetes mellitus. *N. Engl. J. Med* 362, 1563–1574.
- Ackers-Johnson, M., Li, P.Y., Holmes, A.P., O'Brien, S.M., Pavlovic, D., and Foo, R.S. (2016). A simplified, Langendorff-free method for concomitant isolation of viable cardiac myocytes and nonmyocytes from the adult mouse heart. *Circ. Res.* 119, 909–920.
- Azoulay-Alfaguter, I., Yaffe, Y., Licht-Murava, A., Urbanska, M., Jaworski, J., Pietrokovski, S., Hirschberg, K., and Eldar-Finkelman, H. (2011). Distinct molecular regulation of glycogen synthase kinase-3 α isozyme controlled by its N-terminal region: functional role in calcium/calpain signaling. *J. Biol. Chem.* 286, 13470–13480.
- Banks, A.S., McAllister, F.E., Camporez, J.P., Zushin, P.J., Jurczak, M.J., Laznik-Bogoslavski, D., Shulman, G.I., Gygi, S.P., and Spiegelman, B.M. (2015). An ERK/Cdk5 axis controls the diabetogenic actions of PPAR γ . *Nature* 517, 391–395.
- Bugger, H., and Abel, E.D. (2009). Rodent models of diabetic cardiomyopathy. *Dis. Models Mech.* 2, 454–466.
- Choi, J.H., Banks, A.S., Estall, J.L., Kajimura, S., Boström, P., Laznik, D., Ruas, J.L., Chalmers, M.J., Kamenecka, T.M., Blüher, M., et al. (2010). Anti-diabetic drugs inhibit obesity-linked phosphorylation of PPAR γ by Cdk5. *Nature* 466, 451–456.
- Evans, R.M., and Mangelsdorf, D.J. (2014). Nuclear receptors, RXR, and the Big Bang. *Cell* 157, 255–266.
- Finck, B.N., Bernal-Mizrachi, C., Han, D.H., Coleman, T., Sambandam, N., LaRiviere, L.L., Holloszy, J.O., Semenkovich, C.F., and Kelly, D.P. (2005). A potential link between muscle peroxisome proliferator-activated receptor- α signaling and obesity-related diabetes. *Cell Metab.* 1, 133–144.
- Finck, B.N., Han, X., Courtois, M., Aimond, F., Nerbonne, J.M., Kovacs, A., Gross, R.W., and Kelly, D.P. (2003). A critical role for PPAR α -mediated lipotoxicity in the pathogenesis of diabetic cardiomyopathy: modulation by dietary fat content. *Proc. Natl. Acad. Sci. USA* 100, 1226–1231.
- Finck, B.N., Lehman, J.J., Leone, T.C., Welch, M.J., Bennett, M.J., Kovacs, A., Han, X., Gross, R.W., Kozak, R., Lopaschuk, G.D., et al. (2002). The cardiac phenotype induced by PPAR α overexpression mimics that caused by diabetes mellitus. *J. Clin. Invest.* 109, 121–130.
- Goldberg, I.J., Trent, C.M., and Schulze, P.C. (2012). Lipid metabolism and toxicity in the heart. *Cell Metab.* 15, 805–812.
- Gosselin, D., Link, V.M., Romanoski, C.E., Fonseca, G.J., Eichenfield, D.Z., Spann, N.J., Stender, J.D., Chun, H.B., Garner, H., Geissmann, F., et al. (2014). Environment drives selection and function of enhancers controlling tissue-specific macrophage identities. *Cell* 159, 1327–1340.
- Grimm, D., Lee, J.S., Wang, L., Desai, T., Akache, B., Storm, T.A., and Kay, M.A. (2008). *In vitro* and *in vivo* gene therapy vector evolution via multispecies interbreeding and retargeting of adeno-associated viruses. *J. Virol.* 82, 5887–5911.

- Haemmerle, G., Moustafa, T., Woelkart, G., Büttner, S., Schmidt, A., van de Weijer, T., Hesselink, M., Jaeger, D., Kienesberger, P.C., Zierler, K., et al. (2011). ATGL-mediated fat catabolism regulates cardiac mitochondrial function via PPAR- α and PGC-1. *Nat. Med.* *17*, 1076–1085.
- He, F., Popkie, A.P., Xiong, W., Li, L., Wang, Y., Phiel, C.J., and Chen, Y. (2010). GSK3 β is required in the epithelium for palatal elevation in mice. *Dev. Dyn.* *239*, 3235–3246.
- Heinz, S., Romanoski, C.E., Benner, C., and Glass, C.K. (2015). The selection and function of cell type-specific enhancers. *Nat. Rev. Mol. Cell Biol.* *16*, 144–154.
- Hoeflich, K.P., Luo, J., Rubie, E.A., Tsao, M.S., Jin, O., and Woodgett, J.R. (2000). Requirement for glycogen synthase kinase-3 β in cell survival and NF- κ B activation. *Nature* *406*, 86–90.
- Jellusova, J., Cato, M.H., Apgar, J.R., Ramezani-Rad, P., Leung, C.R., Chen, C., Richardson, A.D., Conner, E.M., Benschop, R.J., Woodgett, J.R., et al. (2017). GSK3 is a metabolic checkpoint regulator in B cells. *Nat. Immunol.* *18*, 303–312.
- Kersten, S., Seydoux, J., Peters, J.M., Gonzalez, F.J., Desvergne, B., and Wahli, W. (1999). Peroxisome proliferator-activated receptor α mediates the adaptive response to fasting. *J. Clin. Invest.* *103*, 1489–1498.
- Khan, R.S., Lin, Y., Hu, Y., Son, N.H., Bharadwaj, K.G., Palacios, C., Chokshi, A., Ji, R., Yu, S., Homma, S., et al. (2013). Rescue of heart lipoprotein lipase-knockout mice confirms a role for triglyceride in optimal heart metabolism and function. *Am. J. Physiol. Endocrinol. Metab.* *305*, E1339–E1347.
- Kim, C., Wong, J., Wen, J., Wang, S., Wang, C., Spiering, S., Kan, N.G., Forcales, S., Puri, P.L., Leone, T.C., et al. (2013). Studying arrhythmogenic right ventricular dysplasia with patient-specific iPSCs. *Nature* *494*, 105–110.
- Liu, L., Yu, S., Khan, R.S., Ables, G.P., Bharadwaj, K.G., Hu, Y., Huggins, L.A., Eriksson, J.W., Buckett, L.K., Turnbull, A.V., et al. (2011). DGAT1 deficiency decreases PPAR expression and does not lead to lipotoxicity in cardiac and skeletal muscle. *J. Lipid Res.* *52*, 732–744.
- Lopaschuk, G.D., Ussher, J.R., Folmes, C.D., Jaswal, J.S., and Stanley, W.C. (2010). Myocardial fatty acid metabolism in health and disease. *Physiol. Rev.* *90*, 207–258.
- Maejima, Y., Kyo, S., Zhai, P., Liu, T., Li, H., Ivessa, A., Sciarretta, S., Del Re, D.P., Zablocki, D.K., Hsu, C.P., et al. (2013). Mst1 inhibits autophagy by promoting the interaction between Beclin1 and Bcl-2. *Nat. Med.* *19*, 1478–1488.
- Matsuda, T., Zhai, P., Maejima, Y., Hong, C., Gao, S., Tian, B., Goto, K., Takagi, H., Tamamori-Adachi, M., Kitajima, S., et al. (2008). Distinct roles of GSK-3 α and GSK-3 β phosphorylation in the heart under pressure overload. *Proc. Natl. Acad. Sci. USA* *105*, 20900–20905.
- Neubauer, S. (2007). The failing heart—an engine out of fuel. *N. Engl. J. Med.* *356*, 1140–1151.
- Oka, S., Alcendor, R., Zhai, P., Park, J.Y., Shao, D., Cho, J., Yamamoto, T., Tian, B., and Sadoshima, J. (2011). PPAR α -Sirt1 complex mediates cardiac hypertrophy and failure through suppression of the ERR transcriptional pathway. *Cell Metab.* *14*, 598–611.
- Pacher, P., Nagayama, T., Mukhopadhyay, P., Bátkai, S., and Kass, D.A. (2008). Measurement of cardiac function using pressure-volume conductance catheter technique in mice and rats. *Nat. Protoc.* *3*, 1422–1434.
- Randle, P.J., Garland, P.B., Hales, C.N., and Newsholme, E.A. (1963). The glucose fatty-acid cycle. Its role in insulin sensitivity and the metabolic disturbances of diabetes mellitus. *Lancet* *1*, 785–789.
- Roberts, L.D., Koulman, A., and Griffin, J.L. (2014). Towards metabolic biomarkers of insulin resistance and type 2 diabetes: progress from the metabolome. *Lancet Diabetes Endocrinol.* *2*, 65–75.
- Samuel, V.T., and Shulman, G.I. (2012). Mechanisms for insulin resistance: common threads and missing links. *Cell* *148*, 852–871.
- Sarma, S., Ardehali, H., and Gheorghade, M. (2012). Enhancing the metabolic substrate: PPAR- α agonists in heart failure. *Heart Fail. Rev.* *17*, 35–43.
- Schilling, J.D., and Mann, D.L. (2012). Diabetic cardiomyopathy: bench to bedside. *Heart Fail. Clin.* *8*, 619–631.
- Shulman, G.I. (2014). Ectopic fat in insulin resistance, dyslipidemia, and cardiometabolic disease. *N. Engl. J. Med.* *371*, 1131–1141.
- Silverman, M.G., Ference, B.A., Im, K., Wiviott, S.D., Giugliano, R.P., Grundy, S.M., Braunwald, E., and Sabatine, M.S. (2016). Association between lowering LDL-C and cardiovascular risk reduction among different therapeutic interventions: a systematic review and meta-analysis. *JAMA* *316*, 1289–1297.
- Vega, R.B., and Kelly, D.P. (2017). Cardiac nuclear receptors: architects of mitochondrial structure and function. *J. Clin. Invest.* *127*, 1155–1164.
- Watanabe, K., Fujii, H., Takahashi, T., Kodama, M., Aizawa, Y., Ohta, Y., Ono, T., Hasegawa, G., Naito, M., Nakajima, T., et al. (2000). Constitutive regulation of cardiac fatty acid metabolism through peroxisome proliferator-activated receptor α associated with age-dependent cardiac toxicity. *J. Biol. Chem.* *275*, 22293–22299.
- Xu, H.E., Stanley, T.B., Montana, V.G., Lambert, M.H., Shearer, B.G., Cobb, J.E., McKee, D.D., Galardi, C.M., Plunket, K.D., Nolte, R.T., et al. (2002). Structural basis for antagonist-mediated recruitment of nuclear co-repressors by PPAR α . *Nature* *415*, 813–817.
- Zoete, V., Grosdidier, A., and Michielin, O. (2007). Peroxisome proliferator-activated receptor structures: ligand specificity, molecular switch and interactions with regulators. *Biochim. Biophys. Acta* *1771*, 915–925.

STAR★METHODS

KEY RESOURCES TABLE

REAGENT or RESOURCE	SOURCE	IDENTIFIER
Antibodies		
Anti-rabbit monoclonal phospho-GSK-3 α (Ser21) (36E9)	Cell Signaling	9316
Anti-rabbit monoclonal GSK-3 α (D80E6)	Cell Signaling	4337
Anti-rabbit monoclonal GSK-3 α (D80D1) XP	Cell Signaling	4818
Anti-rabbit monoclonal GSK-3 α / β (D75D3) XP	Cell Signaling	5676
Anti-rabbit polyclonal phospho-GSK-3 α / β (Ser21/9)	Cell Signaling	9331
Anti-rabbit monoclonal GSK-3 β (27C10)	Cell Signaling	9315
Anti-mouse monoclonal GSK-3 α (H-12)	Santa Cruz	sc-5264
Anti-rabbit polyclonal GSK-3 β (H-76)	Santa Cruz	sc-9166
Anti-rabbit polyclonal PPAR α	Cayman Chemical	101710
Anti-rabbit polyclonal PPAR α	Abcam	ab24509
Anti-rabbit polyclonal RXR α (D-20)	Santa Cruz	sc-553
Anti-rabbit polyclonal RXR α / β / γ (Δ N197)	Santa Cruz	sc-774X
Anti-rabbit monoclonal β -Catenin (6B3)	Cell Signaling	9582
Anti-rabbit polyclonal phospho- β -catenin (Ser33/37/T41)	Cell Signaling	9561
Anti-rabbit polyclonal Akt	Cell Signaling	9272
Anti-rabbit polyclonal phospho-Akt (Ser473)	Cell Signaling	9271
Anti-rabbit polyclonal Histone H3	Cell Signaling	9715
Anti-rabbit monoclonal GAPDH (14C10)	Cell Signaling	2118
Anti-rabbit monoclonal GFP (D5.1) XP	Cell Signaling	2956
Anti-rabbit polyclonal GST	Cell Signaling	2622
Anti-mouse monoclonal α -actinin (Sarcomeric)	Sigma-Aldrich	A7811
Anti-mouse IgG, HRP-linked antibody	Cell Signaling	7076
Anti-rabbit IgG, HRP-linked antibody	Cell Signaling	7074
Anti-rabbit polyclonal Troponin T antibody	Abcam	45932
Goat anti-mouse IgG secondary antibody, Alexa Fluor 488	Thermo Fisher Scientific	A-11029
Goat anti-rabbit IgG secondary antibody, Alexa Fluor 488	Thermo Fisher Scientific	A-11034
Goat anti-rabbit IgG secondary antibody, Alexa Fluor 594	Thermo Fisher Scientific	A-11037
Clean-Blot IP Detection Reagent (HRP)	Thermo Fisher Scientific	21230
Anti-rabbit polyclonal phospho-specific PPAR α (Ser280)	GeneScript	This paper
Bacterial and Virus Strains		
Subcloning Efficiency DH5 α Competent Cells	Thermo Fisher Scientific	18265017
One Shot BL21(DE3) Chemically Competent <i>E. coli</i>	Thermo Fisher Scientific	C600003
BAC clone	BACPAC	RP24-545F24

(Continued on next page)

Continued

REAGENT or RESOURCE	SOURCE	IDENTIFIER
Biological Samples		
Human heart samples	Taipei Veterans General Hospital	This paper
Chemicals, Peptides, and Recombinant Proteins		
Anti-GFP mAb-Magnetic beads	MBL	D153-11
Anti-FLAG M2 Affinity Gel	Sigma-Aldrich	A2220
Protein A/G PLUS-Agarose	Santa Cruz	sc-2003
Glutathione Sepharose 4B	VWR/GE	17-0756-01
GSK-3 α protein, active	Millipore	14-492
GSK-3 β protein, active	Millipore	14-306
Recombinant GST-PPAR α (full-length and truncated)	This paper	N/A
Recombinant GST- β -catenin	This paper	N/A
PPAR α LBD (human recombinant)	Cayman Chemical	10009088
Recombinant GSK-3 α	This paper	N/A
IPTG	Invitrogen	15529-019
FuGENE 6 Reagent	VWR/Promega	E2691
LipofectamineTM 2000 Transfection Reagent	Invitrogen	11668-019
Palmitic acid	Sigma-Aldrich	P0500
Oleic acid	Sigma-Aldrich	O1008
Linoleic acid	Sigma-Aldrich	L1376
Bovine Serum Albumin	Boston BioProducts	P753
Palmitic Acid, [9,10-3H(N)]-, 5mCi (185MBq)	Perkin Elmer	NET043005MC
Oleic Acid, [9,10-3H(N)]-, 1mCi	Perkin Elmer	NET289001MC
Etomoxir sodium salt hydrate	Sigma-Aldrich	E1905
2-Deoxy-D-glucose	Sigma-Aldrich	D8375
L-Carnitine hydrochloride	Sigma-Aldrich	C0283
Sodium Pyruvate	Sigma-Aldrich	P4562
Fenofibrate	Sigma-Aldrich	F6020
WY-14643	R&D Systems, Tocris	1312
Rodent Diet with 60% kcal% fat	Research Diets	D12492
Rodent Diet with 10% kcal% fat	Research Diets	D12450B
High-fat diet containing 0.2% (wt/wt) fenofibrate	Research Diets	This paper
High-fat diet without Fenofibrate	Research Diets	This paper
Insulin solution human	Sigma-Aldrich	I9278
2,2,2-Tribromoethanol	Sigma-Aldrich	T48402
Oil Red O solution in 0.5% in isopropanol	Sigma-Aldrich	O1391
Phosphatase Inhibitor Cocktail 3	Sigma-Aldrich	P0044
Protease Inhibitor Cocktail	Sigma-Aldrich	P8340
Maxima SYBR Green/ROX qPCR Master Mix (2x)	Thermo/Fermentas	K0223
TRIzol Reagent (Ambion)	Life Technologies	15596-018
Adenosine 5'-diphosphate sodium salt	Sigma-Aldrich	A2754
Collagenase Type 2 CLS2	Worthington	LS004177
Percoll	GE Healthcare	17-0891-01
Biotinylated Thrombin	EMD Millipore	69672-3
Streptavidin Agarose	EMD Millipore	69203-3

(Continued on next page)

Continued

REAGENT or RESOURCE	SOURCE	IDENTIFIER
Critical Commercial Assays		
XF24 Extracellular Flux Analyzer	Seahorse Bioscience	https://www.agilent.com/en/products/cell-analysis-(seahorse)/seahorse-analyzers
XF96 Extracellular Flux Analyzer	Seahorse Bioscience	https://www.agilent.com/en/products/cell-analysis-(seahorse)/seahorse-analyzers
BriteLite Plus	Perkin Elmer	6066761
Luciferase assay system	VWR/Promega	E1501
Duolink In Situ PLA probe anti-Mouse MINUS	Sigma-Aldrich	92004-0030
Duolink In Situ PLA probe anti-Rabbit PLUS	Sigma-Aldrich	92002-0030
TnT T7 Coupled Reticulocyte Lysate System	VWR/Promega	L4610
QIAGEN HiSpeed Plasmid Maxi Kit	QIAGEN	12663
QIAGEN HiSpeed Plasmid Midi Kit	QIAGEN	12643
QIAprep Spin Miniprep Kit	QIAGEN	27104
QIAquick PCR Purification Kit	QIAGEN	28106
QIAquick Gel Extraction Kit	QIAGEN	28706
Deposited Data		
GSK-3 α / β knockin mice microarray data	Matsuda et al., 2008	GSE112160
PPAR α mutants RNaseq data	This paper	GSE112309
Experimental Models: Cell Lines		
H9C2	Oka et al., 2011	N/A
HEK293	Maejima et al., 2013	N/A
Experimental Models: Organisms/Strains		
Mouse: GSK-3 α heterozygous floxed	Gift from Dr. P.S. Klein (University of Pennsylvania)	N/A
Mouse: GSK-3 β floxed	Gift from Dr. C.J. Phiel (Nationwide Children's Hospital)	He et al., 2010
Mouse: GSK-3 α -Ser21Ala knockin	Gift from Dr. D.R. Alessi (University of Dundee)	N/A
Mouse: GSK-3 β -Ser9Ala knockin	Gift from Dr. D.R. Alessi (University of Dundee)	N/A
Mouse: α -myosin heavy chain promoter-driven heterozygous Cre transgenic	Gift from Dr. M.D. Schneider (Imperial College London)	N/A
Mouse: α -myosin heavy chain promoter-driven FLAG-PPAR α transgenic	Gift from Dr. D. Kelly (University of Pennsylvania)	N/A
Mouse: C57BL/6J	Jackson Laboratory	JAX 000664
Mouse: ob/ob; B6.Cg-Lepob/J	Jackson Laboratory	JAX 000632
Mouse: PPAR α -Ser280Ala knockin	This paper	N/A
Rat: Primary cultured neonatal ventricular cardiomyocytes	Harlan	1-day-Crl:(WI)BR-Wistar rats
Oligonucleotides		
Oligonucleotides used in this study are provided in Table S5	This paper	NCBI PRIMER-BLAST
Recombinant DNA		
pDC316 shuttle vector	Microbix	N/A
pDC316-YFP shuttle vector	Sadoshima lab	Maejima et al., 2013
pDC316-FLAG shuttle vector	Sadoshima lab	Maejima et al., 2013
pDCsilencer	Microbix	N/A
pBHGlox Δ E1.3 Cre	Microbix	N/A
pCold-GST	Takara/Clontech	3372

(Continued on next page)

Continued

REAGENT or RESOURCE	SOURCE	IDENTIFIER
CTNNB1 (untagged)-Human catenin, beta 1	Origene	SC107921
GSK3 alpha pMT2	Addgene	15896
pPPRE-tk-luciferase reporter	Gift from Dr. Ronald Evans (Salk Institute)	N/A
pCITE-GSK-3 α	This paper	N/A
pL451	Gift from Dr. Takeda (Osaka University)	N/A
pMCS-DTA	Gift from Dr. Takeda (Osaka University)	N/A
pMCS-Neo-PPAR α -S280A-DTA	This paper	N/A
pCold-GST-PPAR α -full-length	This paper	N/A
pCold-GST-PPAR α -truncate 1	This paper	N/A
pCold-GST-PPAR α -truncate 2	This paper	N/A
pCold-GST-PPAR α -truncate 3	This paper	N/A
pCold-GST-PPAR α -truncate 4	This paper	N/A
pCold-GST-PPAR α -truncate 5	This paper	N/A
pDC316-YFP-PPAR α -wild type	This paper	N/A
pDC316-YFP-PPAR α -S280A	This paper	N/A
pDC316-YFP-PPAR α -S280D	This paper	N/A
pDC316-YFP-PPAR α -S280E	This paper	N/A
pDC316-YFP-PPAR α -WT-H440A	This paper	N/A
pDC316-YFP-PPAR α -WT-H440Q	This paper	N/A
pDC316-YFP-PPAR α -WT-K448A	This paper	N/A
pDC316-YFP-PPAR α -WT-K448N	This paper	N/A
pDC316-YFP-PPAR α -WT-K449A	This paper	N/A
pDC316-YFP-PPAR α -WT-K449N	This paper	N/A
pDC316-YFP-PPAR α -WT-K448A/K449A	This paper	N/A
pDC316-YFP-PPAR α -WT-K448N/K449N	This paper	N/A
pDC316-YFP-PPAR α -WT-H440A/ K448A/K449A	This paper	N/A
pDC316-YFP-PPAR α -WT-H440Q/ K448N/K449N	This paper	N/A
pDC316-YFP-PPAR α -WT-H440A	This paper	N/A
pDC316-YFP-PPAR α -S280D-H440Q	This paper	N/A
pDC316-YFP-PPAR α -S280D-K448A	This paper	N/A
pDC316-YFP-PPAR α -S280D-K448N	This paper	N/A
pDC316-YFP-PPAR α -S280D-K449A	This paper	N/A
pDC316-YFP-PPAR α -S280D-K449N	This paper	N/A
pDC316-YFP-PPAR α -S280D- K448A/K449A	This paper	N/A
pDC316-YFP-PPAR α -S280D- K448N/K449N	This paper	N/A
pDC316-YFP-PPAR α -S280D-H440A/ K448A/K449A	This paper	N/A
pDC316-YFP-PPAR α -S280D-H440Q/ K448N/K449N	This paper	N/A
pDC316-GSK-3 α	This paper	N/A
shRNA-GSK-3 α #1	This paper	N/A
shRNA-GSK-3 α #2	This paper	N/A
shRNA-GSK-3 α #3	This paper	N/A

(Continued on next page)

Continued

REAGENT or RESOURCE	SOURCE	IDENTIFIER
pBluescript II	Maejima et al., 2013	N/A
AAV-DJ/8-CMV	UPenn Vector Core	N/A
AAV-DJ/8-CMV-PPAR α -wild type	This paper	N/A
AAV-DJ/8-CMV-PPAR α -S280D	This paper	N/A
Software and Algorithms		
R version 3.3.1	The R Project	https://www.r-project.org/
CLC Genomics Workbench 8.5 version	Qiagen	http://www.clcbio.com/products/clc-genomics-workbench/
GSEA ver 2.0	Broad institute of MIT and Harvard	http://software.broadinstitute.org/gsea/
IPA pathway analysis software	Qiagen	https://www.qiagenbioinformatics.com/products/ingenuity-pathway-analysis/
MEME Suite ver 5.0.2	The MEME SUITE	http://meme-suite.org/
UCSC Genome Browser	UCSC	http://genome.ucsc.edu/
ImageJ	NIH	https://imagej.nih.gov/ij/
Prism version 6	GraphPad	https://www.graphpad.com
Metaboanalyst ver 3.0	MetaboAnalyst	http://www.metaboanalyst.ca/
MultiExperiment Viewer ver4.9.0	MeV	http://mev.tm4.org/#/welcome

CONTACT FOR REAGENT AND RESOURCE SHARING

Further information and requests for resources and reagents should be directed to and will be fulfilled by the Lead Contact, Junichi Sadoshima (sadoshju@njms.rutgers.edu).

EXPERIMENTAL MODEL AND SUBJECT DETAILS

Mice

GSK-3 α heterozygous floxed mice (C57BL/6 background) were a kind gift from Dr. P.S. Klein (University of Pennsylvania). GSK-3 β floxed mice (C57BL/6 background) were a kind gift from Dr. C.J. Phiel ([He et al., 2010](#)). GSK-3 α and β knockin (KI) mice were a kind gift from Dr. D.R. Alessi (University of Dundee). Cardiomyocyte-specific deletion of GSK-3 α or GSK-3 β was obtained by crossing the mice with α -myosin heavy chain promoter-driven heterozygous Cre mice (a kind gift from Dr. M.D. Schneider). Cardiomyocyte-specific Tg-FLAG-PPAR α (α -myosin heavy chain promoter) mice were a kind gift from Dr. D. Kelly. Male C57BL/6J *ob/ob* mice and male C57BL/6J wild-type mice were purchased from Jackson Labs at 5–6 weeks of age. For diet-induced obesity, male 5 to 6-week-old animals were fed a high-fat (60%) diet (Research Diets, D12492). The PPAR α ligand, fenofibrate (Sigma-Aldrich), was provided via *ad libitum* feeding with a high-fat diet containing 0.2% (wt/wt) fenofibrate (custom diet purchased from Research Diets) for the indicated periods ([Haemmerle et al., 2011](#)). For cardiac insulin resistance tests, mice were fasted for 4 h, followed by intraperitoneal injection of 0.75 U/kg body weight insulin. Fifteen minutes after insulin injection, the hearts were harvested to evaluate phosphorylation of Akt by immunoblot. For intraperitoneal glucose tolerance tests in HFD-fed mice, mice were fasted for 6 h and body weight and fasting glucose level from a small tail clip were measured. Glucose (1 mg/g body weight) was injected intraperitoneally and blood glucose values were obtained at 15, 30, 45, 60, 90, and 120 mins. Mice were housed in a temperature-controlled environment within a range of 21°C–23°C with 12-hour light/dark cycles and were fed an indicated diet. We used age-matched male mice in all animal experiments. All protocols concerning the use of animals were approved by the Institutional Animal Care and Use Committee at New Jersey Medical School, Rutgers University.

Gene Targeting Mouse

PPAR α genomic DNA was isolated from BAC clone (RP24-545F24) to construct the PPAR α S280A KI targeting vector. PCR-based site-directed mutagenesis was performed to introduce a single mutation of T to G in codon 280 in exon 8 of PPAR α to change codon 280 from Ser to Ala. A pGK neo cassette flanked by two FRT sites (a kind gift from Dr. Takeda, Osaka University) was inserted into intron 8 for selection of the targeted allele. Diphtheria Toxin A fragment was used for negative selection. The DNA sequences used for constructing the targeting vector, including introns 7 and 8 and exon 8, were confirmed by DNA sequencing. The targeting vectors were linearized with *PmeI* and subsequently electroporated into ESCs. G418-resistant ES clones were screened for homologous recombination by long range PCR using the primers listed in [Table S5](#) with the Expand Long Template PCR system (Roche #11681842001). Three positive clones were identified out of 288 clones. Homologous recombinant ES clones were microinjected into blastocysts from C57BL/6J mice and transferred into pseudo-pregnant recipients to generate male chimeras. The chimeric

male mice resulting from the microinjection were bred with C57BL/6J female mice to generate germline-transmitted heterozygous S280A KI mice. PCR analysis was performed on tail DNA from offspring. Sequence analysis was performed on PCR products to verify the presence of the mutations using standard procedures. The mutant offspring were backcrossed into the C57BL/6J background.

GSK-3 α flox/flox mice were generated in Dr. Peter S. Klein's laboratory (University of Pennsylvania, Philadelphia). Briefly, a conventional targeting vector with neomycin resistance and TK was generated to insert loxP sites on either side of exon 2 in the Gsk3a gene. The neomycin resistance cassette, inserted downstream of exon 2, was also flanked by FRT sites. The construct was electroporated into ESCs derived from C57BL/6 mice and positive and negative selection was used to isolate positive clones, which were then screened by PCR for the correct insertion and confirmed by Southern blot. Cre-mediated excision removes exon 2, which encodes an essential portion of the catalytic domain, to generate a null allele.

Human Samples from Implanted Hearts

The samples from explanted hearts used in this study were obtained from 14 non-diabetic (mean age 52.0 \pm 11.8 years; 13 males) and 7 diabetic (mean age 50.4 \pm 11.6 years; 6 males) patients who had received heart transplants at the Taipei Veterans General Hospital. The study was approved by the Ethics Committee of Taipei Veterans General Hospital, and all patients or their families expressed their willingness to participate through an informed consent form. Myocardial samples from near the mitral annulus were obtained at the time of therapeutic transplantation. Immediately after tissue procurement, the samples for biochemical studies were stored in liquid nitrogen and kept at -80°C.

Cell Line

H9C2 cells were maintained at 37°C with 5% CO₂ in Dulbecco's modified Eagle's medium/Nutrient Mixture F-12 supplemented with 10% fetal bovine serum. Information on the sex is not available.

Primary Rat Neonatal Cardiomyocytes

Primary cultures of ventricular CMs were prepared from 1-day-old Crl:(WI)BR-Wistar rats (both sexes) (Harlan Laboratories, Somerville) and maintained in culture. A cardiomyocyte-rich fraction was obtained by centrifugation through a discontinuous Percoll gradient. CMs were cultured in complete medium containing Dulbecco's modified Eagle's medium/F-12 supplemented with 5% horse serum, 4 μ g/mL transferrin, 0.7 ng/mL sodium selenite, 2 g/l bovine serum albumin (fraction V), 3 mM pyruvate, 15 mM Hepes pH 7.1, 100 μ M ascorbate, 100 mg/l ampicillin, 5 mg/l linoleic acid, and 100 μ M 5-bromo-2'-deoxyuridine (Sigma). Culture dishes were coated with 0.3% gelatin or 2% gelatin for immunofluorescence staining on chamber slides.

METHOD DETAILS

Antibodies and Reagents

The following commercial antibodies were used at the indicated dilutions: phospho-GSK-3 α (Ser21) (36E9) (1:1,000), total GSK-3 α (D80E6, for WB) (1:2,000), total GSK-3 α (D80D1, for IF) (1:100), total GSK-3 α/β (D75D3) (1:4,000), phospho-GSK-3 α/β (1:2,000), histone H3 (1:5,000), GAPDH (14C10) (1:5,000), GFP (D5.1, for IF) (1:500), and secondary antibodies (anti-mouse or rabbit IgG) conjugated with horseradish peroxidase (1:4,000) (Cell Signaling); secondary antibodies (anti-mouse or rabbit IgG) conjugated with Alexa Fluor 488 or 555 (1:100) (Life Technologies); GFP-magnetic beads (Fisher/MBL); total PPAR α (1:3,000) (Cayman Chemical); RXR α (D-20) (1:4,000) (Santa Cruz); α -actinin (1:4,000) (sarcomeric) (Sigma-Aldrich). For detection of phosphorylation of PPAR α at Ser280, a polyclonal phosphorylation-specific antibody was generated by immunizing rabbits with a phospho-peptide corresponding to residues surrounding Ser280 of PPAR α (1:1,000). Antibodies were diluted in either 5% (w/v) BSA or 5% (w/v) non-fat dry milk in 1xTBS/0.5% Tween 20, depending on the level of background intensity. The following reagents were used: WY-14643 and fenofibrate (R&D Systems, Tocris for *in vitro* experiments); Palmitic acid, Duolink *In Situ* PLA, and Etomoxir (Sigma-Aldrich).

Adenovirus Constructs

Recombinant adenovirus vectors for overexpression and short hairpin RNA-mediated gene silencing were constructed, propagated, and titered as previously described (Oka et al., 2011). pBHGlox Δ E1,3Cre plasmid was co-transfected with the pDC316 shuttle vector (Microbix) or pDCSilencer (Microbix) containing YFP-PPAR α -WT, YFP-PPAR α -mutants, or GSK-3 α targeting sequences into HEK293 cells using Lipofectamine 2000 (Life Technologies). The cDNA of mouse PPAR α was amplified using pDC316-PPAR α (Oka et al., 2011) as a template and ligated into pDC316-YFP-N terminal vector (Maejima et al., 2013). The shuttle vector for the short hairpin sequence of rat GSK-3 α was generated by insertion of a complementary hairpin sequence of rat GSK-3 α (see Key Resources Table) into pDCSilencer (Microbix). The luciferase reporter plasmid (pPPRE-tk-luc) was a kind gift from Dr. Ronald Evans at the Salk Institute. Mutations were performed by site directed mutagenesis. Adenovirus vectors harboring LacZ (Ad-LacZ) and sh-Scramble (Ad-shScr) were used as controls. The total MOI of adenovirus was kept constant using LacZ or Scramble virus.

Adeno-Associated Virus

The recombinant adeno-associated virus (AAV) vectors used to generate AAV-DJ/8-PPAR α -WT or S280D were constructed by cloning the cDNA of PPAR α -WT or S280D (mouse) from the pDC316-YFP-PPAR α -WT or S280D vector into the pAAV-MCS expression vector (Cell Biolabs, Inc, #VPK-410) downstream of the CMV promoter with BamHI and Sall. 293AAV cells (Cell Biolabs) were

co-transfected with the recombinant AAV vectors, pAAV-DJ/8 vector, and helper plasmid in a 1:1:1 ratio using polyethylenimine (PEI) at the AAV core, Department of Cell Biology and Molecular Medicine, New Jersey Medical School, Rutgers University, Newark, NJ (Grimm et al., 2008). The recombinant AAV produced was purified by the iodixanol gradient/ultra-centrifugation method, and the AAV fraction was concentrated using a VIVASPIN 20 concentrator (100 kDa cut-off, Sartorius, Germany). The virus titer was determined using the Cell Biolabs AAV quantitation kit (Cat. # VPK-145). To administer recombinant AAVs, doses of 2×10^{11} vector genome per mouse were injected intravenously via the jugular vein of C57BL/6J wild-type mice.

Recombinant Proteins

The bacterial expression vectors for GST-fused PPAR α -full-length and -truncates (T1-5) were generated by insertion of mouse PPAR α cDNA amplified by PCR into the pCold-GST-vector. The BL21 *E. coli* strain was transformed with pCold-GST-PPAR α -full-length or truncates. The *E. coli* was grown in 3 mL LB medium containing ampicillin overnight at 37°C, and then transferred to 250 mL LB medium containing ampicillin. Protein expression was induced by addition of 1 mM isopropylthio- β -galactoside. After overnight culture at 15°C, the *E. coli* were lysed in lysis buffer (1% Triton X-100 and 1 mM DTT in PBS) with sonication. The lysate was incubated with 0.5 mL Glutathione-sepharose 4B (GE Healthcare) for 1 h at 4°C. The sepharose was washed 3 times with 5 mL lysis buffer, and then suspended with 1 mL cleavage buffer (20 mM Tris pH 7, 150 mM NaCl, 1 mM DTT).

In Vitro Kinase Assay

Recombinant active GSK-3 α was purchased from Millipore. Recombinant PPAR α -LBD (human) was purchased from Cayman Chemical. GST-tagged full-length PPAR α protein was generated using the pCold-GST-vector. Recombinant active GSK-3 α (10 ng) was incubated with recombinant GST-full-length-PPAR α (1 μ g) or PPAR α -LBD (1 μ g) in a kinase buffer (50 mM HEPES (pH 7.4), 15 mM MgCl₂ and 200 μ M sodium vanadate containing 100 μ M ATP in the presence or absence of 10 μ Ci [γ -³²P]ATP per reaction) at 30°C for 15 min. Phosphorylated proteins were separated by SDS-PAGE and analyzed by autoradiography or immunoblot.

Mass Spectrometry

A kinase reaction was performed using recombinant GST-tagged PPAR α and GSK-3 α proteins. Phosphorylated proteins were separated by SDS-PAGE and stained with Coomassie Brilliant Blue. The gel band of interest was excised for in-gel trypsin digestion. The resulting peptides were subjected to LC-MS/MS analysis on an Ultimate 3000 (Dionex, Sunnyvale, CA, USA) LC system coupled with an Orbitrap Velos tandem mass spectrometry instrument (Thermo Fisher Scientific). The MS spectra were acquired in positive mode with a spray voltage of 2 kV and a capillary temperature of 275°C. The Lock Mass feature was used for accurate mass measurement. The automatic gain control (AGC) target was set to 1.0E+6 for full scan in the Orbitrap mass analyzer and 3.0E+4 for MS/MS scans in the ion trap mass analyzer. The precursor was selected within a 2 m/z isolation window and fragmented using collision-induced dissociation (CID) fragmentation. The MS/MS spectra were searched against the Swissprot mouse database with an MS error tolerance of 10 ppm and an MS/MS error tolerance of 0.5 Da. Methionine oxidation, cysteine carbamidomethylation (IAM) and serine/threonine phosphorylation were set as variable modifications. One % false discovery rate (FDR) was used for both protein and peptide identification.

RNA-Seq Library Preparation, Sequencing, and Data Analysis

Total RNA was isolated from H9C2 cells transduced with the indicated plasmid using TRIzol (Invitrogen). Isolated RNA was first checked for integrity on an Agilent Bioanalyzer 2100; samples with RNA integrity number (RIN) >7.0 were used for subsequent processing. Total RNA was subjected to two rounds of poly(A) selection using oligo-d(T)₂₅ magnetic beads (New England Biolabs). A paired-end (strand specific) cDNA library was prepared using the NEB Next Ultra-directional RNA-seq protocol. Briefly, poly(A)⁺ RNA was fragmented by heating at 94°C for 10 min followed by reverse transcription and second strand cDNA synthesis using the reagents provided in the NEB Next kit. End-repaired cDNA was then ligated with double stranded DNA adapters, followed by purification of ligated DNA with AmpureXP beads. cDNA was then amplified by PCR for 15 cycles with a universal forward primer and a reverse primer with bar code. The sequencing of the cDNA libraries was performed on the Illumina HiSeq 2500 platform (Illumina, San Diego, CA) using the single-read 1x50 cycles configuration. The raw reads files have been deposited in the NCBI Gene Expression Omnibus.

CLC Genomics Workbench version 8.5 (<http://www.clcbio.com/products/clc-genomics-workbench/>; Qiagen) was used for RNA-seq analysis. De-multiplexed fastq files from RNA-seq libraries were imported into the CLC software. Adaptor sequences and bases with low quality were trimmed and reads were mapped to a reference genome, *Rattus norvegicus* (assembly Rnor_6.0). Read mapping was carried out with the RNA-Seq Analysis Tool of CLC Genomics Workbench. RPKM values were calculated for each gene to quantify absolute expression. Statistical analysis of differentially expressed genes was carried out with the Empirical analysis of Digital Gene Expression data tool in CLC Genomic Workbench. Functional Pathway analysis of PPAR α -Ser280 phosphorylation-regulated genes (SD vs SA) was performed using IPA pathway analysis software (QIAGEN). Expression patterns of regulated genes were graphically represented in a heat map. Hierarchical clustering was performed to group genes with similar features in the expression profile. The clustering and visualization were carried out using the MultiExperiment Viewer (MeV).

The following publicly available microarray datasets were used: OB/OB (GSE16790), DB/DB (GSE36875), and streptozotocin-induced type I diabetic model (GSE5606). Raw intensity values were normalized using the Robust Multi-array Average (RMA) method on *R*. A *p* value less than 0.05 in the empirical analysis was considered statistically significant. Normalized expression data were also

analyzed with GSEA v2.0.13 software using the JAVA program (Broad Institute, Cambridge, MA). All gene sets were obtained from the Molecular Signatures Database v4.0 distributed on the GSEA Web site.

Quantitative RT-PCR

Total RNA was prepared from mouse hearts and CMs using TRIzol (Invitrogen). cDNA was generated using 300 ng total RNA and SuperScript III Reverse Transcriptase (ThermoFisher). Using Maxima SYBR Green qPCR master mix (Fermentas), real-time RT-PCR was performed under the following conditions: 94°C for 10 min; 40 cycles of 94°C for 15 seconds, 58°C for 30 seconds, 72°C for 30 seconds; and a final elongation at 72°C for 15 min. Relative mRNA expression was determined by the $\Delta\Delta$ -Ct method normalized to the ribosomal RNA (18S) level. Primer sequences are shown in Table S5.

Metabolomics Analysis

Myocardial tissue samples were harvested from heterozygous PPAR α -S280A KI and littermate control mice at the age of 18 to 20 weeks (n=5). Untargeted screening of the metabolome in ventricular tissue was performed using GC/MS at the University of Utah Metabolomics Core Facility. The freeze-clamped tissue samples (~15 mg) were homogenized in the extraction solution (methanol/water (8:1) with amino-acid standards and D4 succinate) using a ceramic bead tube kit (MO BIO Laboratories, Carlsbad, CA) and Bead Ruptor (Omni International, Kennesaw, GA). After incubation for 2 h at -20°C followed by centrifugation at 13,000 at 4°C for 10 min, the extraction samples were dried using a Speed-vac (MiVac Duo, Barnstead/Genevac, Gardiner, NY) overnight and suspended in 40 μ L of 40 mg/mL O-methoxylamine hydrochloride (MOX) in pyridine. GC/MS analysis was performed with a Waters GCT Premier mass spectrometer fitted with an Agilent 6890 gas chromatograph and a Gerstel MPS2 autosampler. A 30 m Phenomenex ZB5-5 MSi column with a 5 m long guard column was employed for chromatographic separation. Data were collected by MassLynx 4.1. Initial analysis of known metabolites was performed using QuanLynx with data transfer to Excel. Peak picking was performed using MarkerLynx with data mining performed using SIMCA-P ver. 12.0.1. The values were normalized by wet tissue weight. Bioinformatic analysis of the metabolomic data was carried out using Metaboanalyst 3.0 software, including the generation of heat maps. Differences in the abundance of individual metabolites were determined using a Student's t test (2 tails, unpaired comparison). A value of $p < 0.05$ was considered statistically significant. Data are given as mean \pm SEM.

Immunoblotting

CM lysates and heart homogenates were prepared in RIPA buffer containing protease and phosphatase inhibitors (Sigma-Aldrich). Lysates were centrifuged at 13,200 r.p.m. at 4°C for 15 min. Total protein lysates (10–30 μ g) were incubated with SDS sample buffer (final concentration: 100 mM Tris pH 6.8, 2% SDS, 5% glycerol, 2.5% 2-mercaptoethanol, and 0.05% bromophenol blue) at 95°C for 5 min. The denatured protein samples were separated by SDS-PAGE, transferred to polyvinylidene difluoride membranes by wet electrotransfer, and probed with primary antibodies.

Subcellular Fractionation

Cultured neonatal rat CMs were washed with PBS and collected with ice-cold PBS, followed by centrifugation at 600g for 5 min. CMs were then resuspended in hypotonic lysis buffer (10 mM K-HEPES pH 7.9, 1.5 mM MgCl₂, 10 mM KCl, 0.1 mM EGTA, 0.1 mM EDTA, 1% IGEPAL, 1% Phosphatase Inhibitor Cocktail, and 1% Protease Inhibitor Cocktail) and were incubated for 15 min on ice with intermittent pipetting. Whole-cell lysates were centrifuged at 1200g for 5 min. The supernatant was collected for the cytosolic fraction, and the pellets were resuspended in lysis buffer (20 mM K-HEPES, 25% Glycerol, 0.45 M NaCl, 1.5 mM MgCl₂, 1 mM EGTA, 1 mM EDTA, 1% Phosphatase Inhibitor Cocktail, and 1% Protease Inhibitor Cocktail) and were incubated for 15 min on ice with intermittent pipetting. The total homogenate was centrifuged at 13,000rpm for 10 min to collect the nuclear fraction. The pelleted nuclei were resuspended in lysis buffer and protein content was determined for all fractions. The nuclear fraction from mouse hearts was prepared with NE-PER Extraction Reagent (Thermo Scientific).

Immunoprecipitation

CMs or heart samples were lysed with lysis buffer containing 50 mM Tris-HCl pH 7.4, 150 mM NaCl, 1% Triton-X 100, 1% Sodium Deoxycholate, Protease Inhibitor Cocktail (Sigma), and Phosphatase Inhibitor Cocktail (Sigma). Primary antibody was covalently immobilized on protein A/G agarose using the Pierce Crosslink Immunoprecipitation Kit according to the manufacturer's instructions (Thermo Scientific). Samples were incubated with immobilized antibody beads for at least 2 hours at 4°C. After immunoprecipitation, the samples were washed with TBS five times. They were then eluted with glycine-HCl (0.1 M, pH 3.5) and the immunoprecipitates were subjected to immunoblotting using specific primary antibodies and a conformation-specific secondary antibody that recognizes only native IgG (Cell Signaling).

Immune Complex *In Vitro* Kinase Assay

The nuclear fraction was obtained as described in the section on subcellular fractionation. GSK-3 α was immunoprecipitated as described in the section on immunoprecipitation. Immunoprecipitated endogenous GSK-3 α protein or recombinant GSK-3 α protein was incubated with recombinant GST- β -catenin or GST alone as a control in kinase buffer as described in the section on *in vitro* kinase assays, then incubated with 5xSDS sample buffer at 95°C for 5 min, followed by SDS-PAGE. Proteins were detected by immunoblot using β -catenin antibody.

In Vitro Binding Assays

Recombinant GST-fused proteins in a slurry of glutathione sepharose were incubated with CM lysates, recombinant GSK-3 α , or recombinant GSK-3 β in lysis buffer containing 50 mM Tris-HCl pH 7.4, 150 mM NaCl, 1% Triton-X 100, 1% Sodium Deoxycholate, Protease Inhibitor Cocktail (Sigma), and Phosphatase Inhibitor Cocktail (Sigma) with rotation for 1 h at 4°C, followed by pull-down with glutathione-sepharose. After washing five times with PBS, proteins were eluted with 5xSDS sample buffer, followed by SDS-PAGE and immunoblots.

Reporter Gene Assay

PPRE reporter gene activity in rat neonatal CMs was measured with a luciferase assay system (Promega). Cardiomyocytes were transfected with 3xPPRE luciferase reporter plasmids (0.2 μ g) overnight (24 well plate) using LipofectAmine 2000 (Invitrogen). The PPRE reporter gene assay was performed after 9 h of palmitic acid treatment. CMs were lysed with 50 μ l Reporter lysis buffer (24 wells each). The luminescence reaction was started by adding 5 μ l lysate to 50 μ l Reaction buffer, and luminescence was measured for 10 seconds using an OPTOCOMP I luminometer (MGM Instruments). The luminescence was normalized by protein content measured by protein assay kit (BioRad). H9C2 cells were transfected in bulk with 7 μ g of total DNA consisting of 6.4 μ g of 3xPPRE-luciferase reporter and 0.6 μ g of PPAR α in a pDC316 vector using FuGene 6 (Roche) at a lipid to DNA ratio of 3:1. Following 18 h of transfection, cells were trypsinized and replated into 96 well plates (Perkin Elmer) and incubated for 4 h at 37°C and 5% CO₂. Palmitic acid and PPAR α ligands were added and the cells were further incubated for 9 h. Luciferase levels were assayed using BriteLite Plus (Perkin Elmer) and read using a multi-label plate reader (Perkin Elmer).

Chromatin Immunoprecipitation (ChIP) Assay

CMs were transduced with Ad-YFP-PPAR α -WT or -mutants or Ad-YFP as a control (10 cm dish). Two days after transduction, CMs were fixed to cross-link protein-DNA complexes for 10 min with 1% formaldehyde in complete medium containing Dulbecco's modified Eagle's medium/F-12 supplemented with 5% horse serum, 4 μ g/mL transferrin, 0.7 ng/mL sodium selenite, 2 g/l bovine serum albumin (fraction V), 3 mM pyruvate, 15 mM Hepes pH 7.1, 100 μ M ascorbate, 100 mg/l ampicillin, 5 mg/l linoleic acid, and 100 μ M 5-bromo-2'-deoxyuridine (Sigma) at room temperature. Cross-linking was stopped by addition of 1 M Glycine to a final concentration of 125 mM for 5 min. CMs were washed twice with ice-cold PBS and the nuclear fraction was collected as described in the section on subcellular fractionation. The nuclear fractions were subjected to ultrasonic treatment with a Diagenode Bioruptor to generate 200- to 1000-bp DNA fragments and were then diluted 10-fold with dilution buffer [16.7 mM Tris-HCl pH 8.1, 1.2 mM EDTA, 0.01% SDS, 1.1% Triton X-100, protease inhibitor cocktail]. After the addition of EDTA to a final concentration of 0.1 mM, the digested sample was centrifuged at 15,000g for 10 min at 4°C and the resulting supernatant was incubated with rotation at 4°C overnight with anti-GFP-YFP conjugated magnetic beads. The immunoprecipitated chromatin was washed five times with low salt buffer [20 mM Tris-HCl, 150 mM NaCl, 2 mM EDTA, 1% Triton X, and 0.1% SDS] and high salt buffer [20 mM Tris-HCl, 500 mM NaCl, 2 mM EDTA, 1% Triton X, and 0.1% SDS], followed by elution with elution buffer [0.1 M NaHCO₃ and 1% SDS]. Protein-DNA cross-links were reversed by incubation overnight at 65°C with 1% SDS in Tris-EDTA buffer, followed by incubation at 45°C for 1 h with proteinase K and RNase A. DNA fragments were purified with a Qiaquick PCR Purification kit (QIAGEN). The DNA was then used as a template for RT-PCR analysis. The PCR primer sequences are listed in [Table S5](#).

In Vitro Oligo Pull-Down Assay

Recombinant Glutathione S-transferase (GST)-fused PPAR α -WT or PPAR α -S280A proteins were purified from the BL21 *E. coli* strain transformed with pCold-GST backbone plasmids. The recombinant proteins were subjected to *in vitro* kinase assays using recombinant GSK-3 α protein, followed by purification with Glutathione-sepharose 4B (GE Healthcare), washing with binding buffer 3 times and resuspension with 150 μ l binding buffer [10 mM Hepes pH 7.9, 2.5 mM MgCl₂, 50 mM KCl, 150 mM NaCl, 5% glycerol, 1 mM DTT, 0.1% IGEPAL CA-630]. The recombinant proteins were incubated with biotin-labeled double-stranded DNAs with streptavidin-beads at 4°C for 2 h. The recovered proteins were washed 3 times and resolved by SDS-PAGE. The sequences of the double-stranded DNAs are listed in [Table S5](#).

Generation of the PPRE/DR1 Sequence Logos

We searched the PPRE/DR1 sequences in the promoters of genes upregulated in PPAR α -S280D- or -S280A-transduced H9C2 cells (SD vs SA, fold change > 1.5 using the RNA-seq data) and in the promoters of fatty acid uptake- or oxidation-related genes using the MEME software (Multiple EM for Motif Elicitation Version 5.0.2, The MEME SUITE). The sequence of the PPRE element containing direct repeats of the AGGTCA half-site separated by one base pair (canonical PPRE/DR1) together with the upstream and downstream three base pairs (nnnAGGTCAAnAGGTCAAnnn) was used as an input motif for matches to the DR1 sequences in the promoters with a threshold of $p < 1.0E-4$. Based on previously published reports, the following genes were assigned for fatty acid uptake/transport or oxidation-related genes in the heart: *Slc27a1*, *Lpl*, *Acs11*, *Cd36*, *Fabp3*, and *Fabp4* for uptake/transport; *Acadvl*, *Acadm*, *Acadl*, *Acads*, *Acadsb*, *Hadha*, *Hadhb*, *Echs1*, and *Hadh* for oxidation. Using the identified sequences, we generated the PPRE/DR1 sequence logos with the MEME software. Finally, we identified rat genes containing each PPRE/DR1 motif in their promoters with a threshold of $p < 1.0E-5$ using MEME. The 5000 bp promoter sequences in the rat genome were obtained using the UCSC

Genome Browser (RGSC 6.0/m6). Genes containing both fatty acid uptake- and oxidation-related motifs were excluded. Genes containing both PPAR α -S280D- and -S280A-related motif were excluded as well. The remaining genes were plotted in a Venn Diagram using Bioinformatics & Evolutionary Genomics website.

Echocardiography

Mice were anesthetized using 12 μ L/g body weight of 2.5% avertin (Sigma-Aldrich), and echocardiography was performed using ultrasound (Vivid 7, GE Healthcare). A 13-MHz linear ultrasound transducer was used. Mice were subjected to 2-dimension guided M-mode measurements of LV internal diameter to measure systolic function and wall thickness, and transmitral inflow Doppler echocardiography in apical 4-chamber view to measure deceleration time of early filling of mitral inflow. Both were taken from at least three beats and averaged. LV ejection fraction was calculated as follows: Ejection fraction = $[(LVEDD)^3 - (LVESD)^3]/(LVEDD)^3 \times 100$. For all mouse experiments, data analysis was conducted in a blinded manner.

Pressure-Volume (PV) Loop Analysis

Mice were anesthetized with pentobarbital (60 mg/kg, intraperitoneal injection) and subjected to PV loop analyses to measure diastolic and systolic cardiac function. The right common carotid artery was surgically isolated and clamped proximally and distally. A small incision (5-10 mm) was made on the carotid artery, and a 1.4-French pressure-conductance catheter (Millar Instruments) was inserted in the vessel and introduced into the left ventricle. The PV relation and hemodynamics were continuously recorded. After stabilization, the end-systolic PV relation and its slope and the end-diastolic PV relation and its slope were obtained by intermittent occlusion of the inferior vena cava.

Metabolic Assay

The oxygen consumption rate (OCR, pmol/min) in cultured CMs was determined using a Seahorse XF24 or XF96 Extracellular Flux Analyzer (Seahorse Bioscience) according to the Installation and Operation Manual from Seahorse Bioscience. CMs were plated at a density of 200,000 cells/well in 24-well Seahorse assay plates or at a density of 50,000 cells/well in 96-well Seahorse assay plates, followed by transduction with Ad-PPAR α -WT or Ad-PPAR α -mutants for 34 h and additional incubation with 500 μ M BSA-conjugated fatty acids for 14 h prior to measurement. One hour prior to the beginning of measurements, the medium was replaced with XF assay medium containing unbuffered DMEM, 5.5 mM glucose, and 0.5 mM carnitine, and CMs were incubated for 1 h in a 37°C incubator without CO₂. Etomoxir (100 μ M), a specific Cpt-1 inhibitor, was added to assess the degree of FAO (Kim et al., 2013).

Adult CMs Isolation and Metabolic Assay

Adult CMs were isolated as described previously with a modification (Ackers-Johnson et al., 2016). Briefly, the heart of a male mouse was perfused with 12 mL EDTA buffer [130 mM NaCl, 5 mM KCl, 0.5 mM NaH₂PO₄, 10 mM HEPES, 10 mM Glucose, 10 mM BDM, 10 mM Taurine, 5 mM EDTA] to stop the beating of the heart. Digestion was achieved using 30 mL perfusion buffer [130 mM NaCl, 5 mM KCl, 0.5 mM NaH₂PO₄, 10 mM HEPES, 10 mM Glucose, 10 mM BDM, 10 mM Taurine, 1 mM MgCl₂] containing Collagenase type II (0.5mg/mL) and Protease XIV (0.05mg/mL). Cellular dissociation was stopped by addition of 5 mL Perfusion buffer containing 5% FBS and 500 μ M BSA-conjugated fatty acid cocktail (palmitic acid: oleic acid: linoleic acid = 2:1:1 and BSA: fatty acid = 1:5). CMs and non-CMs were separated by 4 sequential rounds of gravity settling with calcium reintroduction medium containing 500 μ M BSA-conjugated fatty acid cocktail. Adult CMs were plated at a density of 200 cells/well in 96-well Seahorse assay plates with XF assay medium, containing 5.5 mM glucose, 500 μ M BSA-conjugated fatty acid cocktail, 10 mM BDM and 0.5 mM carnitine. Adult CMs were incubated in a 37°C incubator with CO₂ for 30 min and without CO₂ for 30 min prior to measurement. The FAO rate was determined by Etomoxir (250 μ M)-inhibitable OCR using a Seahorse XF96 Extracellular Flux Analyzer (Seahorse Bioscience).

Fatty Acid Oxidation

Fatty acid β -oxidation was measured using heart homogenates as described previously (Watanabe et al., 2000). The left ventricle (LV) of a fresh heart was washed with PBS, weighed and homogenized in four volumes of homogenate buffer [0.25 M Sucrose, 1 mM EDTA] per LV weight (mg). Forty μ L of the heart homogenate was dispensed per tube and centrifuged at 800g for 1.5 min and the precipitates were incubated with 200 μ L of Reaction buffer [10 mM Hepes pH 7.4, 150 mM KCl, 0.1 mM EDTA, 1 mM K₂HPO₄, 10 mM MgCl₂, 1 mM Malate, 10 mM Glucose, 1 μ Ci [9,10-³H] palmitic acid and 50 μ M of unlabeled palmitic acid, both bound to BSA at the molecular ratio of 1:3.7 (BSA : fatty acid)] at 37°C for 10 min. The reaction was stopped by the addition of 1 mL chloroform/methanol (2:1) and the samples were mixed well. The samples were kept at -20°C for 4 h and centrifuged at 12,000g at room temperature for 10 min. The supernatants containing ³H₂O were mixed with 4 ml scintillation fluid and the radioactivity was measured with a scintillation counter.

Fatty Acid Uptake In Vitro

Rat neonatal CMs were transduced with adenovirus harboring PPAR α -WT, PPAR α -S280A, PPAR α -S280D or YFP alone. Two days after transduction, CMs were incubated in CM culture medium containing 500 μ M unlabeled BSA-conjugated palmitic acid or 500 μ M

unlabeled BSA-conjugated fatty acid cocktail (palmitic acid, oleic acid, and linoleic acid (2:1:1 ratio)) with 1 μ Ci/mL of [9,10-³H(N)]-palmitic acid alone or 1 μ Ci/mL of combined [9,10-³H(N)]-palmitic acid and [9,10-³H(N)]-oleic acid and 1.25% BSA for 10 min (Liu et al., 2011). After washing CMs with ice-cold PBS four times, CMs were harvested with trypsin-EDTA and centrifuged at 800g at room temperature for 3 min. The pellet was resuspended with 1 mL PBS and centrifuged at 800g at room temperature for 3 min again. CMs were lysed with 1 mL of 0.5 M NaOH and neutralized with 6 M HCl. The radioactivity was measured with a scintillation counter.

Palmitate Uptake into the Heart *In Vivo*

In vivo palmitic acid uptake was measured as previously described with modifications (Khan et al., 2013). Palmitic acid [9, 10-³H(N)]-5 mCi (PerkinElmer, NET043005MC) was complexed with 6% BSA at 37°C. Male GSK-3 α S21A KI and control mice were fasted for 2 h and were intravenously administered the labeled BSA-conjugated palmitic acid and 400 μ M of unlabeled BSA-conjugated palmitic acid via the femoral vein with $\sim 10^6$ counts and euthanized 5 min post-injection. Blood samples collected 2 min after the injection were used for normalization. The heart was quickly washed with PBS to remove the blood from the ventricles and weighed. The heart was lysed with 1 mL of 0.5 M NaOH and neutralized with 6 M HCl. Radioactivity was determined in 20 μ L of blood and a whole heart on an LS 6500 multipurpose scintillation counter (Beckman-Coulter). Palmitic acid uptake into the heart was normalized by the radioactivity of the blood and the heart weight.

Oil Red O Staining

Neonatal CMs were cultured on coverslips and fixed in 4% paraformaldehyde. The left ventricle of the heart was frozen with O.C.T. compound and Cryomold Biopsy (Tissue-Tek). The heart tissue was cut into 10 μ m thick sections on a glass slide. Frozen sections were air-dried for 10 min at room temperature and fixed with 10% formalin for 5 min. After washing with PBS, the sections were dipped into 60% isopropyl alcohol three times and then put into Oil Red O working solution [0.5% Oil Red O (Sigma) dissolved in isopropyl alcohol (W/V)] for 15 min. The sections were washed with 60% isopropyl alcohol three times and then water for 30 min. Cover glasses were mounted with mounting medium. Images were obtained in a blinded manner and analyzed with ImageJ software (NIH).

Immunohistochemistry

The heart tissue was washed with PBS, fixed in 4% paraformaldehyde overnight, embedded in paraffin, and sectioned at 10- μ m thickness onto a glass slide. After de-paraffinization, sections were stained with Picric acid sirius red (PASR) or Periodic acid-Schiff for evaluation of fibrosis or glycogen accumulation, respectively. Images were obtained in a blinded manner. The cross-sectional area of CMs was measured after wheat germ agglutinin (WGA) staining using ImageJ software (NIH).

Immunofluorescence Staining

Rat neonatal CMs were cultured on coverslips, transduced with adenoviruses for 2 to 4 days, washed with PBS, and fixed in 4% paraformaldehyde for 10 min. Samples were permeabilized with PBST (0.5% Triton-X in PBS) for 15 min and blocked in 5% BSA, 5% goat serum in PBST for 30 min at 37°C. Samples were incubated with specific antibodies at 4°C overnight, washed, and incubated with secondary antibody conjugated with Alexa Fluor 488, 555, or 594 dye (Life Technologies). Samples were washed with PBS and mounted on glass slides with mounting medium containing DAPI to stain nuclei (VECTASHIELD, Vector Laboratories). Cells were observed under a fluorescence microscope. Images were obtained in an unblinded manner.

Proximity Ligation Assay

The interaction between GSK-3 α and PPAR α was examined *in situ* using Duolink. Rat neonatal CMs were transduced with adenovirus harboring YFP-PPAR α , followed by incubation with 100 μ M or 500 μ M of BSA-conjugated palmitic acid in the presence or absence of fenofibrate. After fixation, slides were incubated for 10 min at 95°C in antigen retrieval buffer (100 mM Tris, 5% urea, pH 9.5). Slides were then blocked for 4 h at 4°C with PBS containing 5% normal goat serum. Anti-GSK-3 α and anti-GFP-YFP primary antibodies were added (diluted 1:100 in blocking buffer) and slides were incubated in a humidity chamber overnight at 4°C. Slides were further blocked at 37°C in Duolink blocking buffer for 1 h in a humidity chamber. Slides were then washed in Duolink Wash Buffer A twice at room temperature. PLA PLUS Anti-mouse and PLA MINUS Anti-rabbit probes were then incubated with slides in a pre-heated humidity chamber for 1 h at 37°C. After washing in Wash Buffer A twice for 5 min, slides were incubated with Duolink Ligation Stock for 30 min at 37°C. After that, slides were washed in Wash Buffer A and incubated with Duolink Polymerase in Duolink Amplification Stock for 100 min at 37°C. After two washes with Wash Buffer B, slides were mounted with Duolink Mounting Medium with DAPI. Images were obtained in an unblinded manner.

QUANTIFICATION AND STATISTICAL ANALYSIS

All values for continuous data are expressed as mean \pm SEM. Statistical analyses were carried out by two-tailed unpaired Student's t test for 2 groups or one-way ANOVA followed by the Newman-Keuls post-hoc analysis for 3 groups or more, assuming independent variables, normal distribution, and equal variance of samples. Categorical variables were compared using Fisher's exact test.

A *p* value of less than 0.05 was considered significant. Statistical parameters can be found in the figure legends. Statistical analyses were performed using GraphPad Prism (GraphPad Software).

DATA AND SOFTWARE AVAILABILITY

The RNA sequencing data on H9C2 cell lines transduced with PPAR α mutants have been deposited in NCBI's Gene Expression Omnibus and are accessible through GEO Series accession number GSE112309. The microarray data on the hearts of GSK-3 α and GSK-3 β KI mice have been deposited in NCBI's Gene Expression Omnibus and are accessible through GEO Series accession number GSE112160.

Cell Metabolism, Volume 29

Supplemental Information

Glycogen Synthase Kinase-3 α Promotes

Fatty Acid Uptake and Lipotoxic Cardiomyopathy

Michinari Nakamura, Tong Liu, Seema Husain, Peiyong Zhai, Junco S. Warren, Chiao-Po Hsu, Takahisa Matsuda, Christopher J. Phiel, James E. Cox, Bin Tian, Hong Li, and Junichi Sadoshima

Figure S1. Knockdown of GSK-3 α attenuates high-fat diet (HFD)-induced lipotoxic cardiomyopathy, Related to Figure 1.

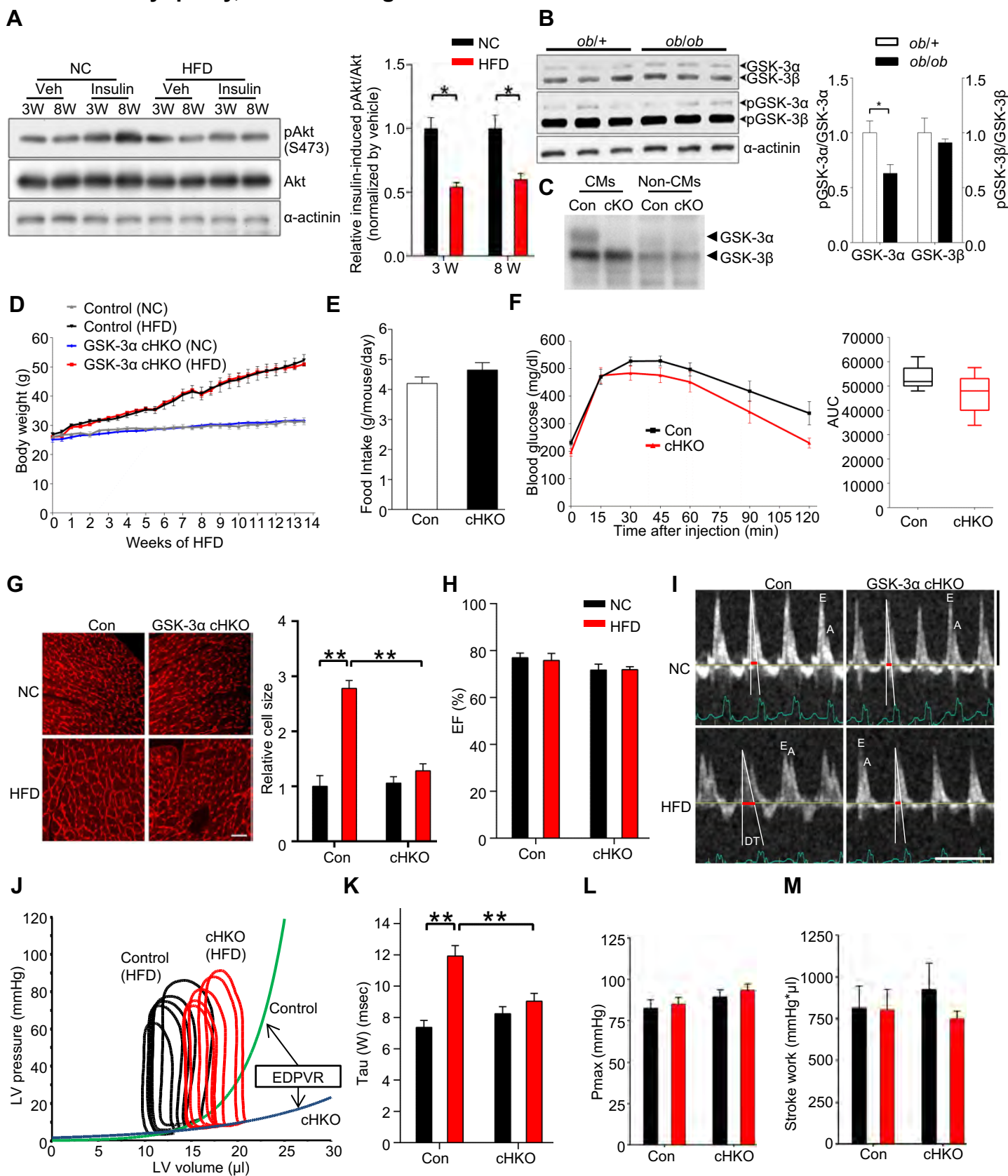


Figure S1. Knockdown of GSK-3 α attenuates high-fat diet (HFD)-induced lipotoxic cardiomyopathy, Related to Figure 1. (A) Immunoblots examining insulin resistance in the hearts of mice fed a HFD or normal chow (NC) for the indicated periods, as shown by insulin-stimulated phosphorylation of Akt (Ser473) (0.75 U/kg body weight, i.p.) (left). Quantification of insulin-induced pAkt normalized by Akt (n = 4) (right). (B) Immunoblots examining activities of GSK-3 α/β in the hearts of *ob/+* and *ob/ob* mice (left). Histograms show the ratios of phosphorylated versus total GSK-3 α/β (n = 6) (right). (C) Immunoblots showing the expression of GSK-3 α/β in cardiomyocytes (CMs) and non-myocytes (non-CMs) isolated from the hearts of GSK-3 α cardiac-specific homozygous knockout (cKO) or control homozygous floxed (Con) mice. (D to M) GSK-3 α cardiac-specific heterozygous knockout (cHKO) mice and heterozygous floxed (control) mice were fed a HFD or NC for 14 weeks. (D) Body weight growth curves (n = 5-7). (E) Food intake in mice fed a HFD (n = 10-12). (F) Intraperitoneal glucose tolerance test in HFD-fed control and GSK-3 α cHKO mice (left) and area under curve (n = 6) (right). (G) Wheat germ agglutinin staining of left ventricular (LV) cardiomyocyte cross sections. Scale bar, 100 μ m. Histograms show relative cardiomyocyte size, a marker of individual cardiomyocyte hypertrophy (n = 8) (right). (H) Echocardiographic analyses showing LV ejection fraction (EF, %) (n = 8 -15). (I) Representative images of transmitral flow obtained by Doppler echocardiography. Deceleration time (DT) is indicated by red bars. Transverse scale bar, 100 cm/s. Vertical scale bar, 100 ms. (J) Representative pressure-volume (PV) loop plots. Exponential curves show end-diastolic PV relation (EDPVR). (K to L) Tau, a marker of diastolic dysfunction (K), LV maximum pressure (L), and Stroke work (M), obtained by PV loop analysis (n = 5 for NC and n = 9 for HFD). Error bars indicate s.e.m. * $p < 0.05$, ** $p < 0.001$.

Figure S2. Knockdown of GSK-3 β exacerbates high-fat diet (HFD)-induced lipotoxic cardiomyopathy, Related to Figure 1.

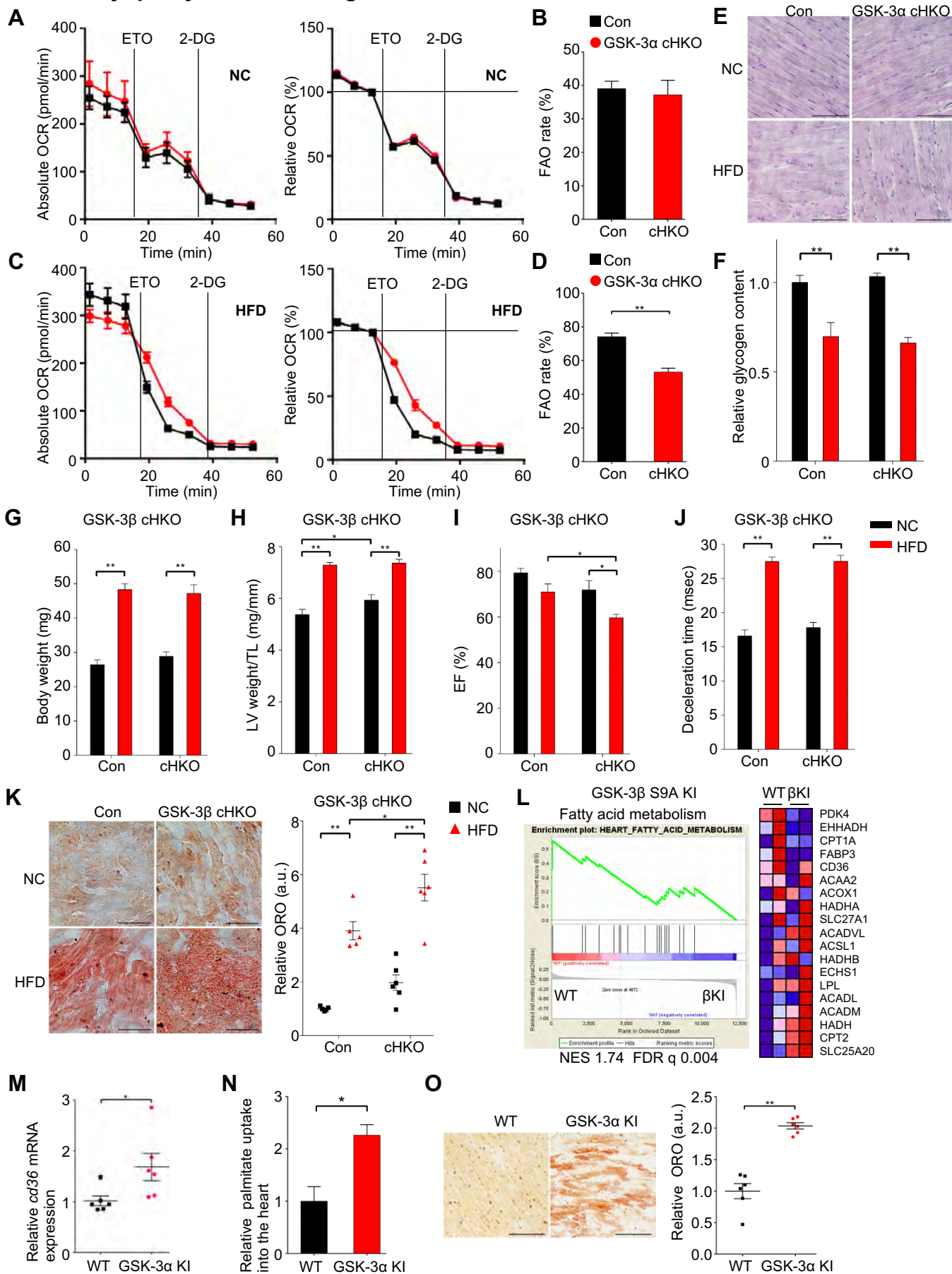


Figure S2. Knockdown of GSK-3 β exacerbates high-fat diet (HFD)-induced lipotoxic cardiomyopathy, Related to Figure 1. (A to D) Representative absolute and relative oxygen consumption rate (OCR) in CMs isolated from the hearts of GSK-3 α cHKO and control mice fed a HFD or normal chow (NC), measured by a Seahorse analyzer in the presence of 500 μ M of BSA-fatty acid cocktail (n = 3-4, A and C). Fatty acid oxidation (FAO) rate was evaluated by etomoxir (ETO)-inhibitable OCR. Histograms show FAO rate (the ratio of FAO versus OCR) (n = 4 (B, NC) and n = 8 (D, HFD)). (E and F) Representative Periodic acid-Schiff staining (E) and quantification of relative glycogen accumulation in the hearts of GSK-3 α cHKO and control mice fed a HFD or NC (n = 6) (F). Scale bar, 50 μ m. (G to K) GSK-3 β cardiac-specific heterozygous knockout (GSK-3 β cHKO) mice and heterozygous floxed (control) mice were fed a HFD or NC for 14 weeks. (G) Body weight after 14 weeks of the indicated diet (n = 5-6). (H) Left ventricular (LV) weight normalized by tibia length (TL), a marker of cardiac hypertrophy (n = 5-6). (I) Ejection fraction (EF), a marker of systolic function, obtained by M-mode echocardiography (n = 5-6). (J) Deceleration time, a marker of diastolic function, obtained by transmitral flow Doppler echocardiography (n = 5-6). (K) Representative Oil Red O staining of the indicated mouse heart sections (left), a marker of lipid accumulation. Scale bar, 25 μ m. Quantification of relative myocardial lipid accumulation (n = 5-6) (right). (L) Custom gene-set analysis representing enrichment of cardiac fatty acid metabolism in GSK-3 β Ser9Ala homozygous knock-in (KI) mouse hearts compared to wild-type (WT) mice at 3 months of age. (M to O) Fatty acid uptake and lipid accumulation were examined in the hearts of GSK-3 α S21A homozygous knockin (KI) and control wild-type (WT) mice fed NC (3 months of age). Relative *CD36* mRNA expression in the hearts (n = 6) (M), BSA-conjugated ³H-palmitate uptake into the hearts (n = 6) (N), and representative Oil Red O staining of the heart sections (left) and quantification of myocardial lipid accumulation (n = 6) (right). Scale bar, 50 μ m (O). Error bars indicate s.e.m. * $p < 0.05$, ** $p < 0.001$.

Figure S3. GSK-3 α , but not GSK-3 β , physically interacts with PPAR α , Related to Figure 2.

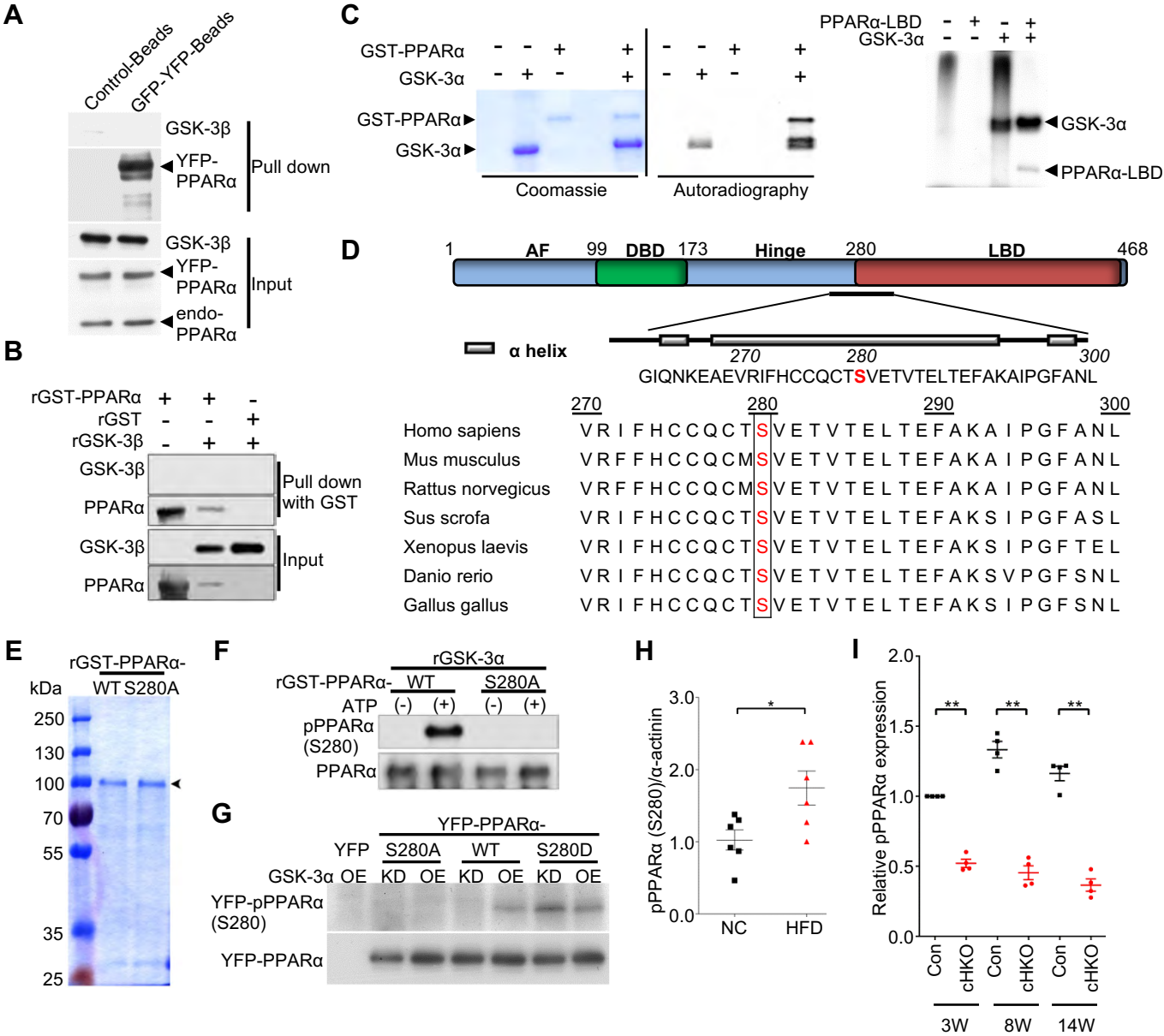


Figure S3. GSK-3 α , but not GSK-3 β , physically interacts with PPAR α , Related to Figure 2.

(A) Immunoprecipitation assays examining the interaction between endogenous GSK-3 β and YFP-tagged PPAR α in cardiomyocytes (CMs). Forty-eight hours after transduction with Ad-YFP-PPAR α , lysates were extracted for immunoprecipitation with anti-GFP-YFP antibody-conjugated or control beads, followed by immunoblotting with anti-GSK-3 β antibody. (B) *In vitro* binding assays examining direct interaction between recombinant (r) GSK-3 β and rGST-PPAR α . (C) *In vitro* kinase assays to test the ability of rGSK-3 α to phosphorylate rGST-PPAR α or rGST alone as a control (left). *In vitro* kinase assays to test the ability of rGSK-3 α to phosphorylate commercially available truncated rPPAR α protein, including the ligand binding domain (amino acids 170-430) (right). (D) Conservation of the PPAR α Ser280 phosphorylation site across species. (E) Coomassie Brilliant Blue staining of the rGST-PPAR α -wild type (WT) protein and phospho-resistant rPPAR α mutant protein with an alanine mutation of the Ser280 residue (rGST-PPAR α -S280A). (F) Immunoblots testing the sensitivity and specificity of the antibody against Ser280-phosphorylated PPAR α . An *in vitro* kinase assay was performed with active rGSK-3 α and rGST-PPAR α -WT or rGST-PPAR α -S280A mutant protein, followed by probing with the antibody against PPAR α -Ser280 phosphorylation. (G) Immunoblots showing Ser280 phosphorylation of PPAR α in CMs transduced with PPAR α -S280A, -WT, or -S280D or YFP alone as a control in the presence of adenovirus-mediated GSK-3 α overexpression (OE) or knockdown (KD) with palmitic acid treatment. (H) Histogram showing the ratio of Ser280-phosphorylated PPAR α versus α -actinin (n = 6). (I) Histogram showing relative expression of Ser280-phosphorylated PPAR α versus Histone H3 (n = 4). Error bars indicate s.e.m. * $p < 0.05$.

Figure S4. GSK-3 α -mediated Ser280 phosphorylation enhances PPAR α activity, Related to Figure 3.

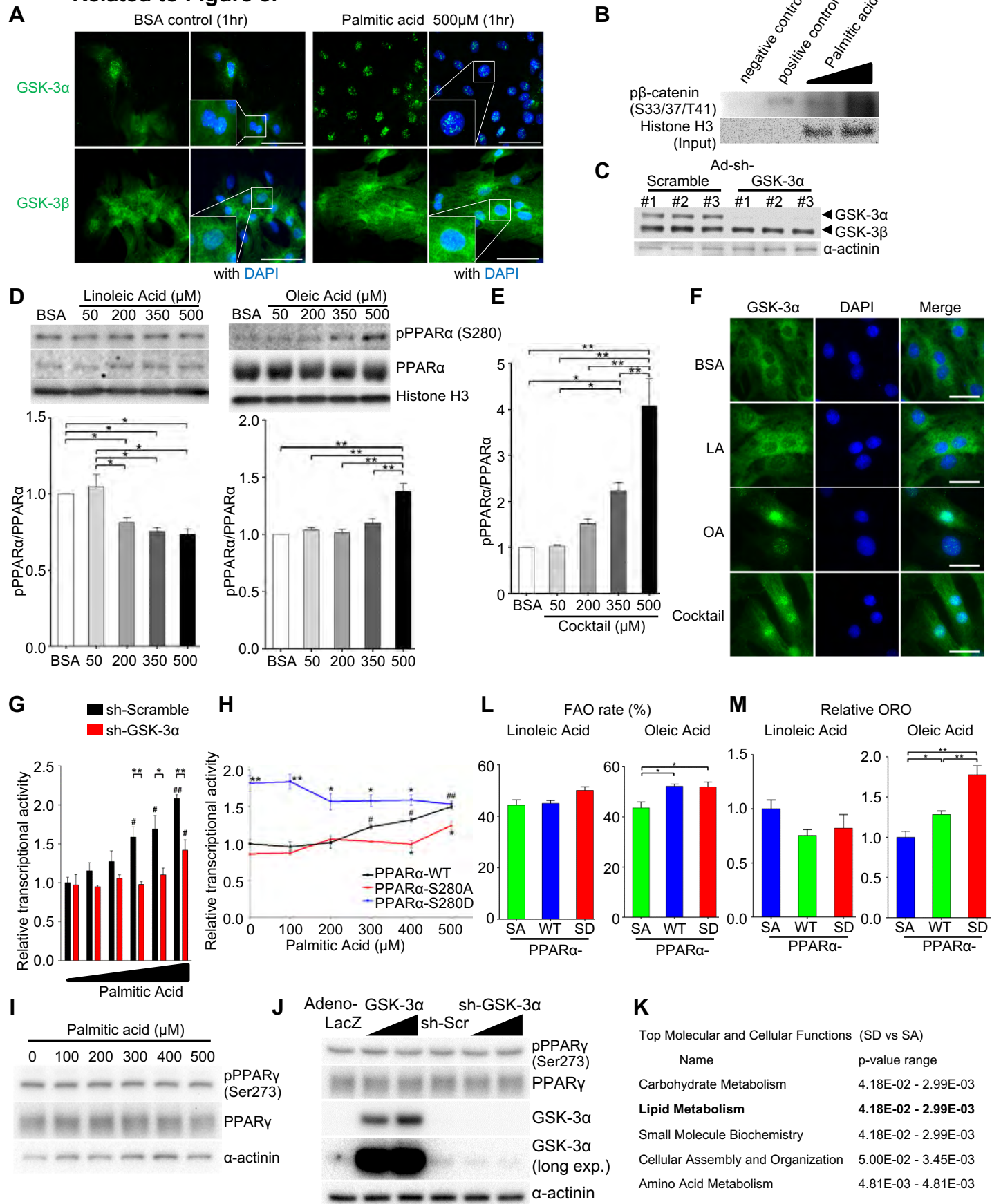


Figure S4. GSK-3 α -mediated Ser280 phosphorylation enhances PPAR α activity, Related to Figure 3. (A) Immunofluorescence staining for GSK-3 α (green, upper) or GSK-3 β (green, lower) and DAPI (blue) in primary cultured rat neonatal cardiomyocytes (CMs) treated with 500 μ M of BSA-conjugated palmitic acid (PA) or BSA control for 1 hour. Images are representative of three independent experiments. Scale bar, 50 μ m. (B) Immune complex *in vitro* kinase assays to examine nuclear GSK-3 α activity in CMs treated with PA. GSK-3 α was immunoprecipitated from the nuclear fraction of cultured CMs, followed by *in vitro* kinase assays with recombinant GST- β -catenin. Positive and negative control experiments were performed in the presence and absence of recombinant active GSK-3 α instead of CM lysate, respectively. (C) Immunoblots testing the efficiency of knockdown of GSK-3 α with adenovirus harboring shRNA-GSK-3 α or shRNA-scramble as a control, using anti-GSK-3 α/β antibody. (D and E) Immunoblots showing the expression of pPPAR α (Ser280) in the nucleus of CMs treated with BSA-linoleic acid (left) or BSA-oleic acid for 9 hours (right) and quantification analyses (n = 4) (D). Histogram showing the ratio of Ser280-phosphorylated PPAR α versus total PPAR α in the nucleus of CMs treated with BSA-fatty acid cocktail (n = 4) (E). (F) Immunofluorescence staining for GSK-3 α (green) and DAPI (blue) in CMs treated with 500 μ M of indicated BSA-conjugated fatty acid or BSA control for 1 hour. Images are representative of three independent experiments. Scale bar, 25 μ m. (G) The effect of GSK-3 α on the PA-induced increase in PPRE-luciferase reporter activity in CMs in the presence or absence of GSK-3 α knockdown (n = 8). # $p < 0.05$ and ## $p < 0.001$ compared to control (PA 0 μ M). (H) The effect of BSA-PA on PPRE-luciferase reporter activity in H9C2 cells transduced with PPAR α -WT, PPAR α -S280D or PPAR α -S280A mutant allele. YFP alone was used for background extraction (n = 4). * $p < 0.05$, ** $p < 0.001$ compared to PPAR α -WT. # $p < 0.05$, ## $p < 0.001$ compared to 0 μ M of PA in H9C2 cells with PPAR α -WT. One-way ANOVA Newman-Keuls post-hoc analysis. (I and J) Immunoblots showing the effect of PA (I) and GSK-3 α activity (J) on the phosphorylation of PPAR γ at Ser273 in CMs. (K) Ingenuity pathway analysis showing top 5 molecular and cellular functions in the PPAR α -SD versus the PPAR α -SA mutant. Gene expression was determined by RNA-seq data. (L) FAO rate in CMs treated with 500 μ M of BSA-linoleic acid (left) or BSA-oleic acid (right), measured by 96-well Seahorse analyzer (n = 7-8). (M) Relative lipid accumulation in CMs treated with 500 μ M of BSA-linoleic acid (left) or BSA-oleic acid (right) (n = 6). Error bars indicate s.e.m. * $p < 0.05$, ** $p < 0.001$.

Figure S5. PPAR α activity is increased by GSK-3 α -mediated Ser280-phosphorylation, Related to Figure 4.

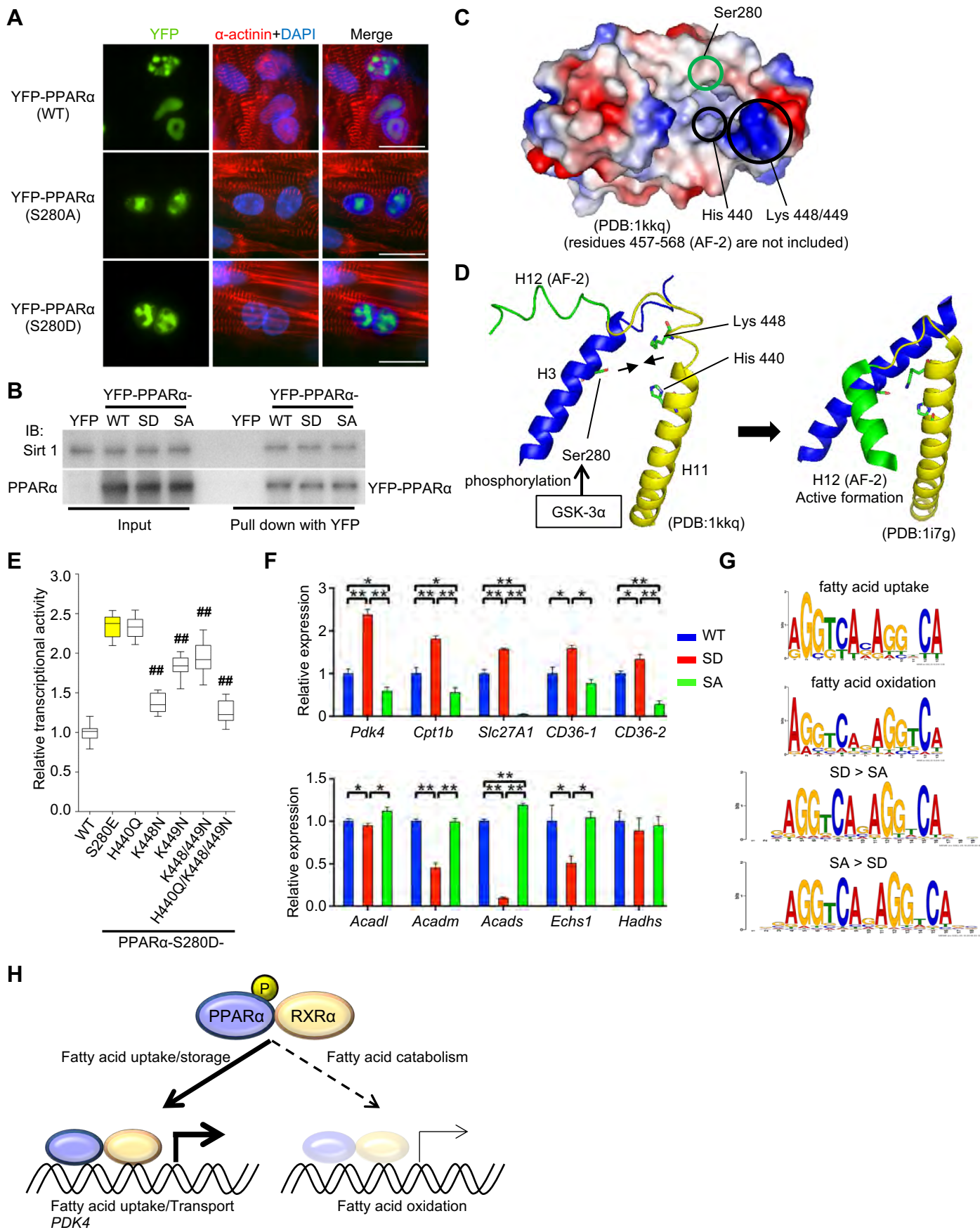


Figure S5. PPAR α activity is increased by GSK-3 α -mediated Ser280-phosphorylation, Related to Figure 4. (A) Immunofluorescence staining in cardiomyocytes (CMs) transduced with Ad-YFP-PPAR α -WT, -S280A or -S280D mutant for DAPI (blue) and α -sarcomeric actinin (red). Scale bar, 20 μ m. (B) Immunoprecipitation assays examining the interaction between Sirt1 and YFP-PPAR α -WT, -S280D, -S280A or YFP alone as a control in CMs. The data shown are representative of three independent experiments. (C) The surface of the PPAR α ligand binding domain (PDB: 1kkq), excluding residues 457-568. Red represents a negative charge and blue represents a positive charge. (D) A ribbon drawing of PPAR α helices 3, 11 and 12 (AF-2) (PDB: 1kkq and 1i7g). (E) PPRE-luciferase reporter activity in H9C2 cells transduced with PPAR α -WT, PPAR α -H440Q/K448N/K449N, PPAR α -S280E or PPAR α -S280D-H440Q/K448N/K449N mutant. YFP alone was used for background extraction (n = 12). ## $p < 0.001$ compared to PPAR α -S280E. (F) Quantification analyses of the ChIP assay normalized by the input level (n = 4). * $p < 0.05$, ** $p < 0.001$. (G) PPRE/DR1 (PPAR α -RXR α complex) sequence logos generated by the canonical PPRE/DR1 sequences enriched in the promoters of the genes related to fatty acid uptake or oxidation or the genes upregulated in PPAR α -S280D or PPAR α -S280A. (H) Schematic representation. S280-phosphorylated PPAR α preferentially binds to the promoters of genes for fatty acid uptake and *PDK4*, but not mitochondrial β -oxidation, thereby stimulating fatty acid uptake/storage. Error bars indicate s.e.m.

Figure S6. The development of lipotoxic cardiomyopathy is mediated by PPAR α -Ser280 phosphorylation, Related to Figure 5.

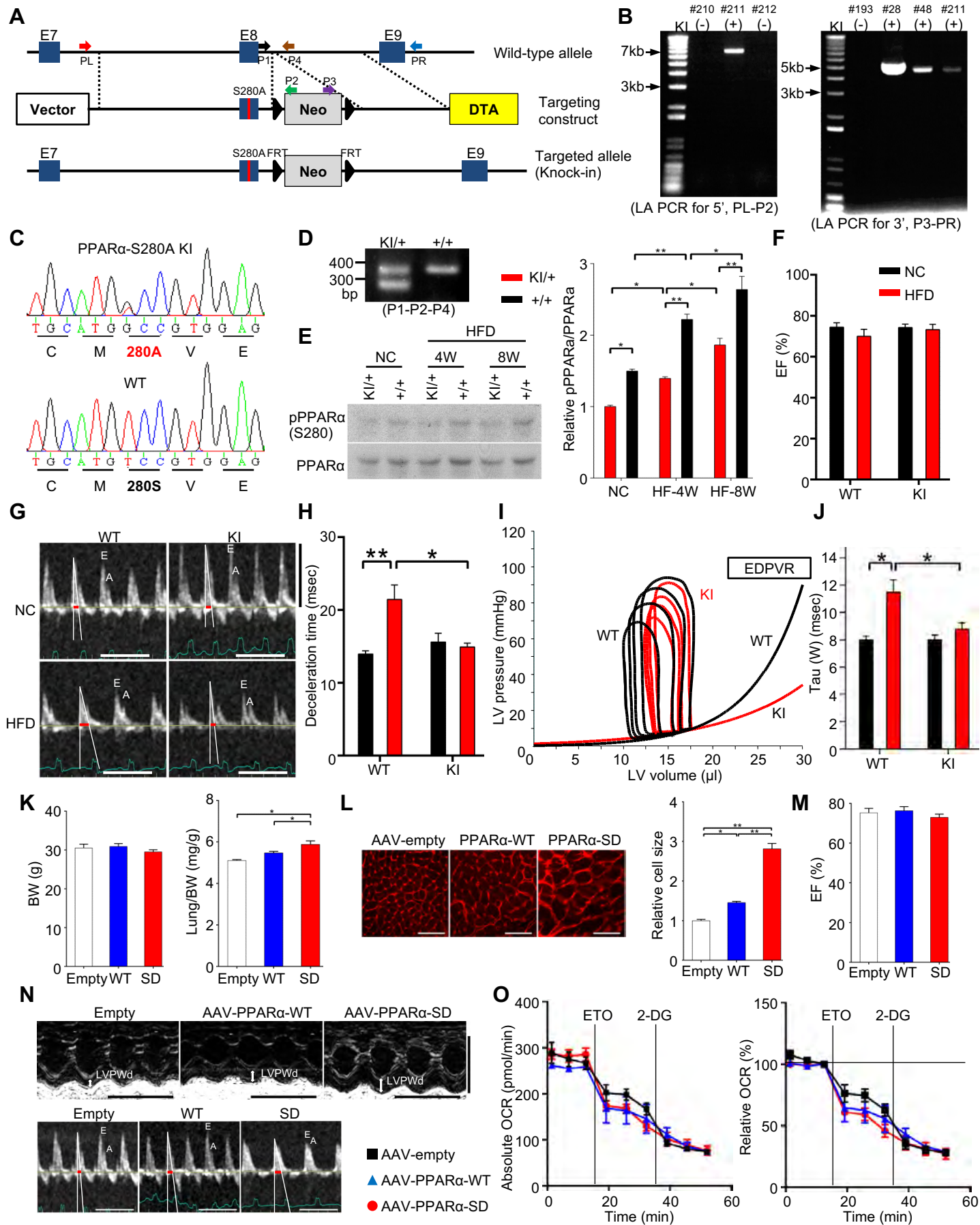


Figure S6. The development of lipotoxic cardiomyopathy is mediated by PPAR α -Ser280 phosphorylation, Related to Figure 5. (A) Schematic diagram of PPAR α -Ser280Ala knock-in (KI) gene targeting. The PPAR α genomic region of interest, the targeting construct, and the mutated Ser280Ala locus after homologous recombination are shown. P, PL and PR denote a primer, left primer, and right primer, used in (B) and (D). (B) DNA isolated from Neo-resistant ES clones was assessed by long range (LA) PCR for wild-type (WT) and heterozygous (het) alleles with the primers shown in (A). Positive ES clones identified by 5' LA-PCR were then verified by 3' LA-PCR. (C) Incorporation of Ser280Ala mutation into KI mice was verified by PCR and sequencing analyses using tail DNA. (D) PCR using tail DNA isolated from WT and heterozygous KI mice. Locations of the primers are shown in (A). (E to J) WT and S280A het KI mice were fed a high-fat diet (HFD) or normal chow (NC) for up to 8 weeks. (E) Immunoblots examining PPAR α -Ser280 phosphorylation in the heart (left). NC data was obtained from heart samples isolated from mice fed NC for 8 weeks. Quantification analyses of pPPAR α (Ser280) normalized by total PPAR α (n = 4) (right). (F) Echocardiographic analyses showing left ventricular (LV) ejection fraction (EF, %) (n = 6-7). (G) Representative images of transmitral flow obtained by Doppler echocardiography. Deceleration time is indicated by a red bar. Transverse scale bar, 100 cm/s. Vertical scale bar, 100 ms. (H) Deceleration time, evaluated by transmitral flow Doppler echocardiography (n = 6-7). (I) Representative pressure-volume (PV) loop plot for the indicated mice fed a HFD. Exponential curves show end-diastolic PV relation (EDPVR). (J) Tau, a marker of diastolic function, obtained by PV loop analysis (n = 5-8). (K to O) Either PPAR α -WT or PPAR α -S280D mutant was expressed in WT mouse hearts (C57BL/6J background) by adeno-associated virus (AAV)-mediated gene delivery and the mice were fed NC for 8 weeks. AAV-empty injection (Empty) was performed as a control. (K) Body weight (BW) (g) 8 weeks after AAV injections (left). Lung weight normalized by BW, a marker of congestive heart failure (n = 5-7) (right). (L) Wheat germ agglutinin staining of LV cardiomyocyte cross sections (left). Scale bar, 50 μ m. Histograms show relative cardiomyocyte size, a marker of individual cardiomyocyte hypertrophy (n = 4-6) (right). (M) LV ejection fraction (EF, %), evaluated by echocardiography (n = 5-6). (N) Representative images of M-mode echocardiogram (upper) and transmitral flow obtained by Doppler echocardiography (lower). Deceleration time is indicated by a red bar. (M-mode) Transverse scale bar, 100 ms. Vertical scale bar, 5 mm. (Doppler) Transverse scale bar, 100 cm/s. Vertical scale bar, 100 ms. (O) Representative absolute and relative oxygen consumption rate (OCR) of adult cardiomyocytes isolated from the hearts of mice transduced with the indicated AAV, measured by a 96-well Seahorse analyzer in the presence of 500 μ M of BSA-conjugated fatty acid cocktail (n = 3-4). Error bars indicate s.e.m. * $p < 0.05$, ** $p < 0.001$.

Figure S7. PPAR α ligands inhibit GSK-3 α -mediated PPAR α phosphorylation and ameliorate high-fat diet (HFD)-induced cardiac dysfunction, Related to Figure 6.

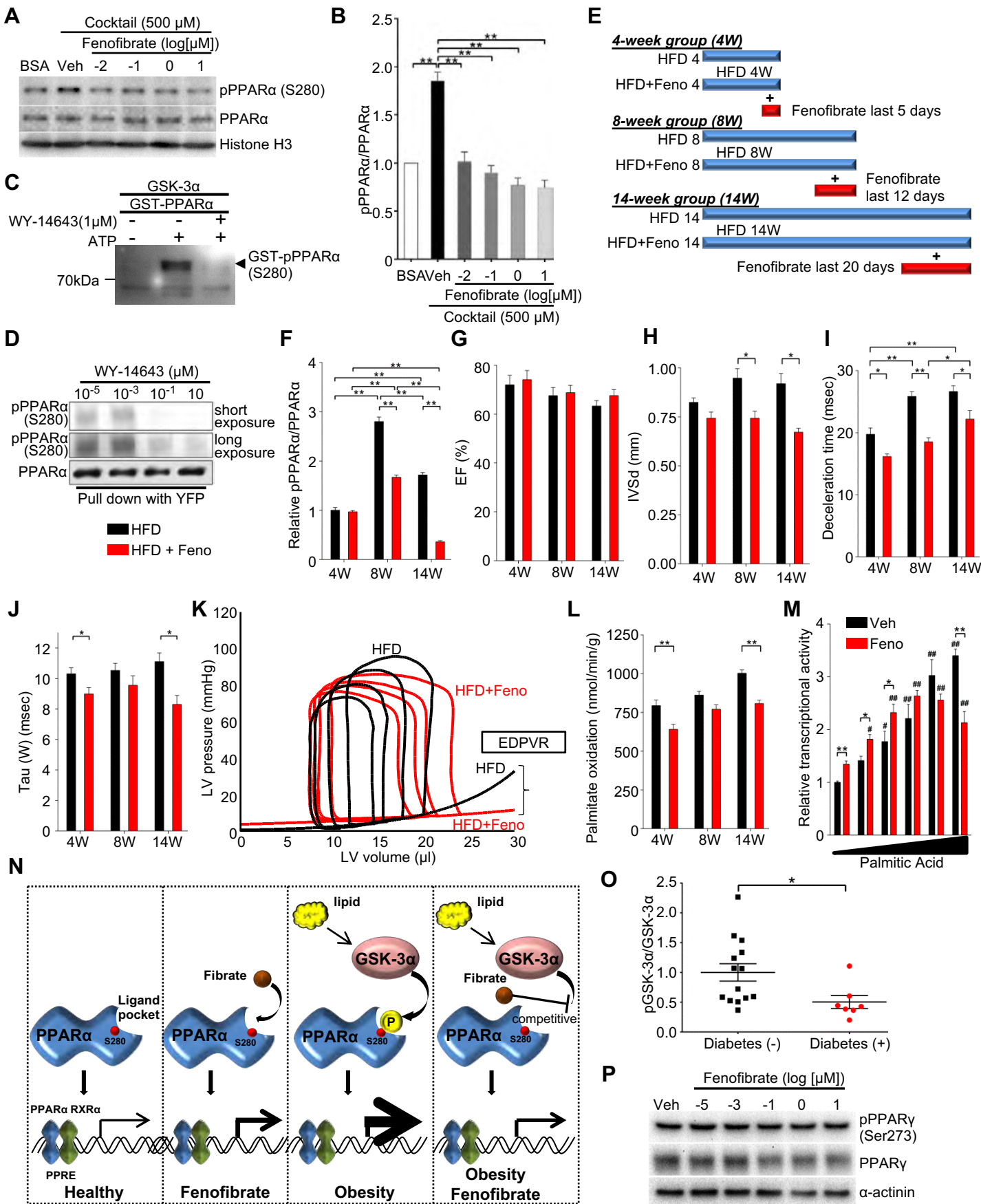


Figure S7. PPAR α ligands inhibit GSK-3 α -mediated PPAR α phosphorylation and ameliorate high-fat diet (HFD)-induced cardiac dysfunction, Related to Figure 6. (A and B) Immunoblots examining the effect of fenofibrate, a PPAR α ligand, on PPAR α -Ser280 phosphorylation in the nucleus of cardiomyocytes (CMs) in the presence of 500 μ M of BSA-fatty acid cocktail (A) and quantification analyses (n = 4) (B). (C) *In vitro* kinase assay using recombinant (r) GSK-3 α and rGST-PPAR α in the presence or absence of WY-14643 (1 μ M), a PPAR α ligand, followed by probing for Ser280-phosphorylated PPAR α . (D) The effect of WY-14643 on PPAR α -Ser280 phosphorylation in CMs. CMs were transduced with Ad-YFP-PPAR α and cultured with the indicated concentration of WY-14643, followed by immunoprecipitation with an anti-GFP-YFP antibody and probing for pPPAR α (Ser280). (E to L) Wild-type (WT) mice were fed a HFD in the presence or absence of fenofibrate for the indicated periods. (E) Schematic representation of HFD experiments with or without fenofibrate (Feno) for the indicated periods. (F) Quantification of the effect of fenofibrate on Ser280 phosphorylation of PPAR α shown in Figure 6B (n = 3). (G and H) Echocardiographic analyses of cardiac morphology and function. Ejection fraction (G, EF, %) and interventricular septal thickness at diastole (H, IVSd, mm) (n = 8-12). (I) Deceleration time, a marker of diastolic function, evaluated by transmitral flow Doppler echocardiography (n = 8-12). (J) Pressure-volume (PV) loop analyses to test diastolic function, as indicated by tau (n = 8-12). (K) Representative images showing PV loop. Exponential curves show end-diastolic PV relation (EDPVR). (L) Palmitate oxidation in the hearts (n = 16). (M) The effect of fenofibrate on PPRE-luciferase reporter activity in primary cultured rat neonatal CMs, depending on the concentration of BSA-palmitic acid (PA) (n = 8). # $p < 0.05$, ## $p < 0.001$ compared to 0 μ M of PA. (N) Schematic representation of fibrates- or lipid-induced PPAR α stimulation through activation of GSK-3 α and PPAR α -Ser280 phosphorylation in CMs. Fibrates inhibit GSK-3 α -mediated PPAR α phosphorylation by interfering with the interaction between GSK-3 α and PPAR α , thereby antagonizing lipid-induced activation of PPAR α and ameliorating cardiac lipotoxicity in obesity. (O) Histogram showing the ratio of phosphorylated versus total GSK-3 α (n = 7 with diabetes and n = 14 without diabetes). (P) Immunoblots showing the effect of fenofibrate on PPAR γ -Ser273 phosphorylation in CMs. Error bars indicate s.e.m. * $p < 0.05$, ** $p < 0.001$.

Table S1. Top 10 upregulated KEGG gene sets in wild-type (vs GSK-3 α knock-in) mouse heart, Related to Figure 1

	GS follow link to MSigDB	SIZE	ES	NES	NOM p-val	FDR q-val
1	KEGG_NEUROACTIVE_LIGAND_RECEPTOR_INTERACTION	221	-0.42	-2.27	0	0.001
2	KEGG_AUTOIMMUNE_THYROID_DISEASE	22	-0.66	-2.21	0	0.001
3	KEGG_ALLOGRAFT_REJECTION	16	-0.68	-2.19	0	0.001
4	KEGG_ASTHMA	15	-0.59	-1.84	0.01	0.019
5	KEGG_HEMATOPOIETIC_CELL_LINEAGE	66	-0.4	-1.81	0.005	0.019
6	KEGG_INTESTINAL_IMMUNE_NETWORK_FOR_IGA_PRODUCTION	31	-0.45	-1.73	0.008	0.028
7	KEGG_JAK_STAT_SIGNALING_PATHWAY	125	-0.31	-1.6	0	0.062
8	KEGG_PRIMARY_IMMUNODEFICIENCY	33	-0.42	-1.6	0.016	0.055
9	KEGG_CYTOKINE_CYTOKINE_RECEPTOR_INTERACTION	201	-0.29	-1.53	0	0.077
10	KEGG_CELL_ADHESION_MOLECULES_CAMS	103	-0.31	-1.52	0	0.074

Table S2. Upregulated KEGG gene sets in PPAR α -S280D vs in PPAR α -WT (FDR q<0.25), Related to Figure 3

	GS follow link to MSigDB	SIZE	ES	NES	NOM p-val	FDR q-val
1	KEGG_RETINOL_METABOLISM	28	0.69	1.84	0	0.03
2	KEGG_TYPE_I_DIABETES_MELLITUS	20	0.71	1.79	0	0.03
3	KEGG_TERPENOID_BACKBONE_BIOSYNTHESIS	15	0.75	1.74	0	0.04
4	KEGG_FATTY_ACID_METABOLISM	33	0.61	1.69	0.003	0.06
5	KEGG_GLYCEROLIPID_METABOLISM	43	0.57	1.67	0.002	0.07
6	KEGG_GAP_JUNCTION	69	0.53	1.64	0.001	0.08
7	KEGG_LONG_TERM_POTENTIATION	64	0.51	1.6	0.003	0.11
8	KEGG_ALLOGRAFT_REJECTION	15	0.68	1.57	0.02	0.13
9	KEGG_BLADDER_CANCER	39	0.52	1.51	0.024	0.21
10	KEGG_GNRH_SIGNALING_PATHWAY	92	0.46	1.5	0.013	0.2
11	KEGG_TASTE_TRANSDUCTION	26	0.57	1.5	0.026	0.2
12	KEGG_STARCH_AND_SUCROSE_METABOLISM	33	0.53	1.48	0.034	0.2
13	KEGG_TRYPTOPHAN_METABOLISM	37	0.52	1.46	0.03	0.23
14	KEGG_CALCIIUM_SIGNALING_PATHWAY	165	0.41	1.46	0.004	0.22

Table S3. Myocardial metabolites in the heart of wild-type and PPAR α -S280A knock-in mice, Related to Figure 5.

PATHWAY		METABOLITE	Mean \pm SEM		FOLD CHANGE	p-value		
			WT	KI				
TCA cycle		citric acid	29.9 \pm 3.0	22.2 \pm 2.5	0.742	0.056		
		isocitric acid	11.7 \pm 1.6	9.1 \pm 0.9	0.777	0.148		
		succinic acid	177.9 \pm 24.0	228.3 \pm 69.3	1.283	0.465		
		fumaric acid	152.2 \pm 19.9	75.9 \pm 11.0	0.499	0.006		
		malic acid	256.0 \pm 38.1	119.3 \pm 20.1	0.466	0.008		
Glucose metabolism		Glycolysis		glucose-1-phosphate	10.7 \pm 2.1	9.7 \pm 1.6	0.905	0.676
		glucose-6-phosphate	72.0 \pm 15.3	59.3 \pm 11.1	0.824	0.475		
		fructose-6-phosphate	75.8 \pm 14.5	66.0 \pm 11.7	0.870	0.572		
		Glycerol 3-phosphate	199.7 \pm 31.9	290.4 \pm 119.4	1.455	0.436		
		3-phosphoglycerate	16.9 \pm 3.6	12.6 \pm 2.7	0.748	0.322		
		pyruvic acid	8.6 \pm 0.6	7.9 \pm 0.8	0.918	0.431		
		lactic acid	447.5 \pm 142.1	999.1 \pm 629.3	2.233	0.367		
		Myoinositol	41.8 \pm 2.9	31.5 \pm 5.6	0.754	0.106		
		myo-inositol 1-phosphate	60.9 \pm 4.4	44.2 \pm 13.3	0.725	0.217		
		Fatty acid metabolism		Saturated FFA		12:0 lauric acid	5.1 \pm 0.7	4.1 \pm 0.6
14:0 myristic acid	16.4 \pm 0.8			14.5 \pm 2.0	0.887	0.362		
16:0 palmitic acid	2163.4 \pm 102.5			1515.3 \pm 234.5	0.700	0.022		
17:0 Heptadecanoic acid	16.6 \pm 0.5			12.2 \pm 2.5	0.734	0.094		
18:0 stearic acid	3786.7 \pm 233.9			2538.3 \pm 600.0	0.670	0.062		
19:0 Nonadecanoic acid	8.3 \pm 0.4			5.7 \pm 1.5	0.683	0.100		
Unsaturated FFA				16:1 Palmitelaidic acid	4.5 \pm 0.4	2.8 \pm 0.5	0.616	0.017
18:2 linoleic acid	249.3 \pm 11.1			175.1 \pm 45.6	0.702	0.115		
18:1 oleic acid	124.3 \pm 5.9			82.5 \pm 20.8	0.664	0.063		
18:1 (trans) elaidic acid	45.6 \pm 1.2			29.9 \pm 8.9	0.656	0.085		
20:4 arachidonic acid	123.7 \pm 4.6			76.0 \pm 28.0	0.614	0.096		
				1-Linoleoyl-glycerol	24.3 \pm 0.6	17.6 \pm 3.3	0.723	0.057
				1-Oleoyl-glycerol	24.8 \pm 1.1	16.8 \pm 3.7	0.678	0.050
				1-monostearoylglycerol	402.6 \pm 22.9	351.2 \pm 29.5	0.872	0.163
				1-monopalmitoylglycerol	295.8 \pm 23.0	240.2 \pm 14.4	0.812	0.051
				2-monooleoylglycerol	12.4 \pm 0.3	9.1 \pm 1.8	0.732	0.075
				glycerol	152.5 \pm 6.9	132.3 \pm 10.8	0.867	0.115
				cholesterol	2328.9 \pm 124.7	1875.4 \pm 114.0	0.805	0.017
Amino acid metabolism				BCAA		valine	310.0 \pm 28.3	333.7 \pm 90.4
		leucine	230.6 \pm 29.0	264.7 \pm 75.7	1.148	0.651		
		isoleucine	113.6 \pm 13.4	132.0 \pm 37.6	1.163	0.619		
				alanine	71.6 \pm 7.6	66.4 \pm 10.0	0.928	0.658
				aspartic acid	5578.5 \pm 874.2	3928.1 \pm 1207.1	0.704	0.251
				asparagine	30.0 \pm 2.6	21.0 \pm 2.9	0.701	0.033
				cysteine	7.9 \pm 0.5	6.9 \pm 1.0	0.866	0.326
				L-Glutamic acid	470.9 \pm 104.4	424.0 \pm 104.6	0.900	0.732
				glutamine	2105.4 \pm 177.2	2001.0 \pm 256.2	0.950	0.718
				glycine	32.7 \pm 3.1	29.3 \pm 1.3	0.896	0.288
				histidine	14.7 \pm 1.9	8.5 \pm 0.6	0.580	0.009
				lysine	161.6 \pm 24.6	94.5 \pm 6.0	0.585	0.018
				L-Methionine	89.0 \pm 11.3	66.2 \pm 8.2	0.744	0.105
				proline	2.3 \pm 0.4	2.3 \pm 0.4	0.993	0.975
				phenylalanine	63.7 \pm 4.8	65.6 \pm 5.2	1.029	0.782
				serine	738.2 \pm 78.4	494.5 \pm 50.5	0.670	0.019
				tyrosine	17.9 \pm 4.3	17.2 \pm 2.5	0.964	0.890
				tryptophan	49.4 \pm 7.9	26.9 \pm 3.6	0.544	0.020
				2-aminoadipic acid	2.8 \pm 0.6	1.4 \pm 0.3	0.505	0.039
				threonine	85.4 \pm 13.2	54.7 \pm 5.9	0.640	0.045
				homoserine	6.1 \pm 0.5	6.2 \pm 0.9	1.011	0.942
				glycolic acid	15.0 \pm 0.9	12.0 \pm 1.0	0.799	0.041
				glyceric acid	7.6 \pm 0.3	7.1 \pm 0.6	0.934	0.436
		2-hydroxyglutarate	6.3 \pm 0.7	8.2 \pm 2.1	1.309	0.349		
		homocysteine	1.6 \pm 0.2	1.4 \pm 0.1	0.836	0.152		
		N-methylalanine	32.5 \pm 5.0	16.3 \pm 2.9	0.502	0.014		
		sarcosine	8.8 \pm 2.3	5.0 \pm 0.8	0.568	0.122		
		Urea cycle		ornithine	18.8 \pm 5.4	14.2 \pm 1.1	0.753	0.377
		urea	131.1 \pm 10.0	129.6 \pm 11.7	0.989	0.915		
		N-acetylaspartate	1.5 \pm 0.4	1.1 \pm 0.1	0.716	0.310		
		B-alanine	1.7 \pm 0.4	1.4 \pm 0.2	0.871	0.617		
		inorganic phosphate		phosphate	11701.2 \pm 926.0	11833.7 \pm 708.6	1.011	0.902
diphosphate	271.6 \pm 48.5	177.0 \pm 53.3	0.651	0.180				
Purine/primidine metabolism		Adnine nucleotides		hypoxanthine	5.4 \pm 3.2	5.3 \pm 2.1	0.977	0.972
		adenosine	75.4 \pm 13.3	60.2 \pm 8.0	0.798	0.306		
		inosine	5.0 \pm 2.2	3.4 \pm 1.2	0.686	0.513		
		adenine	10.7 \pm 0.6	9.1 \pm 0.8	0.845	0.096		
		5'-Adenosine monophosphate	1148.3 \pm 210.8	824.1 \pm 191.5	0.718	0.239		
		uric acid	2.3 \pm 0.7	1.4 \pm 0.3	0.593	0.184		
		uracil	0.9 \pm 0.3	1.3 \pm 0.6	1.477	0.536		
Others		creatinine	1640.6 \pm 68.9	1175.0 \pm 53.2	0.716	0.000		
		pantothenic acid	29.7 \pm 3.9	17.0 \pm 2.7	0.572	0.017		
		3-hydroxybutyrate	12.7 \pm 8.4	13.2 \pm 5.8	1.036	0.961		
		nicotinamide	88.5 \pm 4.1	70.8 \pm 6.3	0.799	0.030		
		glutathione	36.0 \pm 2.1	23.0 \pm 2.6	0.639	0.002		
		2,4-dihydroxybutanoic acid	52.7 \pm 2.1	42.7 \pm 4.2	0.810	0.044		
		serotonin	4.7 \pm 0.5	4.9 \pm 2.1	1.050	0.904		
		dopamine	2.7 \pm 0.4	1.4 \pm 0.4	0.530	0.039		
		1,3-bisphosphoglycerate	1.3 \pm 0.1	0.9 \pm 0.2	0.686	0.090		
		2-hydroxybutyric acid	25.7 \pm 3.4	14.8 \pm 1.8	0.576	0.014		
		kynurenine	0.4 \pm 0.0	0.3 \pm 0.1	0.617	0.063		
		gluconic acid	15.7 \pm 1.8	10.7 \pm 1.5	0.687	0.049		
		ribitol	1.6 \pm 0.2	1.1 \pm 0.1	0.674	0.057		
		phosphoethanolamine	8.4 \pm 0.3	8.0 \pm 0.7	0.949	0.533		

 Decreased metabolite (p<0.05)

Table S4. Information on human heart samples, Related to Figure 6.

	Diabetes (-) (n = 14)	Diabetes (+) (n = 7)	P value
Age (year)	52.0 ± 11.8	50.4 ± 11.6	0.776
Male (n)	13 (92.9%)	6 (85.7%)	1.000
Hypertension (n)	5 (35.7%)	4 (57.1%)	0.397
Body weight (kg)	68.4 ± 2.4	71.4 ± 4.8	0.540
Height (cm)	168.2 ± 2.1	165.2 ± 2.6	0.409
Body mass index (kg/m ²)	24.3 ± 0.9	26.0 ± 1.2	0.259

Table S5. Oligonucleotide used in this paper, Related to STAR Methods

Name	Forward Primer	Reverse Primer
(A) qPCR Primers		
(mouse)		
Cd36	CCTCCAGAATCCAGACAACC	CACAGGCTTTCCTTCTTTGC
Slc27a1	ATCTACGGGTTGACGGTGGTA	GGTAGCGGCAGATTTACCTA
Lpl	AGAGAGGACTCGGAGACGTG	GGAGTTGCACCTGTATGCCT
Cpt1b	TGGCTGAGGTACTTTCTGAACC	AGAGACCCCGTAGCCATCAT
Acadm	GCTAGTGGAGCACCAAGGAG	CCAGGCTGCTCTCTGGTAAC
Acadl	TTCCGGGAGAGTGTAAAGGA	ACTTCTCCAGCTTCTCCCA
Acadvl	GCTCTGCAAGGCTGTATGGA	CGATTCTGTCTCCCGTCTC
Echs1	CCAGTTCGGACAGCCAGAAA	ACAAGACTGCCTGCTTTGC
Pdk4	TGACTCAAAGACGGGAAACC	ACTGGTCGCAGAGCATCTT
Glut4	TTGGGAAGGAAAAGGGCTAT	GAGGAACCGTCCAAGAATGA
Adiponectin	CTCCACCCAAGGGAACCTGT	AGGACCAAGAAGACCTGCATC
Adipsin	CGTACCATGACGGGGTAGTC	GAGTCTCCCCTGCAAGTGTC
Leptin	ACATTTACACACGCAGTCG	ACTCAGAATGGGGTGAAGCC
IL-6	CCGGAGAGGAGACTTCACAG	TGCCATTGCACAACCTTTTT
TNF α	CCCTCACACTCAGATCATCTTCT	GCTACGACGTGGGCTACAG
Pgc1 α	TCACACCAAACCCACAGAAA	TCTGGGGTCAGAGGAAGAGA
Ppara	ATGCAGTACTGCCGTTTTTC	CCGAATCTTTCAGGTCGTGT
Ppar δ	GACAATCCGCATGAAGCTC	CAAAGCGGATACGCTGTGTG
Ppar γ	TTCAGAAGTGCCTTGCTGTG	CCAACAGCTTCTCCTTCTCG
(Rat)		
Cd36	TTCAAGGTGTGCTCAACAGC	CCCCACAAGAGTTTCTTCAA
Slc27a1	TGAGAAGCGCCTAGGACTTTG	TCCGCATCCTTCTCTGGCTTG
Lpl	CCATGGATGGACGGTGACAG	ATAATGTTGCTGGGCCCGAT
Cpt1b	CCATCATGGTGAACAGCAAC	CTCTTCTCGGTCCAGTTTGC
Acadl	GGTTTCAGCCTCCATTCAGA	TCATCTGGGGGATAAACTGC
Acadm	GTCGCCCCAGACTACGATAA	GCCAAGACCACCACAACCTCT
Acadvl	AAGCCAGAGACCCTCTCCTC	CAGATGGGTATGGGAACACC
Echs1	CTCGCTGTTGTCCCCAGTTC	TTCAACTGGATCAGCCCCAC
Hadhb	CGCATCCTTCGCAGACTCTA	TGGGGCAGACTGTACTTGTG
Pdk4	CAAGAATTGCCCGTCAGACT	GACGGAAGGGGTGTCACTA
Atp5b	ACCACCAAGAAGGGCTCGAT	CCCAACTCAGCAATAGCACG
Atp5d	GGCCTGGACAGATGTCCTTC	CAAAGGTCAGGTCAGCGTA
Atp5g1	CTGACGGGGAGTGGGAGT	TACTCAGGAGGGAGGCAGAC
Ndufb6	GTACCGCACCCAGTCTCTCAC	TTCTGGGCTTCGTGCCAAC
Pgc1 α	CAGAACCATGCAAACCACAC	TTGTGGCTTTTGTGTTGAC
(B) ChIP primers (rat)		
Pdk4	TGTAACAAGGACAAGTCTGGGCG	AAGGGGCAAAGGGTGAGAGGGA
Cpt1b	CAGACCCATACCCGACAGA	CGGCTGAGAGTAAGGGTGAA
Slc27A1	TGAGAAGCGCCTAGGACTTT	ATGCTGACCTTCTCTGGCTT
Cd36-1	CAGTTCTAAGATCATGGACCCC	TGTTGCCCTGCAGATCAAAC
Cd36-2	GCGTGCATAGCAAACCAA	TGTGGCCTGGTTCAACTATT
Acadl	GACTGACCCTGGACTCTGAC	CCGCAACAATCACGTTCACT
Acadm	TTAGCCGCTCCAGTGTACAC	ATACCGGGGAAAGCTGGAC
Acads	TGCCATCCGGAACCTTAGAG	GATCTCCGCCCTGTGACC
Echs1	TACTCAAAGAACC GCCGCTA	GGAGACGGAAGCTAAAGGGA
Hadhs	TCTCTGGGAAGCAGCTAATGT	AGAATGGCAAATAGGGAATTGGT
(C) Primers for oligo pull-down		
Cd36	AAAGCAAGGTA AAAAGGTCAAGGGCA	TGCCCTTGACCTTTTACCTTGCTTT
Slc27A1	AGTGGGGCAAAGGGCACAGGAGATG	CATCTCCTGTGCCCTTTGCCCACT
Acadm	GGCACAAGCTCAGAGGTCAGTAAAT	ATTTACTGACCTCTGAGCTTGTGCC
Echs1	CCGCTCAGGTCACGGGTCCACCCCT	AGGGGTGGACCCGTGACCTGAGCGG
(D) Primers for recombinant proteins, adenovirus, and site-directed mutagenesis		
GST-PPAR α -T1	ATTGGATCCGTGGACACAGAGAGCCCCA	ATTATTGTCGACTCACATGCACTGGCAGCAGTG
GST-PPAR α -T2	ATTGGATCCGTGGACACAGAGAGCCCCA	ATTATTGTCGACTCACAGGCACTTGTGAAAAACGG
GST-PPAR α -T3	ATTGGATCCGTGGACACAGAGAGCCCCA	ATTATTGTCGACTCAGATGTTCAAGGGCACTGCC
GST-PPAR α -T4	ATTGGATCCGTGGACACAGAGAGCCCCA	ATTATTGTCGACTCAGTCTGTGATGACAGAGCCCTC
GST-PPAR α -T5	ATGGATCCACCCCTCTCCAGCTTCCAG	ATTATTGTCGACTCAGTACATGTCTCTGTAGATCTCTGC
GST- β -catenin	ATTATTGGTACCCTACTCAAGCTGATTTGATGAGT	ATTATTAGGATCCTTACAGGTGAGTATCAAACCAGGC
PPAR α -S280A	CCAGTGCATGGCCGTGGAGACCG	CGGTCTCCACGGCCATGCACTGG
PPAR α -S280D	CCAGTGCATGGACGTGGAGACCG	CGGTCTCCACGTCCATGCACTGG
PPAR α -S280E	CCAGTGCATGGAGGTGGAGACCG	CGGTCTCCACCTCCATGCACTGG

PPAR α -H440A	GGTCACGGAGGCTGCGCAGCTCG	CGAGCTGCGCAGCCTCCGTGACC
PPAR α -H440Q	GTACACGGAGCAAGCGCAGCTCG	CGAGCTGCGCTTGCTCCGTGAC
PPAR α -K448A	CGTACAGGTCATCGCGAAGACCGAGTCCG	CGGACTCGGTCTTCGCGATGACCTGTACG
PPAR α -K449A	CAGGTCATCAAGGCGACCGAGTCCGACG	CGTCGGACTCGGTTCGCCTTGATGACCTG
PPAR α -K448/449A	CGTACAGGTCATCGCGGCGACCGAGTCCGAC	GTCGGACTCGGTTCGCCGCGATGACCTGTACG
PPAR α -K448N	CGTACAGGTCATCAACAAGACCGAGTCCG	CGGACTCGGTCTTGTTGATGACCTGTACG
PPAR α -K449N	CAGGTCATCAAGAACACCGAGTCCGACG	CGTCGGACTCGGTGTTCTTGATGACCTG
PPAR α -K448/449N	CGTACAGGTCATCAACAACACCGAGTCCGAC	GTCGGACTCGGTGTTGTTGATGACCTGTACG
pDC-YFP- PPAR α	ATTCCCGGGGTGGACACAGAGAGCCCC	ATTATTGTCGACTCAGTACATGTCTCTGTAGATCTCT TG
(E) Primers for mouse generation and genotyping		
Subcloning, long arm	ATTATTGGATCCGGCGCGCCTATCAGCTCCCCT GGAAGTAAA	ATTAGATATCCTCACTCAGTTCCACTCCACAG
Subcloning, short arm	ACTAACTGTCGACGCGGCCGCCTGTGGAGTGG AACTGAGTGAGAACAGTAT	ATTATCTCGAGACCGCCTCTGATGGGTACAGACA
5' Selection (PL-P2)	ACCTGAGCTTGGATCCTTGC	TGGGTCGTTTGTTCGGATCT
3' Selection (P3-PR)	TCCAGACTGCCTTGGGAAAA	GGGAAGGTCAGTAAGGGTGC
PPAR α -KI (P1-P2)	AGTGGATCTGTCACTCGCAG	TGGGTCGTTTGTTCGGATCT
PPAR α -KI (P1-P4)	AGTGGATCTGTCACTCGCAG	AGCACTGCACCTAAACCTGC
α MHC-Cre	ATGACAGACAGATCCCTCCTATCTCC	CTCATCACTCGTTGCATCGAC
GSK-3 α floxed	CCAACCCTCCAGTCCTTATC	CAGGCTACCCAGCCTTTC
GSK-3 β floxed-Neo	GGGAGGATTGGGAAGACAAT	ACAATGTGCCGAGTTCATCA
GSK-3 β floxed-WT	TTGGCAATTTGAAAGGGAAG	ACAATGTGCCGAGTTCATCA
GSK-3 α KI	TTGAAGTGGCTGGTACTGGCTCTG	GTGTGCTCCAGAGTAGTACCTAGC
GSK-3 β KI	TCACTGGTCTAGGGGTGGTGGAAAG	GGAGTCAGTGACAACACTTAACTT
(F) shRNA targeting sequence (rat)		
GSK-3 α #1	GTGATTGGCAATGGCTCAT	
GSK-3 α #2	GGTGTCAAATCTCGGACA	
GSK-3 α #3	GCTTTAACTGAGACTCAGA	